EOS MODIS and SNPP VIIRS Cloud Properties: User Guide for the Climate Data Record Continuity Level-2 Cloud Top and Optical Properties Product (CLDPROP)

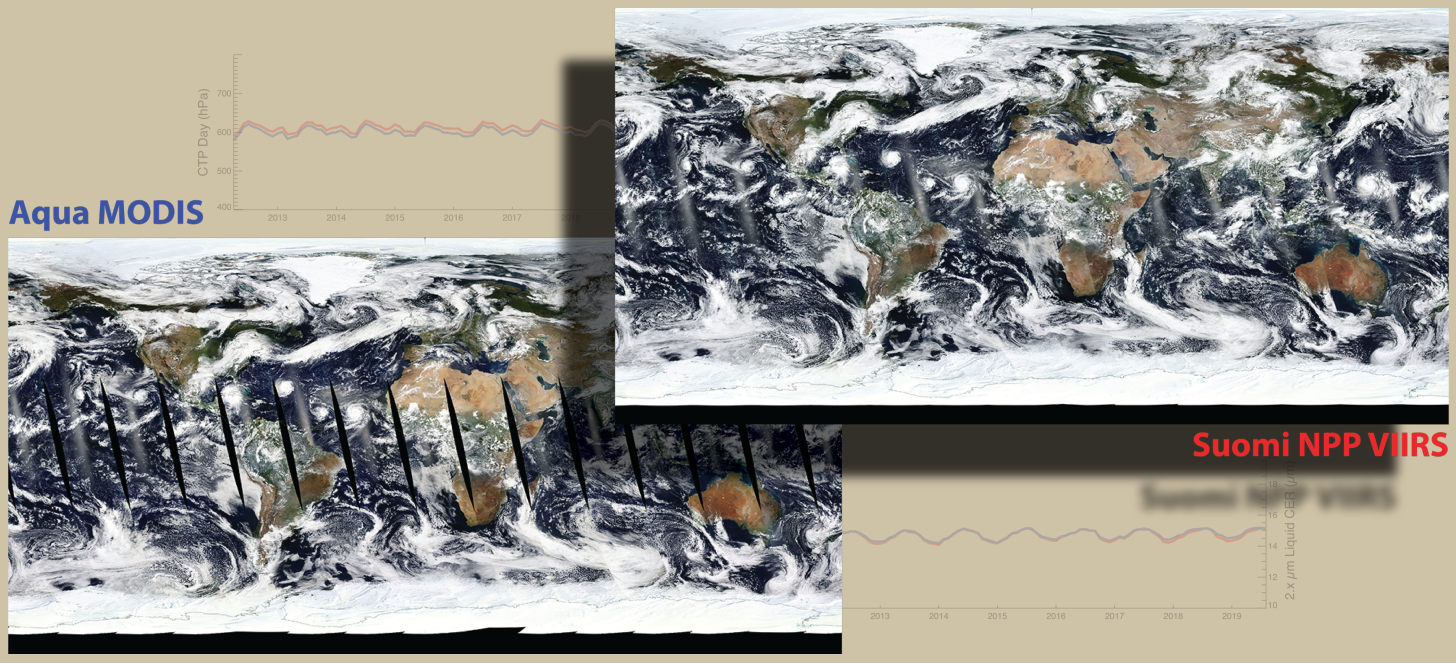

Version 1.1

January 2020

CLOUD MASKING TEAM

STEVEN A. ACKERMAN[6], RICHARD FREY[6]

CLOUD TOP PROPERTY TEAM

ANDREW HEIDINGER[2], YUE LI[6], ANDI WALTHER[6]

CLOUD OPTICAL PROPERTY TEAM

STEVEN PLATNICK[1], KERRY G. MEYER[1], GALA WIND[3,1], NANDANA AMARASINGHE[3,1], CHENXI WANG[4,1], BENJAMIN MARCHANT[5,1]

PRODUCT ASSESSMENT SUPPORT

ROBERT E. HOLZ[6], STEVEN DUTCHER[6], PAUL HUBANKS[7,1]

1 Earth Sciences Division, NASA Goddard Space Flight Center, Greenbelt, MD
2 NOAA NESDIS/STAR/CIMSS, Madison, WI
3 Science Systems and Applications, Inc., Lanham, MD
4 Earth System Science Interdisciplinary Center, University of Maryland, College Park, MD
5 Goddard Earth Sciences Technology and Research, Universities Space Research Association, Columbia, MD
6 Cooperative Institute for Meteorological Satellite Studies, University of Wisconsin, Madison WI
7 ADNET Systems, Inc., Bethesda, MD

1. INTRODUCTION

NASA ushered in a new generation of global imager observations of the Earth with MODIS on the EOS Terra and Aqua missions. MODIS provided unique spectral capability relative to earlier global imagers, allowing for the retrieval of geophysical parameters key to understanding changes in the Earth's land surface, ocean, and atmosphere. For retrievals of clouds, two shortwave infrared (**SWIR**) 1.64 and 2.13 µm window channels were included that, in addition to an AVHRR heritage 3.75 µm channel, provide comprehensive cloud microphysical information. Multiple spectral channels within the thermal infrared (**IR**) 13 µm CO_2 absorption band allowed for application of a CO_2-slicing cloud top property retrieval technique that, along with a SWIR channel centered within the 1.38 µm water vapor absorption band, provided unprecedented sensitivity to high altitude, thin clouds. Furthermore, MODIS also provided unique spatial capabilities, having spectral channels with 250 m (0.66, 0.86 µm), 500 m (SWIR), and 1 km (all other) resolution at nadir. To date, these imagers have proved remarkably successful, exceeding their design lives to produce 18-year (Terra) and 16-year (Aqua) climate data records that are expected to continue into the early 2020s.

Nevertheless, detecting climate trends, including those related to clouds, is a multi-decadal endeavor. For instance, cloud feedback detection for a range of CMIP (Coupled Model Intercomparison Project) models is typically greater than 2-3 decades given the uncertainties of current sensors [*Wielicki et al.*, 2013]. Thus, while their missions are projected to extend into the early 2020s, the EOS Aqua and Terra data records alone are not sufficient for establishing climate trends. Extending these EOS data records to new sensors is therefore imperative. For continuing MODIS-like global cloud records, the only viable imager is VIIRS (375-750 m nadir resolution) on Suomi NPP (SNPP) and the operational NOAA JPSS series (starting with JPSS-1/NOAA-20 in late 2017, with subsequent satellites expected to provide coverage into the mid-2030s). With respect to MODIS, however, the absence of key spectral channels on VIIRS and a significant spectral location change for a key SWIR channel used for cloud microphysical retrievals prohibits the direct porting of the EOS MODIS cloud algorithms to VIIRS to establish a consistent MODIS-VIIRS cloud climate data record. For this reason, a merged MODIS-VIIRS cloud record to serve the science community in the coming decades requires different algorithm approaches than those used for MODIS alone.

Starting in 2013, NASA formed an SNPP Science Team to develop continuity algorithms that would bridge the EOS and SNPP observation era (i.e., MODIS/VIIRS, AIRS/CrIS, OMI/OMPS). These continuity products are intended to enable NASA R&A and Application studies, as well as engage the broader scientific community. Due to the inconsistent spectral coverage between the MODIS and VIIRS imagers, the approach taken by the cloud product team was to develop a continuity algorithm that only uses the common (or near-common) subset of spectral channels available to both imagers, and is run on both the MODIS and VIIRS data streams. All algorithm elements (forward models and assumptions, retrieval mechanics, ancillary datasets, etc.) are kept constant between the two streams. This document describes the imager continuity algorithms, along with associated filenames and science and Quality Assurance (**QA**) datasets. The continuity algorithm sections are focused on differences with the heritage MODIS standard cloud product algorithms. Note that the standard MODIS cloud products (**MOD06**, **MOD35**, **MOD08**), using the full complement of available spectral coverage, will continue to be produced. Both the

continuity and MODIS standard products are archived at the same distribution facility (details in Section 1.3).

1.1. Challenges for Extending MODIS Cloud Products to VIIRS

Recent assessment efforts [e.g., *Stubenrauch et al.*, 2013; *Hamann et al.*, 2014; *Roebling et al.*, 2015] discuss the challenges to producing cloud climate data records and to achieving consistency across different sensors and different algorithms. With respect to bridging the MODIS and VIIRS observational records, these challenges arise from key differences in sensor specifications and project requirements. For instance, VIIRS lacks the IR CO_2 and water vapor absorption channels available on MODIS that provide information on cloud masking, cloud top pressure (particularly for high altitude, thin clouds), and thermodynamic phase. Moreover, the VIIRS 2.25 µm SWIR channel is spectrally offset from the MODIS 2.13 µm channel, with differences in spectral cloud particle absorption impacting cloud microphysical retrievals and thermodynamic phase determination; these two SWIR channels are collectively referred to as the 2.x µm channels in Sect. 4.

Apart from spectral channel differences, the finer spatial resolution of VIIRS compared to MODIS (750 m versus 1 km at nadir) has direct consequences for sub-pixel heterogeneity and its inducement of optical and microphysical property retrieval biases, particularly for liquid phase clouds that are generally more heterogeneous than ice phase clouds. Sub-pixel heterogeneity impacts are expected to be more acute for MODIS than for VIIRS, owing to the latter's on-board detector aggregation scheme that limits pixel growth across swath. Furthermore, while both Aqua and SNPP ostensibly have the same equatorial crossing time (notionally 1:30 pm local time), the stringent requirements of operating within the A-Train constellation limit the variability of Aqua's crossing time to within roughly a minute, while SNPP's crossing time is allowed to drift by up to 10 minutes. In addition, Aqua and SNPP have different orbital altitudes (roughly 705 km vs 834 km, respectively) and inclinations (98.2° vs 98.7°, respectively), limiting reasonable ground track alignment to once every few days. These sensor resolution and orbital differences have important ramifications on the spatial and temporal sampling and, ultimately, the global cloud property statistics derived from MODIS and VIIRS.

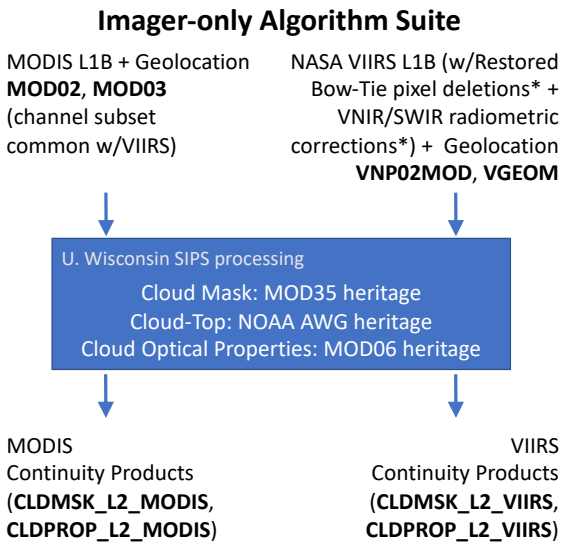

Figure 1.1.1. Processing paradigm for the MODIS-VIIRS climate data record continuity cloud mask (CLDMSK) and cloud optical/microphysical property (CLDPROP) products.

The principal philosophy of the Cloud Team regarding cloud product continuity between MODIS and VIIRS rests in the continuity of approach, i.e., pursuing a common

algorithm applied to both MODIS and VIIRS. However, the above challenges, particularly the spectral channel set differences, preclude a direct porting of the existing EOS MODIS MOD35 and MOD06 algorithms to VIIRS. Thus, the common MODIS-VIIRS algorithm relies on a common spectral channel set that for MODIS represents only a subset of the channels used in the EOS products. Therefore, in addition to the VIIRS continuity cloud products, an analogous MODIS continuity cloud product stream is necessary that is separate from (but shares heritage with) the MOD35 and MOD06 products. Figure 1.1.1 shows the processing paradigm of the MODIS and VIIRS cloud climate data record continuity products, along with the file naming convention. The continuity Level-2 (**L2**) pixel-level products are derived from three separate algorithms: a cloud mask that provides the probability of an unobstructed pixel field-of-view (**CLDMSK**), and a suite of cloud top and cloud optical property algorithms with combined datasets contained in a single file (**CLDPROP**). Note that CLDMSK results are used by both the cloud top and cloud optical property algorithms.

1.2. Cloud Product Heritage

1.2.1. Cloud Mask

The common MODIS-VIIRS Cloud Mask (CLDMSK) is used by the downstream cloud top and cloud optical property algorithms. A separate document describes the CLDMSK algorithm and is not repeated here [Link 1; see Appendix C]. However, for context, the CLDMSK algorithm closely follows the heritage MODIS MOD35 product algorithm to the extent possible, including providing results for individual sets of spectral detection tests (solar reflectance and IR). Because of overlap in the sensitivities of the various spectral tests to the type of cloud, each test is considered as part of one of several groups. The overall detection result is determined from the product of the minimum confidence of each group and is referred to as the Q value as defined in *Ackerman et al.* [1998]. For CLDMSK, the Q value is output along with a classification of clear, probably clear, probably cloudy, and cloudy.

1.2.2. Cloud Top and Optical Properties

The MODIS MOD06 cloud top algorithm retrieves cloud top pressure (**CTP**), temperature (**CTT**), and height (**CTH**), and provides an IR-only thermodynamic phase retrieval. Due to the absence on VIIRS of the 13-14 μm CO_2 spectral channels used in the MOD06 algorithm, however, a different approach is required for continuity. For CLDPROP, cloud top property and phase retrievals are provided by NOAA operational algorithms developed for AVHRR, VIIRS, and GOES-16/17, specifically the Clouds from AVHRR Extended (CLAVR-x) processing system for cloud top phase (algorithm based primarily on IR spectral channels, with additional information from select SWIR channels) and NOAA's Enterprise Algorithm Working Group (AWG) Cloud Height Algorithm (ACHA) (see the ACHA ATBD [*Heidinger and Li*, 2018], Link 2) for cloud top properties.

The Collection 6 (**C6**) MOD06 algorithm provides heritage for the CLDPROP optical property datasets. Multispectral reflectances are used to simultaneously retrieve cloud optical thickness (**COT**), effective radius (**CER**), and derived cloud water path (**CWP**) globally during the day-time for liquid and ice phases. The optical/microphysical algorithm primarily uses six visible (**VIS**), near-infrared (**NIR**), shortwave-infrared (SWIR) and midwave-infrared (**MWIR**) spectral

channels, as well as several thermal channels. In addition to the 1 km MODIS (or 750 m VIIRS) Level-1B data, the optical property algorithm requires as input a cloud mask (i.e., CLDMSK), the cloud-top pressure portion of CLDPROP, and a variety of ancillary datasets including gap-filled MODIS land and snow/ice surface spectral albedos, snow/ice data (Near-real-time Ice and Snow Extent, **NISE**), and forecast analysis fields (**NCEP GDAS**).

The MOD06 User's Guide [Link 3] and *Platnick et al.* [2017] (and references therein) provide extensive detail on the MODIS Collection 6 cloud optical properties algorithm. Essential differences between C6 MOD06 and CLDPROP are described in Section 4.1.

1.3. Cloud Product Names and Data Distribution

Product and file naming conventions for the Atmosphere Team climate data record continuity products are changed with respect to their heritage EOS MODIS counterparts. Furthermore, data product file formats have been updated to NetCDF-4 to facilitate ease of use by ensuring their compatibility with modern tools widely used by the climate and modeling communities. For the cloud mask and cloud top and optical/microphysical properties, ESDIS product names are CLDMSK and CLDPROP, respectively, for both Aqua-MODIS and SNPP-VIIRS; note that the heritage MODIS MOD35 cloud mask and MOD06 cloud top and optical property products will continue to be produced and archived under their original EOS-era product names. An example of the standardized Atmosphere Team Level-2 and Level-3 climate data record continuity product file naming convention is below.

CLDPROP_L2_MODIS_Aqua.AYYYYDDD.HHMM.VVV.YYYYDDDMMHHSS.nc

The interpretation of this file name is as follows:

CLDPROP: Data product type (cloud mask: **CLDMSK**; cloud top/optical: **CLDPROP**)

L2: Data product level (Level-2 pixel-level: **L2**; Level-3 global gridded: **L3**)

MODIS: Sensor name (**MODIS**, **VIIRS**)

Aqua: Platform name (**Aqua**, **SNPP**)

AYYYYDDD: Data acquisition year (**YYYY**) and day of year (**DDD**)

HHMM: Data acquisition hour (**HH**) and minute (**MM**) start time, in UTC

VVV: Data version number

YYYYDDDMMHHSS: Data production date and time, in UTC

nc: Denotes NetCDF-4 file format

All Atmosphere Team Level-2 and Level-3 continuity products, including the CLDMSK and CLDPROP products for both Aqua-MODIS and SNPP-VIIRS, are produced by the Atmosphere Science Investigator Led Processing System (**SIPS**) [Link 4] located at the University of

Wisconsin – Madison and are archived and distributed at the Level-1 and Atmosphere Archive and Distribution System (**LAADS**) Distributed Active Archive Center (**DAAC**) [Link 5] located at NASA GSFC. Note that LAADS also distributes the MODIS standard cloud products that are produced at the NASA MODIS Adaptive Processing System (**MODAPS**).

1.4. Product Version 1.1 Change Summary

CLDPROP Version 1.1 reprocessing began in August 2019 in response to an issue with the cloud optical properties (**COP**) thermodynamic phase algorithm (algorithm details in Section 4.1.2) yielding spurious liquid cloud results. Algorithm changes are limited solely to the phase algorithm, and impacts are only on the COP phase results and downstream optical properties retrievals (COT, CER, CWP) and uncertainties.

The COP phase algorithm for CLDPROP is a modified version of the C6/C6.1 MOD06 COP phase algorithm that employs a voting scheme consisting of numerous tests based on the IR thermodynamic phase results [*Baum et al.*, 2012], cloud top temperature retrievals, and dual phase spectral CER retrievals (full algorithm details are provided in *Marchant et al.* [2016] and Section 2.4 and Appendix E of the MOD06 C6/C6.1 User's Guide [Link 3]). For CLDPROP Version 1.0, this algorithm was implemented without a key cold cloud sanity check that in C6 MOD06 overrides an undetermined phase or ambiguous liquid phase result provided that the IR phase indicates an ice cloud and that the cloud is cold (CTT < 240 K) with the reported cloud top property solution provided by the CO_2-slicing technique (cloud top solution method being an indicator of high-altitude clouds). Because VIIRS does not have IR channels in the 13 µm CO_2 absorption region that are required for the CO_2-slicing approach, and the C6 MOD06 cloud top algorithm has been replaced in CLDPROP by the ACHA cloud top retrieval (see Section 3.1.2) that uses only the 8.5, 10.8, and 12 µm IR window channels, the heritage cloud top solution method information (CO_2-slicing vs IR-window) is unavailable in CLDPROP and the cold cloud sanity check was outright removed from the COP phase algorithm.

The removal of the cold cloud sanity check had unintended consequences, namely spurious liquid phase clouds around the edges of otherwise cold, ice phase clouds. An example from Aqua MODIS is shown in Figure 1.4.1, where the red arrow in the CLDPROP V1.0 plot (bottom row, center panel) indicates a region of liquid phase where retrieved cloud top temperature (top row, right panel) is less than 240 K. In these cases, the spectral CER tests, which are in fact thresholds applied to ice phase CER retrievals, indicated liquid clouds because the ice CER was smaller than the threshold for liquid phase results. Thus the CER tests outvoted the cloud top temperature test and a liquid phase result for found. This in turn yielded a discontinuity in aggregated ice phase CER statistics exactly at the ice phase CER thresholds used in the spectral CER tests (20 µm for ice CER retrievals from the 1.6 and 2.x µm channels, and 15 µm for ice CER retrievals from the 3.7 µm channel). This discontinuity is shown by the monthly (February 2014) Aqua MODIS 2.1 µm CER retrieval histograms in Figure 1.4.2 (top panel).

For CLDPROP Version 1.1, the cold cloud sanity check has been restored, albeit in modified form, in the COP phase algorithm. In the event of an undetermined or ambiguous liquid phase result, an ice phase decision is now forced if the cloud top properties phase indicates ice and the cloud top temperature is less than 240 K or, for optically thick clouds (COT > 40), if either of these conditions are met. The impact of this sanity check on granule-level phase results is shown in the bottom right

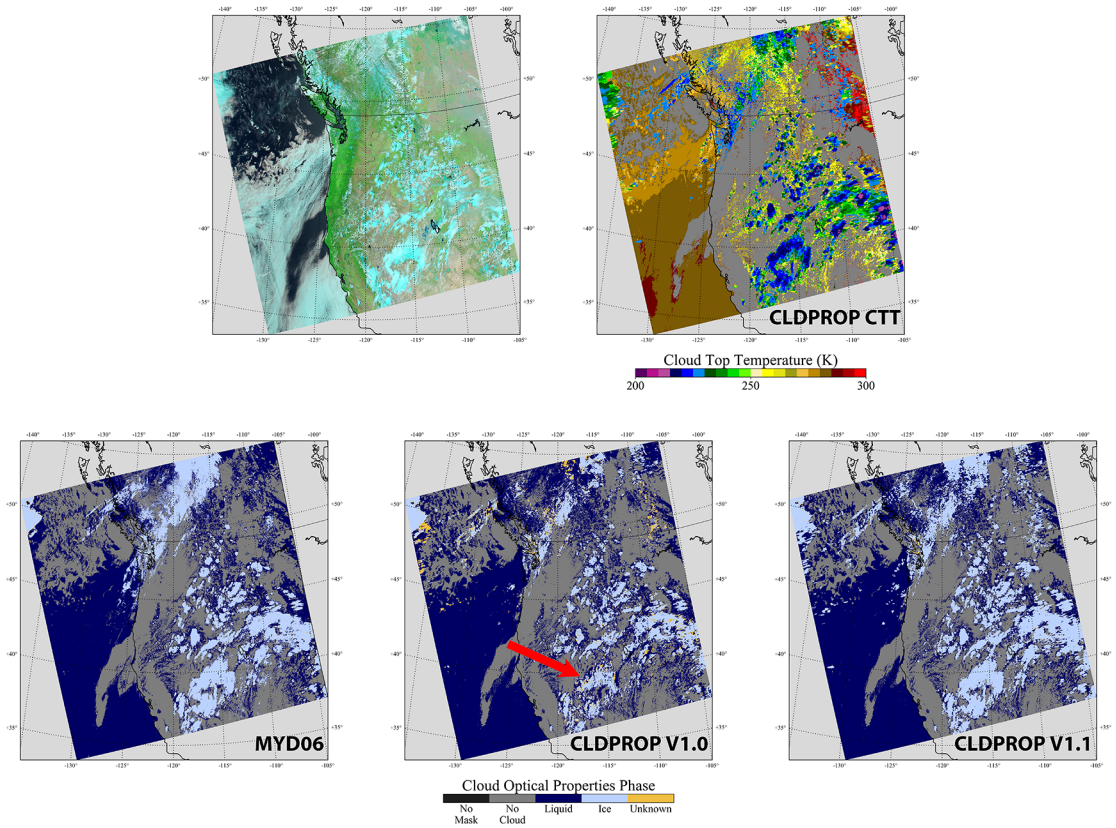

Figure 1.4.1. Example Aqua MODIS granule imagery (1 June 2019, 2100 UTC) illustrating the spurious liquid phase clouds in the CLDPROP Version 1.0 cloud optical properties phase (red arrow, bottom row center panel). The cloud optical properties phase results from C6.1 MYD06 (bottom row, left panel) and CLDPROP Version 1.1 (bottom row, right panel), are also shown. The spurious liquid clouds are correctly identified as ice in V1.1.

panel of Fig. 1.4.1, where the CLDPROP COP phase better matches that of MYD06 (bottom row, left panel). The impact on monthly ice phase CER statistics is shown in the bottom panel of Fig. 1.4.2, where the discontinuity at 20 µm is no longer evident.

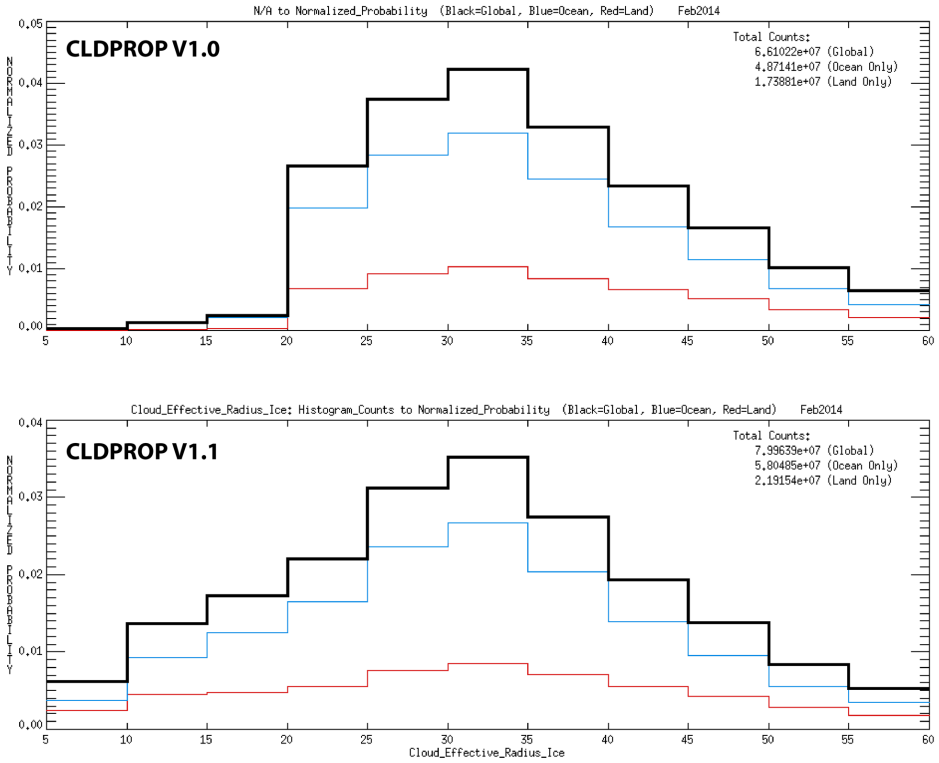

Figure 1.4.2. Monthly (February 2014) histograms of Aqua MODIS CLDPROP ice phase 2.1 μm CER retrievals from Version 1.0 (top panel) and Version 1.1 (bottom panel) after restoring the cold cloud sanity check in the COP thermodynamic phase algorithm.

2. LEVEL-1B USAGE

Required inputs to the CLDPROP algorithms include Level-1B (L1B) geolocated and calibrated pixel-level spectral reflectance (solar channels) and radiance (thermal IR channels) data and uncertainties. For the CLDPROP-MODIS product stream, the L1B data are the 1 km resolution (at nadir) Aqua-MODIS MYD021KM product produced by MODAPS; this L1B usage is consistent with the heritage MYD06 cloud top and optical/microphysical property products. For CLDPROP-VIIRS, reflectance/radiance data are from the moderate-resolution 750 m (at nadir) VIIRS M-band spectral channels. However, rather than relying on the NOAA vendor IDPS L1B products, NASA specified the creation of its own L1B data products to be used by all algorithm teams in the Land, Ocean, and Atmosphere disciplines. The NASA VIIRS L1B software and products largely follow the model previously developed for EOS-MODIS. The files are produced by the respective VIIRS SIPSs and include all metadata required for archiving in the EOSDIS DAACs. Differences from the MODIS L1B products include the archive file format (NetCDF4 rather than HDF4) and granule length (6 minutes rather than 5 minutes), in addition to the key sensor-driven differences discussed in detail below. Additional information on the NASA VIIRS L1B products and software can be found in the NASA VIIRS Level-1 Data Product User's Guide [Link 6].

2.1. Sensor Swath Geometry

VIIRS represents an advancement over MODIS in several respects. For instance, with a sensor scan angle range of ±56.28°, VIIRS views a 3060 km-wide swath on the ground at its nominal altitude of 834 km, allowing for complete daily global coverage free of gaps. MODIS, on the other hand, has gaps between orbital swaths over the tropics, as it only views a 2330 km-wide swath (±55° sensor scan angle range at 705 km altitude). Figure 2.1.1 shows example global RGB imagery from (a) Aqua-MODIS and (b) SNPP-VIIRS from 10 September 2018 (images courtesy of NASA Worldview, Link 7). Note the lack of orbital gaps in the SNPP-VIIRS image.

Moreover, while the 750 m nadir pixel size of the VIIRS M-bands is not substantially different from the MODIS 1 km nadir pixel size, VIIRS uniquely employs an on-board detector aggregation scheme that limits along-scan (across-track) pixel growth towards swath edge. The 16 VIIRS M-band detectors are rectangular with a native footprint size at nadir of 250 m along scan (width) by 750 m along track (length). To achieve the 750 m nadir resolution of the M-band L1B data, three along-scan detectors are aggregated for observations with sensor scan angles less than 31.72°, two detectors are aggregated for scan angles between 31.72° and 44.86°, and no aggregation is performed beyond 44.86° (see the sample aggregation zones in Figure 2.1.2, green text). Thus along-scan pixel width increases roughly only to 1.625 km at scan edge, comparable to the along-track pixel length growth; note that no along-track detector aggregation is performed. The pixel growth (represented as horizontal sampling interval) in the along-scan and along-track directions is shown by the blue lines in Figure 2.1.3. Because the detector aggregation occurs on-board, the native detector data is discarded and only the aggregated data are downlinked. Further information

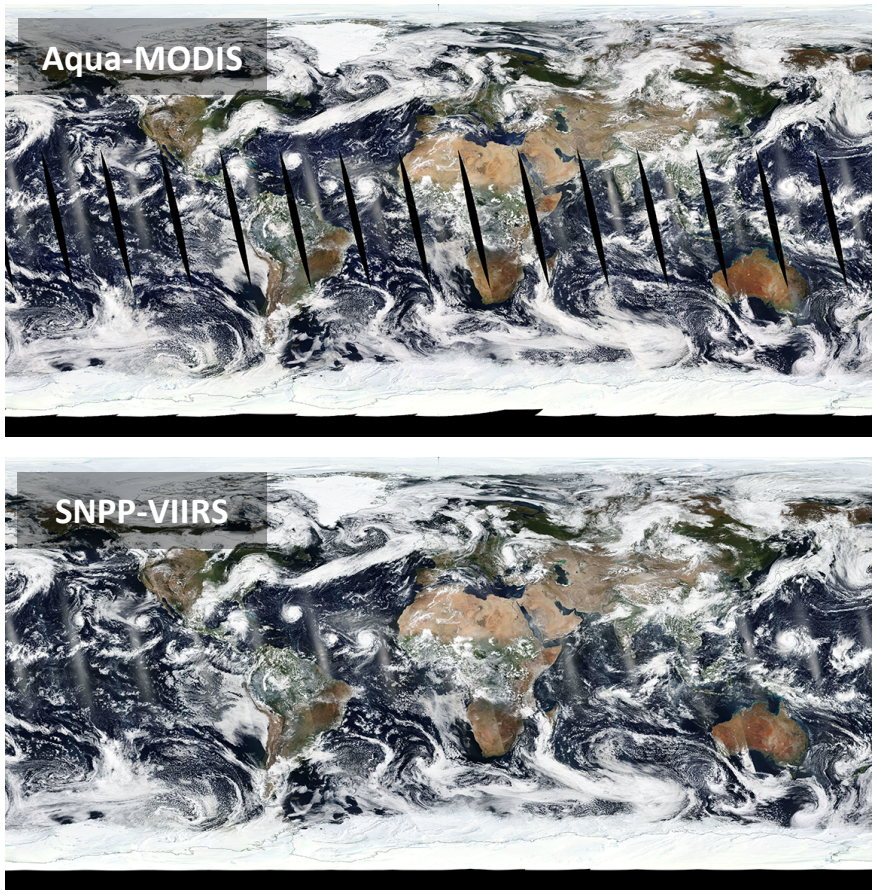

Figure 2.1.1. True color corrected reflectance RGBs from 10 September 2018. (a) Aqua-MODIS. (b) SNPP-VIIRS. The vertical black strips over the tropics in the Aqua-MODIS image are the gaps between MODIS swaths from successive orbits. Note that the VIIRS image does not have these orbital gaps due to its wider swath. Images courtesy of NASA Worldview (Link 7).

regarding the on-board detector aggregation of the VIIRS M-bands can be found in the NOAA VIIRS Sensor Data Record (SDR) User's Guide, specifically Section 2.1.1 [*Cao et al.*, 2013].

MODIS is not designed to allow for such a detector aggregation scheme for all 1 km spectral channels. While channels 1-2 (0.66, 0.86 µm) and 3-7 (0.47, 0.55, 1.24, 1.64, 2.13 µm) are aggregated during L1B processing to 1 km (nadir) pixels from detectors having native nadir resolutions of 250 m and 500 m, respectively, L1B pixel sizes grow from the nominal 1 km at nadir to more than 2×4.9 km at scan edge [*Justice et al.*, 2011].

These differences in sensor swath geometry between MODIS and VIIRS can have profound impacts on the continuity of the cloud products derived from each. The wider swath of VIIRS allows for greater sampling at all latitudes, removing orbital gaps in the tropics while increasing swath overlap at higher latitudes. However, known view angle-dependent biases, such as artificially increasing cloud fraction towards scan edge or the increased likelihood of viewing the sides of clouds (with implications on cloud top, optical, and microphysical retrievals), are likely larger in these additional VIIRS pixels. Furthermore, the limited pixel size growth of the VIIRS M-bands towards the edge of scan also reduces the impact of sub-pixel cloud heterogeneity and 3D effects that increase as pixel size grows and that have been shown to significantly impact the MODIS cloud optical/microphysical property retrievals under various conditions [e.g., *Zhang and Platnick*, 2011; *Zhang et al.*, 2012; *Cho et al.*, 2015]. That said, the lack of direct sub-pixel information on VIIRS, available on MODIS from its 250 m VIS/NIR channels, limits the ability to identify and provide useful QA information (via sub-pixel heterogeneity indices, partially

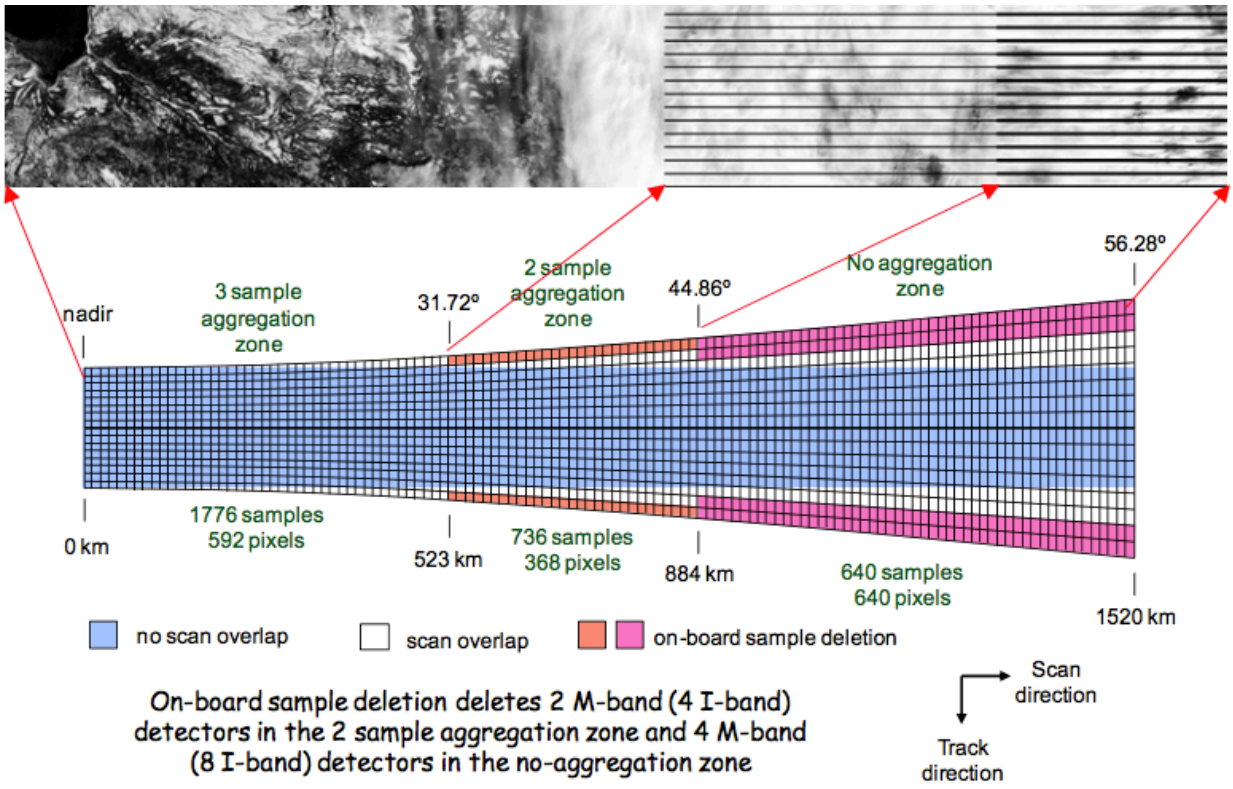

Figure 2.1.2. Illustration of VIIRS on-board along-scan detector aggregation zones (green text) and bow-tie pixel deletion. Figure obtained from the NOAA VIIRS SDR User's Guide [Figure 3, *Cao et al.*, 2013].

cloudy Clear Sky Restoral tests, etc.) on VIIRS pixels for which sub-pixel heterogeneity may nevertheless be impactful. It is possible that the VIIRS 375 m I-band (imaging) channels have the potential to provide useful sub-pixel information for the M-bands. However, these channels are not inherently co-located with the M-bands and, because they are coarser than the 250 m MODIS channels and do not map into the M-band 750 m pixels in the same way as the 250 m channels do into the MODIS 1 km pixels, they cannot provide the same level of information on heterogeneity. Further investigation is needed to determine the efficacy of the I-bands for assessing M-band sub-pixel heterogeneity.

2.2. Handling of VIIRS Bow-Tie Deleted Pixels

In addition to on-board aggregation of the native M-band detectors along scan, VIIRS also employs an on-board M-band pixel row deletion scheme aimed at limiting the so-called "bow-tie" effect at the edge of scan. The bow-tie effect results from the increase in the horizontal sampling interval in the along-track direction moving away from nadir towards the edge of swath due to the increased distance between the sensor and the ground. The end result of this panoramic effect, illustrated by the VIIRS scan illustration in Fig. 2.1.2 and along-track pixel growth plot in Fig. 2.1.3, is that successive instrument scans have pixel overlap. For VIIRS, this overlap starts to occur roughly at 19° scan angle. To mitigate scan overlap, which in effect represents pixel oversampling at scan edge, and to save downlink bandwidth, portions of VIIRS M-band pixel rows that overlap the preceding or succeeding scans are deleted on board and are assigned fill values in ground processing. In practice, the first and last pixel row of a given scan are deleted (assigned fill values

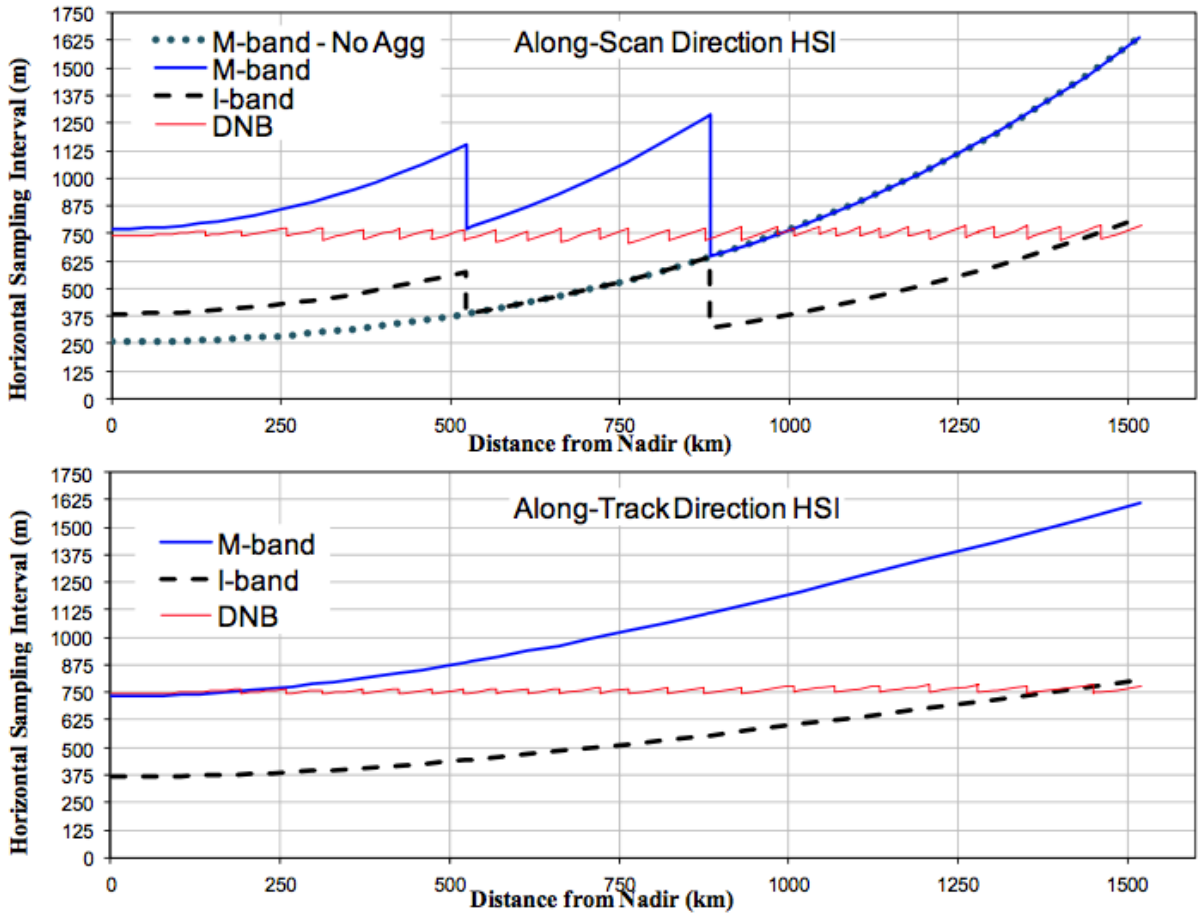

Figure 2.1.3. Illustration of VIIRS M-band detector (green dotted line) and pixel (blue line) growth in the along-scan (top) and along-track (bottom) directions. Figure obtained from the NOAA VIIRS SDR User's Guide [Figure 4, *Cao et al.*, 2013].

in the L1B) for scan angles greater than 31.72° (orange pixels in Fig. 2.1.2), and the first and last two pixel rows are deleted for scan angles greater than 44.86° (pink pixels in Fig. 2.1.2); note that these scan angle thresholds match those of the on-board M-band detector aggregation. Further information regarding the VIIRS bow-tie deletion scheme can be found in the NOAA VIIRS SDR User's Guide, specifically Section 2.1.1 [*Cao et al.*, 2013].

MODIS also suffers from overlap of successive scans due to the bow-tie effect. However, no bow-tie pixel deletion scheme is implemented, and all pixel data are reported in the MODIS L1B file. To maintain sampling consistency between the two sensors, rather than implement a post-processing bow-tie deletion scheme on MODIS, the Atmosphere Team decided to "restore" the deleted VIIRS M-band bow-tie pixels via nearest-neighbor sampling of the surviving pixels in either the preceding or succeeding scans. This scheme is implemented via post-processing the SIPS-produced NASA VIIRS L1B to produce an intermediate L1B file that includes restored bow-tie pixels for ingestion by the Atmosphere Team L2 geophysical retrieval algorithms. Note that the intermediate VIIRS L1B file is discarded after use and is not archived, though the L1B post-processing tool will be made publicly available for users to recreate these files themselves.

Note that the Cloud Team's CLDPROP_L3 global aggregation algorithm uses a pixel sampling scheme that avoids these restored bow-tie pixels so that no duplicated/artificial pixels will be included in the aggregations (see Section 3.0 of the CLDPROP_L3 User Guide, Link 10). Namely, every fourth along-scan pixel in the along-track pixel rows 4, 8, and 12 within each VIIRS scanline will be aggregated. The use of a pixel sampling approach for L3 aggregations has heritage in the MODIS Atmosphere Team MOD08 product algorithm.

2.3. Inter-Sensor Shortwave Radiometric Assessments and Adjustments

Assessments of initial SNPP-VIIRS CLDPROP retrievals against their co-located Aqua-MODIS CLDPROP counterparts revealed significant differences in liquid phase COT retrievals, with VIIRS yielding significantly larger COT. Figure 2.3.1 shows results from a scene over the Kamchatka Peninsula on 6 July 2014, which Aqua-MODIS (0200 UTC granule) and SNPP-VIIRS (0154 and 0200 UTC granules) observed within a few minutes of each other from a nearly coincident ground track. The false color RGBs from both instruments (MODIS at left: 2.13-0.86-0.66 μm; VIIRS at right: 2.25-0.87-0.67 μm) are shown in the top row. A scatterplot comparing liquid phase COT retrievals from MODIS and VIIRS from an early CLDPROP development test is shown at bottom left, where it is evident that VIIRS retrieves larger COT than does MODIS. Note that the pixels in this scatterplot have been filtered to include only those over ocean for which the MODIS and VIIRS sensor view zenith and scattering angle differences are less than 1°, therefore mitigating the impact of viewing geometry differences.

Further investigation of the COT differences in Fig. 2.3.1 implicated potential differences in relative radiometry between the two instruments, as VIIRS appeared to observe brighter spectral reflectance, particularly in the VIS/NIR spectral channels used for COT retrievals. To evaluate this possibility, the MYD06 algorithm was used to test the impact of applying a 3% increase to reflectance in the 0.86 μm channel that is used for COT retrievals over ocean. A comparison of the resulting liquid phase COT retrievals using biased 0.86 μm reflectance and the original MYD06 retrievals is shown in the scatterplot at bottom right in Fig. 2.3.1. For this granule, it is evident that even a relatively small 3% radiometric increase to the 0.86 μm channel yields large liquid phase COT retrieval biases comparable to those found with VIIRS. Similar conclusions were concurrently being drawn by other Atmosphere Team algorithm developers, particularly the Deep Blue aerosol team.

In response to these findings by the Atmosphere Team, and in lieu of a near-term strategy from the MODIS and VIIRS Characterization Support Teams to address the issue, the Atmosphere SIPS agreed to produce MODIS-VIIRS match files to facilitate Atmosphere Team inter-sensor radiometric analyses. These match files contain pixel-level co-located reflectance and radiance data from Aqua-MODIS and the SNPP-VIIRS M-bands, as well as cloud masking and cloud top/optical retrievals from the EOS Aqua-MODIS products (MYD35, MYD06) for the entire SNPP mission. The co-located data in the match files are limited to those MODIS and VIIRS pixels that have view zenith and scattering angle differences less than 10° and observation time differences less than 15 minutes. Because VIIRS M-band pixel sizes are smaller than MODIS, the match files provide multiple co-located VIIRS pixels for each MODIS pixel. The goal of the match file analyses is to derive radiometric adjustment factors that can be applied to VIIRS such that its relative radiometric calibration is close to that of Aqua-MODIS.

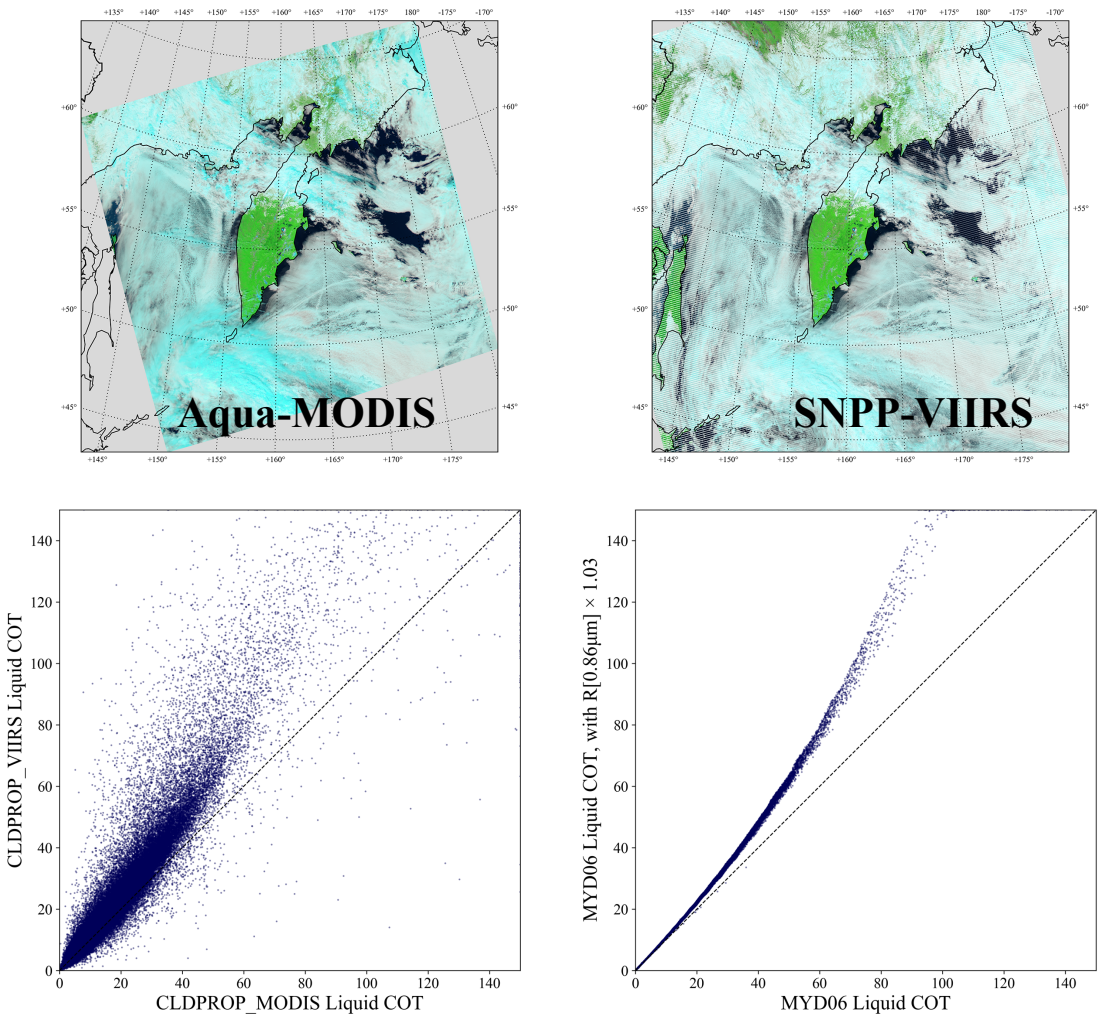

Figure 2.3.1. Coincident observations of the Kamchatka Peninsula from Aqua-MODIS (0200 UTC granule) and SNPP-VIIRS (0154 and 0200 UTC granules) on 6 July 2014. *Top Row*: False color RGBs (MODIS B7-B2-B1; VIIRS M11-M7-M5). *Bottom Left*: Scatterplot of co-located MODIS and VIIRS liquid phase COT retrievals from an early CLDPROP development test for pixels over the ocean in this scene having inter-sensor view zenith and scattering angle differences less than 1°. *Bottom Right*: Scatterplot of MYD06 liquid COT for the same pixel population, but with ordinate COT retrieved after increasing MODIS 0.86 μm (B2) reflectance by 3%. The similarity between the two scatterplots implies that much of the VIIRS COT bias with respect to MODIS at lower left is due to a radiometric bias between the two sensors (i.e., VIIRS observes brighter reflectance than MODIS).

The analysis performed by the Cloud Product team focused solely on overcast liquid phase clouds over the ocean (as determined by the MYD06 cloud optical properties phase product), pixels for which the cloud forward model assumptions are thought to be better understood. Furthermore, stricter thresholds are applied to the inter-sensor angle differences, specifically requiring view zenith and scattering angle differences to be less than 1° to mitigate potential impacts of the angular dependence of the cloud BRDF on the radiometric comparison results. The analysis focuses only on those solar reflectance channels used in the CLDPROP cloud optical property retrieval algorithm (see Table 2.3.1); note that concurrent analyses of dark clear sky scenes by the Deep Blue aerosol team include additional shortwave channels [*Sayer et al.*, 2017].

The radiometric analysis relies on comparisons of VIIRS expected and observed spectral cloud-top reflectance. Observed cloud-top reflectance is obtained by correcting TOA reflectance for above-cloud atmospheric absorption in a manner consistent with the approach of the MYD06 and CLDPROP cloud optical property retrieval algorithms, using cloud altitude determined by the co-located MYD06 cloud top pressure. The expected VIIRS cloud-top reflectance is calculated via forward radiative transfer modeling based on the co-located MYD06 COT and CER retrievals. In practice, the CLDPROP-VIIRS COT-CER retrieval look-up tables are searched to find the spectral reflectance that matches the co-located MYD06 COT-CER solution, essentially reversing the cloud optical property retrieval process. A linear fit is applied to the expected vs observed VIIRS cloud-top reflectances for each spectral channel for each month of the match file dataset, the slope of which represents the radiometric adjustment factor that must be applied to each VIIRS spectral channel such that it better matches Aqua-MODIS. Time series of these adjustment factors are used to determine radiometric stability and trends.

Figure 2.3.2 (left panel) shows an example monthly joint histogram of expected vs observed VIIRS cloud-top reflectance in the 0.87 µm channel (MODIS B2, VIIRS M7) for February 2014. The slope, or radiometric adjustment factor, derived from the linear fit (dotted magenta line) is shown inset; the one-to-one line is plotted in black. For this month, an adjustment factor value of 0.96 indicates that VIIRS reflectance is estimated to be roughly 4% brighter than MODIS. The time series of monthly VIIRS radiometric adjustment factors for this spectral channel from the beginning of the SNPP mission through April 2018 is shown in the right panel of Fig. 2.3.2. The blue dashed line denotes radiometric adjustment factors derived using the Aqua-MODIS C6.1 L1B and MYD06 COT-CER retrievals as the baseline; the magenta line denotes adjustment factors derived using the C6 L1B and MYD06 retrievals. Mean values for each time series over the entire SNPP mission are shown within parentheses. The differences between the C6.1- and C6-derived adjustment factors highlight the obvious fact that changes to the radiometry of either MODIS or VIIRS can impact the relative radiometric consistency between the two. Furthermore, there appears to be a small trend in the time series since 2017, at least for the 0.87 µm channel shown here. It is therefore critical to continue to monitor the stability of both instruments, particularly as MODIS continues to age.

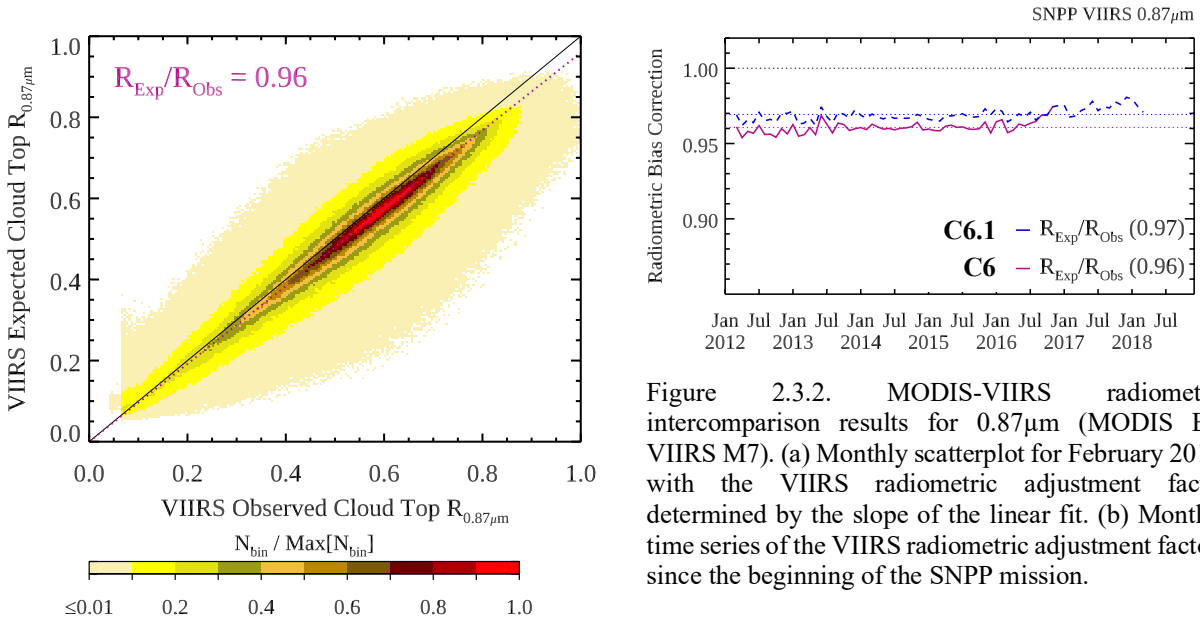

Figure 2.3.2. MODIS-VIIRS radiometric intercomparison results for 0.87µm (MODIS B2, VIIRS M7). (a) Monthly scatterplot for February 2014, with the VIIRS radiometric adjustment factor determined by the slope of the linear fit. (b) Monthly time series of the VIIRS radiometric adjustment factors since the beginning of the SNPP mission.

Table 2.3.1 shows the SNPP-VIIRS radiometric adjustment factors for the five spectral channels used in the CLDPROP cloud optical property retrieval algorithm. These factors represent the February 2012 through March 2018 monthly time series means for each channel, derived as shown in Fig. 2.3.2. While adjustment factors derived using both the C6 and C6.1 Aqua-MODIS L1B and MYD06 products are included here, only those based on the more recent C6.1 are applied to the VIIRS L1B prior to CLDMSK (cloud mask) and CLDPROP (cloud top and optical/microphysical property) product processing. Note that these adjustment factors are applied to the intermediate L1B that includes the "restored" bow-tie pixels (see Section 2.2) that are discarded after use and are not archived, though they are reported in the CLDPROP L2 file global metadata. Note also that, for the spectral channels considered in both analyses, these adjustment factors are generally consistent with those found by the Deep Blue Aerosol team for dark scenes [*Sayer et al.*, 2017].

Table 2.3.1. SNPP-VIIRS radiometric adjustment factors derived from comparisons with Aqua-MODIS. VIIRS observes brighter reflectance than MODIS in these spectral channels.

VIIRS Channel		M5 (0.67µm)	M7 (0.87µm)	M8 (1.24µm)	M10 (1.61µm)	M11 (2.25µm)
Radiometric Bias Correction (Expected VIIRS TOC/Observed)	vs C6	0.94	0.96	0.98	0.98	0.97
	vs C6.1	0.95	0.97	0.99	0.98	0.97

Figure 2.3.3 shows the impact of the radiometric adjustment factors in Table 2.3.1 on the CLDPROP-VIIRS liquid COT retrievals in Fig. 2.3.1 (y-axis, bottom left panel). After applying the radiometric adjustment factors to the VIIRS spectral reflectance, the agreement between Version 1.1 CLDPROP-VIIRS and CLDPROP-MODIS liquid COT retrievals for this relatively homogeneous cloud scene is significantly improved, with the distribution centered around the 1-to-1 line. As will be shown in Section 4.2, however, disagreement between MODIS and VIIRS aggregated COT statistics continues to persist due to the effects of pixel size differences in heterogeneous broken cloud scenes.

2.4. Ongoing Efforts

The consistency of the cloud optical and microphysical property retrievals from Aqua-MODIS and SNPP-VIIRS is quite dependent on their relative radiometry, as shown in Fig. 2.3.1 for the case of liquid phase COT retrievals. Furthermore, as is evident by the apparent latter year trend in the 0.87 µm radiometric adjustment factor time series plot in Fig. 2.3.2, the stability of the relative radiometry between MODIS and VIIRS can be impacted by temporal radiometric drifts in one or both instruments. An ongoing challenge for the CLDPROP products, and the Atmosphere Team products in general, is that climate data record continuity across Aqua-MODIS and SNPP-VIIRS requires continuous monitoring of the relative radiometry of two different instruments and accounting for temporal radiometric changes.

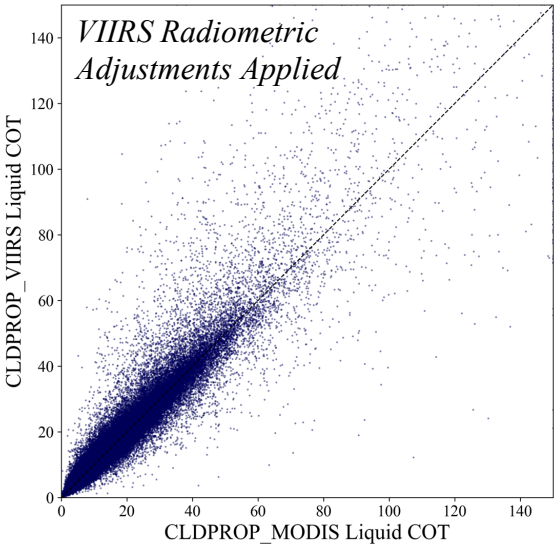

Figure 2.3.3. Scatterplot of Version 1.1 CLDPROP-VIIRS and CLDPROP-MODIS liquid COT retrievals for the pixel population in Fig. 2.3.1. Here, the radiometric adjustments shown in Table 2.3.1 have been applied to VIIRS, resulting in improved agreement over the early CLDPROP implementation shown in Fig. 2.3.1.

3. Cloud Top Properties

3.1. Algorithm Overview

The CLDPROP cloud top properties, which include pixel-level cloud top temperature, pressure, and height along with the corresponding thermodynamic phase used for the cloud top solution (note that this phase is different from the cloud optical properties phase, see Section 4.1.2), are provided by NOAA operational algorithms developed for AVHRR, VIIRS, and GOES-16/17. These cloud top properties are derived in a two-step process, with thermodynamic phase identification occurring first and determining the cloud top property solution path. The cloud top phase algorithm is taken from the Clouds from AVHRR Extended (CLAVR-x) NOAA processing system while the cloud top property algorithm is based on NOAA's Enterprise Algorithm Working Group (AWG) Cloud Height Algorithm (ACHA) (see the ACHA ATBD [*Heidinger and Li*, 2018], Link 2). Table 3.1 lists the MODIS and VIIRS spectral channels used in the cloud top properties algorithm and their application.

Table 3.1. Spectral channels used in the CLDPROP cloud top properties algorithm.

MODIS	VIIRS	Retrieval Parameter(s)
1.64μm (B6)	1.61μm (M6)	Phase
3.75μm (B20)	3.7μm (M12)	Phase
8.5μm (B29)	8.5μm (M14)	Phase, Cloud Height
11.03μm (B31)	10.8μm (M15)	Phase, Cloud Height
12μm (B32)	12μm (M16)	Phase, Cloud Height

3.1.1. Cloud Top Properties Thermodynamic Phase Determination

Unlike the heritage EOS MYD06 cloud top property IR thermodynamic phase algorithm, the CLAVR-x phase algorithm used in the CLDPROP cloud top properties employs multiple spectral channels from both the IR and solar spectra, as shown in Table 3.1 for MODIS and VIIRS. The phase retrieval starts with the identification of local radiative center (LRC) pixels and follows with non-LRC pixels. The LRC approach allows the algorithm to consider spectral information within the same cloud while avoiding signals from weaker radiative pixels, such as at cloud edge. A detailed description of the LRC approach can be found in the GOES-R ABI Cloud Type/Phase ATBD [Pavolonis, 2010, Link 8] and Cloud Mask ATBD [*Heidinger and Straka*, 2013, Link 9].

The cloud top properties phase algorithm first determines a general liquid or ice phase by computing the ice probability for both LRC and non-LRC pixels (Appendix E, Figure E1), after which various tests are performed to determine cloud type (Appendix E, Figure E2). While LRC pixels retain their original phase designation, the phase of non-LRC pixels may be adjusted if their cloud type differs from that of their corresponding LRC pixels. When LRC phase is liquid but non-LRC is ice, the non-LRC pixels are forced to liquid phase. When LRC phase is ice but non-LRC is liquid, the non-LRC are forced to ice if the LRC type is non-overshooting ice cloud and the non-

LRC pixel is liquid water, fog, or supercooled liquid water types. Note that only the final phase designation (liquid, ice, mixed) is reported in the CLDPROP files.

3.1.2. Cloud Top Temperature/Pressure/Height Algorithm

The NOAA Enterprise AWG Cloud Height Algorithm (ACHA) that provides the CLDPROP retrievals of cloud top temperature, pressure, and height uses an analytical, numerically efficient IR radiative transfer model imbedded within an optimal estimation (OE) solution approach. ACHA directly retrieves pixel-level cloud top temperature, while cloud top pressure and height are derived using co-located atmospheric profiles from ancillary Numerical Weather Prediction (NWP) reanalysis data. Because full details on ACHA can be found in the ACHA ATBD [*Heidinger and Li*, 2018, link], only modifications specific to its implementation within CLDPROP are discussed here.

ACHA supports multiple IR channel combinations, referred to as modes, and the physics, mathematics, and retrieval methodology are consistent across each. Since VIIRS does not have absorbing IR channels, the retrieval is limited only to the 8.5, 11, and 12 μm channels (mode 5). Because the OE solution logic is physically based, ACHA also requires assumptions on the cloud radiative model. For internal consistency, all cloud radiative model assumptions are consistent with those of the CLDPROP cloud optical property retrievals; for ice clouds, the severely roughened column aggregate model of *Yang et al.* [2013] is used following MOD06 C6/6.1 convention. Furthermore, while ACHA supports the retrieval of multilayer scenes consisting of two cloud layers, i.e., ice overlying liquid water clouds as identified by the cloud top properties phase/type algorithm (see Appendix E, Figure E2), for CLDPROP these pixels are retrieved as single-layer ice phase clouds, thus the cloud top retrievals correspond to the uppermost cloud layer.

3.2. Continuity Assessment

Figure 3.2.1 shows the daily zonal mean ice cloud fraction computed from the CLDPROP MODIS (red line) and VIIRS (blue line) cloud top properties phase product for 1 February 2014, in addition to ice fraction computed from the C6.1 MYD06 cloud optical properties phase (green line). Note that the MYD06 phase product uses additional spectral information not available to the CLDPROP cloud top phase algorithm. All three phase products show generally consistent patterns, though better agreement surprisingly exists between MYD06 and CLDPROP VIIRS. CLDPROP MODIS indicates higher ice cloud fractions, a result likely due to spectral differences between the MODIS and VIIRS sensors. For instance, the split window liquid water test is sensitive to the brightness temperature difference (BTD) between the 8.5 μm and 11 μm channels. Figure 3.2.2 shows the comparison of this BTD between SNPP VIIRS and Aqua MODIS for one day of co-located observations on 8 November 2016. BTD from VIIRS are evidently lower than that from MODIS, and it is expected that better accounting for the spectral differences between the two sensors can result in more consistent cloud phase products.

For the cloud top properties, specifically cloud top height, in addition to comparisons with C6.1 MYD06 cloud top retrievals, initial continuity assessments also include an evaluation using co-located lidar observations from CALIOP. Figure 3.2.3 shows the global gridded daily mean cloud top height (CTH) from C6.1 MYD06 (top panel) and CLDPROP MODIS (middle panel) and VIIRS (bottom panel). From a cursory comparison of these three images, the two CLDPROP

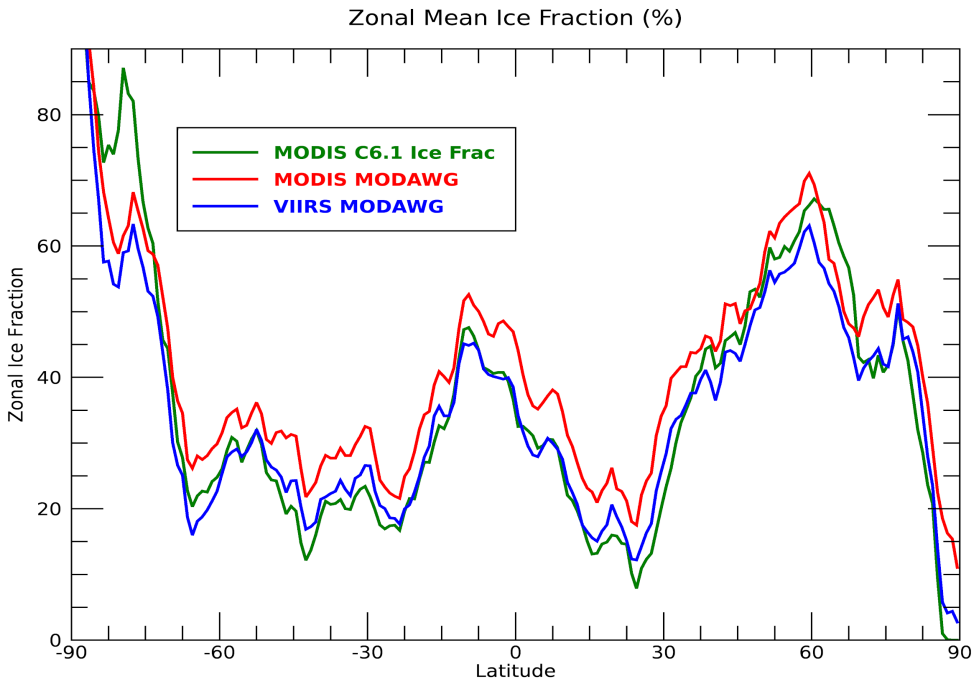

Figure 3.2.1. Zonal mean ice cloud fraction from the CLDPROP MODIS (red line) and VIIRS (blue line) products, as well as the C6.1 MYD06 cloud optical properties phase, for 1 February 2014.

products appear to be quite similar. Moreover, in the tropics, all three datasets are visually similar, except over the tropical Pacific near the international dateline where C6.1 MYD06 tends to be slightly lower. Over midlatitudes, differences between the CLDPROP products and C6.1 MYD06 become larger, particularly over the northern hemisphere land regions; the largest differences are observed over high latitude regions for both hemispheres.

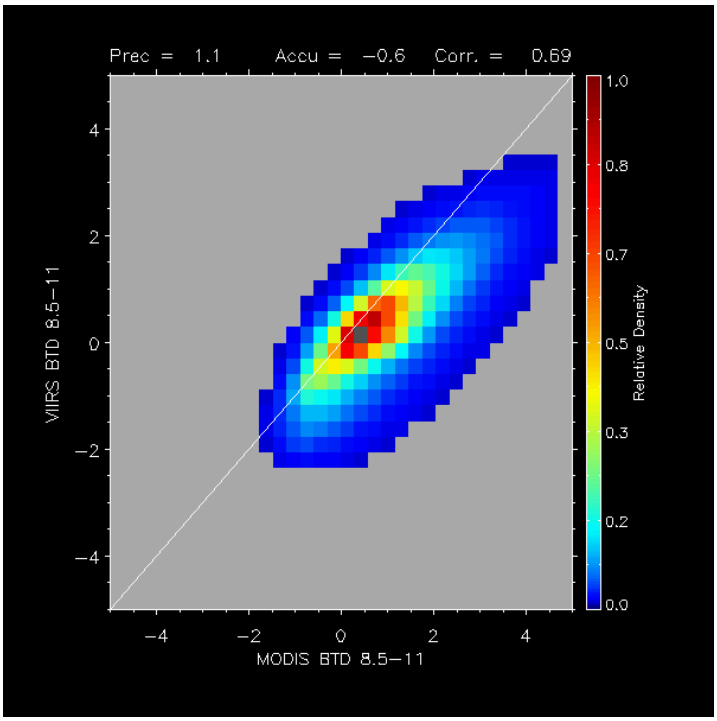

Figure 3.2.2. Comparison of 8.5-11μm BTD between SNPP VIIRS and Aqua MODIS for a full day of co-located data from 8 November 2016.

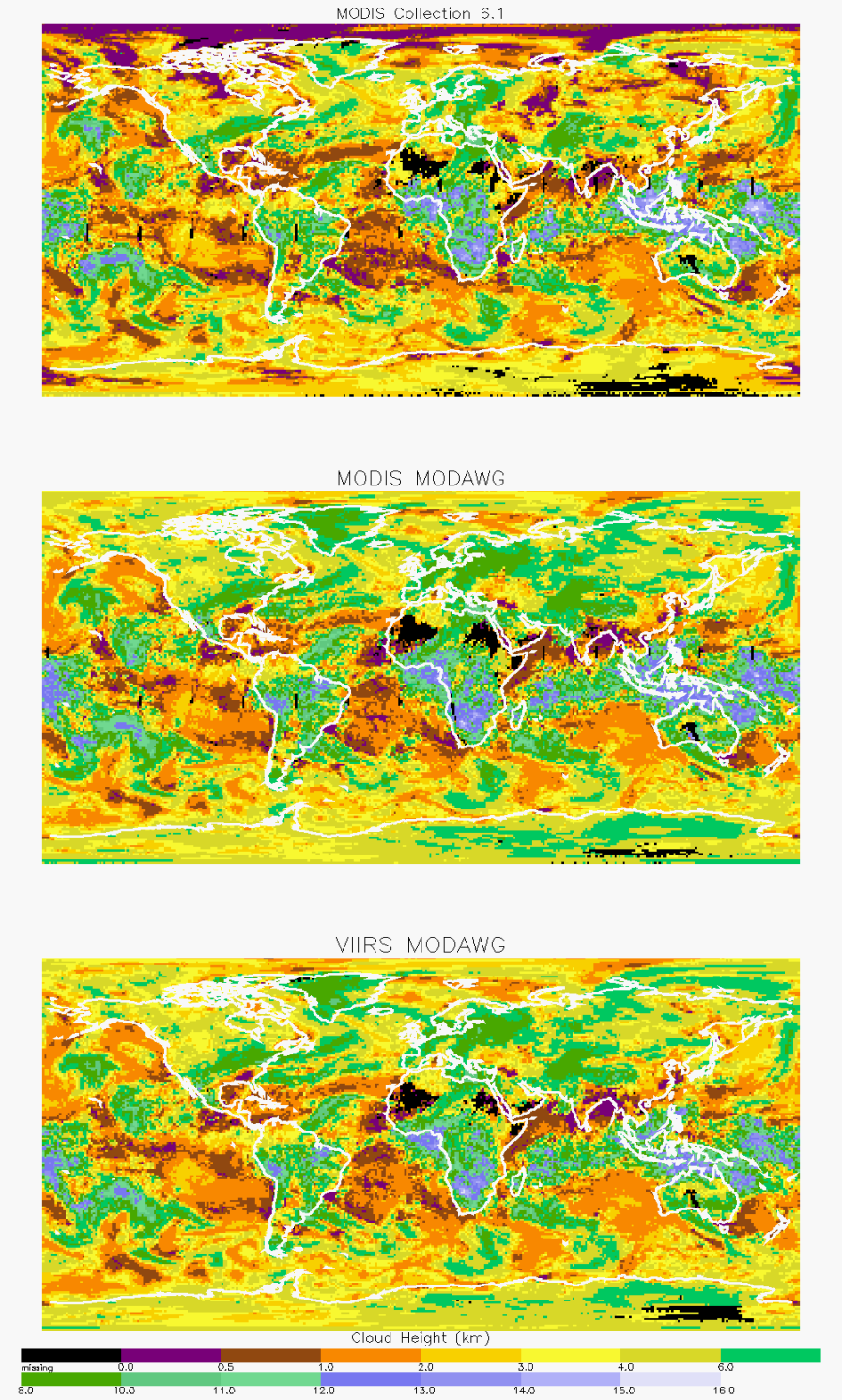

Figure 3.2.3. Global mean cloud top height from C6.1 MYD06 (top) and CLDPROP MODIS (center) and VIIRS (bottom) for 1 February 2014. The units are in km. The spatial resolution is 1° longitude by 1° latitude. Black regions indicate where data are not available.

These differences at higher latitudes are evident in the zonal means shown in Figure 3.2.4. A generally consistent performance is evident over tropical regions. Surprisingly, but consistent with Fig. 3.2.3, the CLDPROP CTH products begin to diverge from MYD06 at higher latitudes (roughly at 45°N and 60°S), where the differences can reach as large as 2 km. There are three main

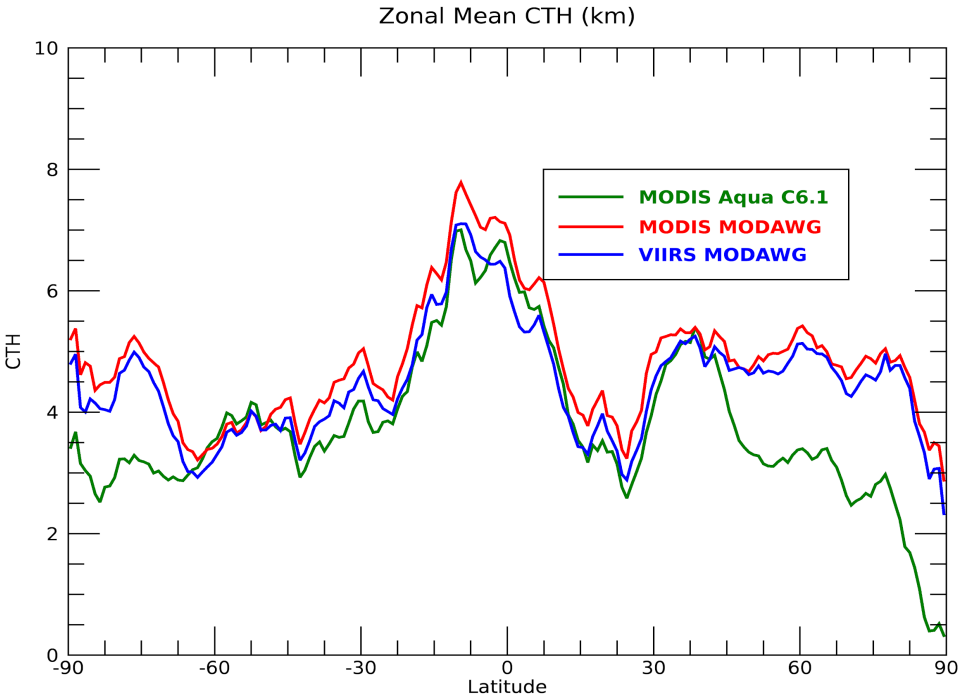

Figure 3.2.4. Daily zonal mean CTH from C6.1 MYD06 (green line) and CLDPROP MODIS (red line) and VIIRS (blue line) for 1 February 2014.

reasons for this divergence from MYD06: 1) C6.1 MYD06 can report a 0 value in its CTH retrieval, which commonly occurs over high latitude regions and can cause lower mean CTH. In contrast, CLDPROP implements a quality check procedure using the larger value of surface elevation and a constant value (75 m) as its lower limit. Removing pixels with value of 0 from the MYD06 product prior to aggregating largely reduces the differences, with the largest differences within 1.5 km (not shown). 2) The CO_2 slicing method employed in MYD06 is known to have issues over mid- and high-level clouds over very cold surfaces. If the CO_2 slicing fails, the IR-window method tends to report low CTH [*R. Frey, personal communication*]. 3) Cloud mask and cloud phase differences also have an impact on the observed CTH differences. The C6.1 MYD35 cloud mask tends to over-identify clouds over snow-covered surfaces and, due to the aforementioned IR-window issue, a low CTH will be reported for these falsely detected cloud scenes. Another noticeable feature is that CLDPROP MODIS tends to retrieve slightly higher clouds than does CLDPROP VIIRS. This is likely related to the higher ice cloud fractions from CLDPROP MODIS as shown in Fig. 3.2.1.

An evaluation of CLDPROP VIIRS CTH against the CALIPSO/CALIOP lidar products is shown in Figure 3.2.5. Here, the VIIRS CTH bias is defined as the VIIRS-CALIOP difference, and is derived from a full day of co-located pixel-level retrievals. Phase matching between VIIRS (cloud top phase) and CALIOP is applied due to the dependence of ACHA on known phase. CTH from CALIOP is adjusted using in-cloud extinction to better compare with IR retrievals from satellite imagers that are sensitive to the radiating height rather than the physical cloud top [*Heidinger et al.*, submitted]. This has a general impact of slightly lowering CALIOP CTH for thin high clouds but not for thick clouds. The comparison indicates a reasonable performance of the CLDPROP CTH products, with biases centered around 0 and near-normal distributions for both liquid water

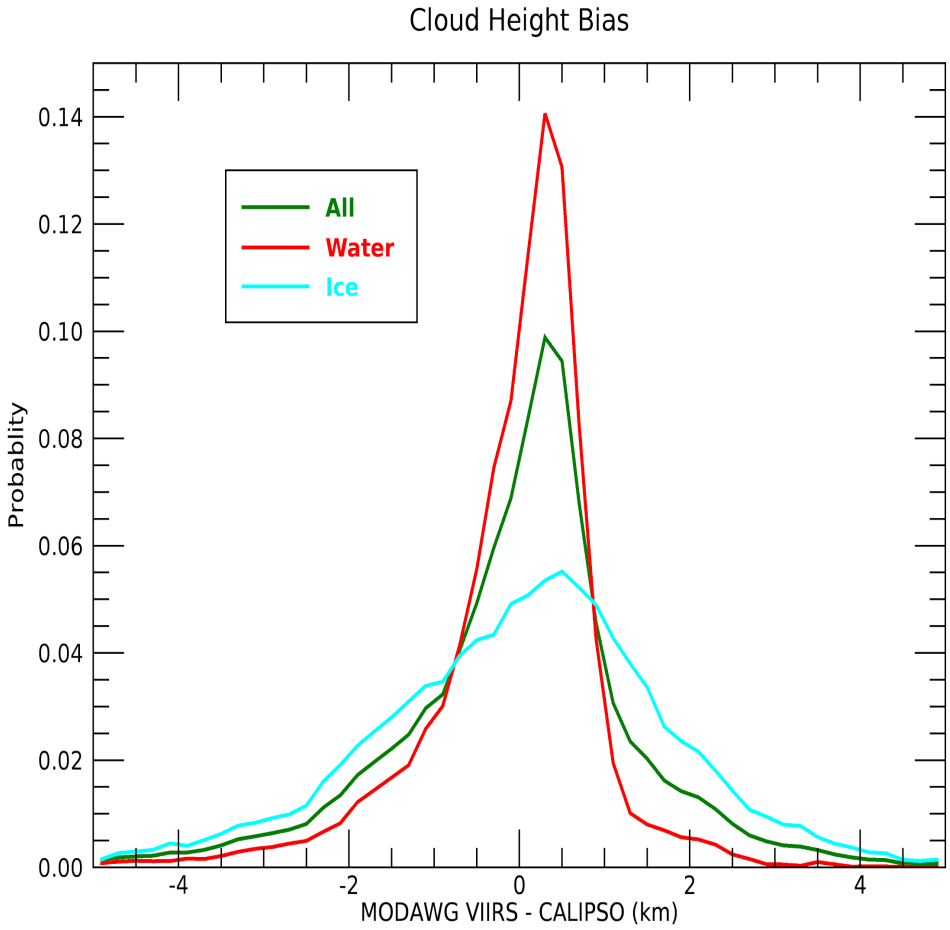

Figure 3.2.5. Histogram showing the CLDPROP VIIRS CTH bias with respect to CALIPSO/CALIOP. Cloud phase matching between VIIRS and CALIOP is applied.

and ice phase clouds. As expected, performance of ice clouds is not as well as liqud water clouds due to more complex structures. Table 3.2.1 lists the bias statistics for the comparisons in Fig. 3.2.5.

Table 3.2.1. Bias and standard deviation of CLDPROP VIIRS CTH compared to CALIPSO/CALIOP. Both phase matched and non-phase matched results are shown.

VIIRS-CALIOP Statistics	Non-Phase Matched			Phase Matched		
	All Clouds	Ice	Liquid	All Clouds	Ice	Liquid
Bias (km)	-1.27	0.22	-2.42	0.05	-0.08	0.18
Std Dev (km)	3.72	1.57	4.42	1.41	1.11	1.67

Figure 3.2.6 shows the zonal mean CTH from CLDPROP VIIRS and CALIOP computed using one day of co-located observations (1 February 2014). Similar to Fig. 3.2.5 and Table 3.2.1, the

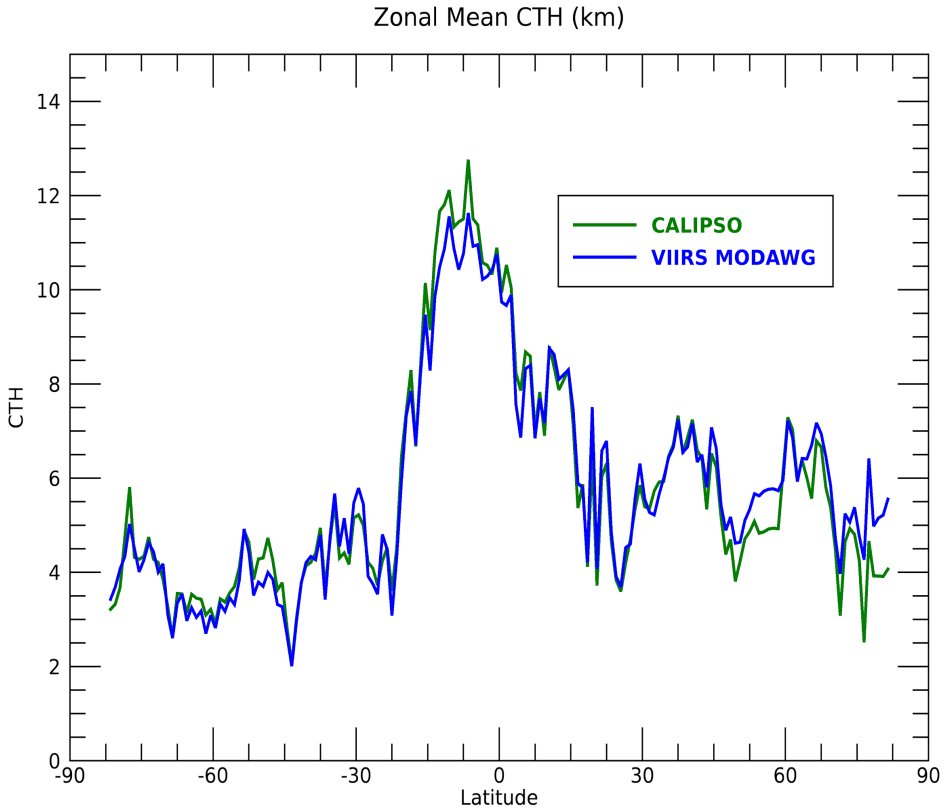

Figure 3.2.6. Zonal mean CTH derived from co-located CALIOP and CLDPROP VIIRS pixel-level retrievals for 1 February 2014.

CALIOP CTH has been adjusted using in-cloud extinction. As shown in this figure, the CLDPROP VIIRS CTH retrievals compare very well with those from CALIOP, even over polar regions.

3.3. Ongoing Efforts

The lack of CO_2 absorption channels around the 13.3 μm spectral region on the VIIRS instrument limits the information content for cirrus cloud top retrievals, thus the retrieval heavily relies on *a priori* information (from a CALIOP-derived climatology) and retrieval uncertainty is higher, particularly for optically thin cirrus. However, CO_2 absorption channels are available on the hyperspectral CrIS sounder also onboard the SNPP platform. As discussed in Section 3.4.2.10 in the ACHA ATBD [Link 2], there is an option to use cirrus cloud heights retrieved from the sounder (e.g., using a CO_2 slicing technique) as an additional constraint in ACHA's optimal estimation approach [*Heidinger et al.*, submitted] for VIIRS pixels identified as cirrus cloud type by the upstream cloud phase algorithm (Section 3.1.1). This is a novel approach in that it uses the CrIS-derived cirrus CTH as a solution constraint rather than incorporating the coarser spatial resolution CrIS radiances directly into the optimal estimation measurement vector. Figure 3.2.7 demonstrates ice cloud top height biases for VIIRS IR window channels alone (dashed lines) and the VIIRS/CrIS combined retrievals (solid lines) compared to CALIPSO/CALIOP. The largest improvements are observed for the thinnest ice clouds (emissivity range 0-0.4, panel a), as expected. For CLDPROP

continuity, a similar approach can be applied to Aqua MODIS using co-located AIRS sounder cirrus cloud top height retrievals.

Additional ongoing efforts include work towards more consistent MODIS and VIIRS cloud top retrievals using different combinations of spectral channels. One way is to explore new ice microphysical models by studying real data from satellite observations in addition to theoretically derived scattering database. Other options under consideration include making ACHA less

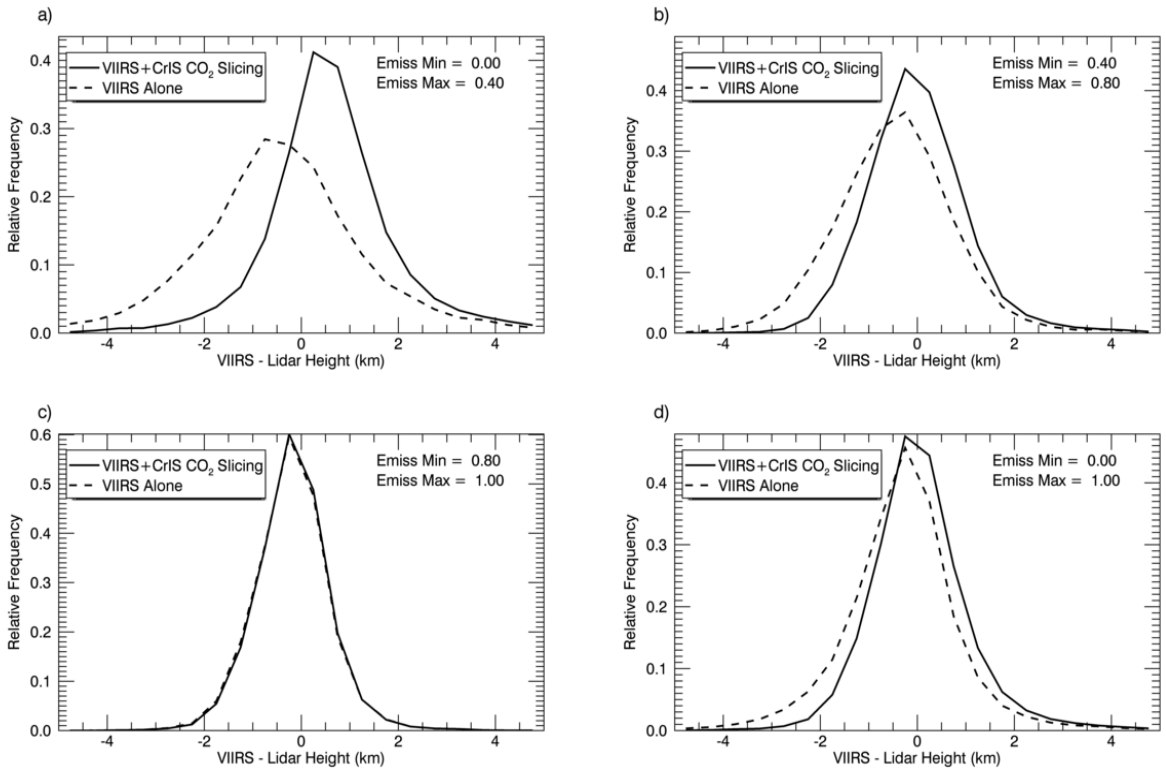

Figure 3.3.1. Bias distribution of VIIRS CTH compared to CALIOP. Two VIIRS retrievals are shown: one using VIIRS IR window channels alone (dashed lines), and one using additional spectral information from CrIS from the 13.3 μm CO_2 absorption region (solid lines). The data are from 15 days in January and August in 2015. Data are grouped based on cloud emissivity ranges for a) 0-0.4 (optically thin clouds); b) 0.4-0.8; c) 0.8-1.0 (optically thick clouds); and d) 0-1.0 (all clouds).

dependent on the upstream cloud type/phase algorithm to reduce the impact due to misclassified cloud phase.

4. Cloud Optical Properties

4.1. Algorithm Overview

The CLDPROP cloud optical and microphysical property product provides pixel-level retrievals of COT and CER and derived CWP, as well as pixel-level estimates of their respective uncertainties accounting for known and quantifiable error sources (e.g., radiometry, atmospheric correction, surface spectral reflectance, cloud forward model), for liquid and ice phase clouds. The theoretical basis of the CLDPROP optical/microphysical property retrieval algorithm has direct heritage with the EOS MODIS MOD06 cloud products, and shares its core scientific code base with the most recent Collections 6 and 6.1. Key C6/C6.1 algorithm updates with respect to previous MOD06 collections can be found in *Platnick et al.* [2017], with additional algorithm details, theoretical basis primer, and Frequently Asked Questions in the C6/C6.1 cloud optical property User's Guide [Link 3].

The simultaneous retrieval of COT and CER is based on the bi-spectral solar reflectance method introduced in *Nakajima and King* [1990]. Reflectance in a non-absorbing visible (VIS), near-infrared (NIR), or shortwave infrared (SWIR) spectral channel (collectively referred to as VNSWIR) provides the primary information on COT (channel selection dependent on surface type), while reflectance in an absorbing SWIR or mid-wave infrared (MWIR) spectral channel provides the primary information on CER. Table 4.1.1 lists the analogous MODIS and VIIRS spectral channels used for CLDPROP COT and CER retrievals, as well as their primary application.

Table 4.1.1. Band numbers and spectral locations of the centers of analogous MODIS and VIIRS channels used in CLDPROP for COT and CER retrievals.

MODIS	VIIRS	Primary Retrieval Parameter
0.66 µm (B1)	0.67 µm (M5)	COT over land
0.86 µm (B2)	0.87 µm (M7)	COT over water
1.24 µm (B5)	1.24 µm (M8)	COT over snow/ice
1.64 µm (B6)	1.61 µm (M10)	CER; supplemental COT over snow/ice coupled with 2.13/2.25µm
2.13 µm (B7)	2.25 µm (M11)	CER
3.75 µm (B20)	3.7 µm (M12)	CER

Because CLDPROP shares its scientific core with the MOD06 cloud optical/microphysical property retrieval algorithm, only key changes with respect to the heritage EOS MODIS algorithm are provided here. These changes include: i) an updated liquid cloud forward radiative model based on a more recent refractive index database for liquid water derived from laboratory measurements at supercooled temperatures; ii) modifications to the cloud thermodynamic phase algorithm used in the optical/microphysical property retrievals; iii) absent datasets that provide information on pixel-level retrieval quality, including removal of sub-pixel cloudiness tests from the Clear Sky Restoral algorithm due to VIIRS's lack of direct sub-pixel information in its M-bands (see Section 2.1), and omission of a multilayer cloud flag due to VIIRS's lack of key water vapor and CO_2 absorption channels in the SWIR and thermal IR. While this document focuses only on the changes

and updates to the MOD06 algorithm that were implemented during the development of the CLDPROP algorithm, relevant sections of the aforementioned MOD06 C6/C6.1 User's Guide [Link 3] will be referenced for further reading as appropriate.

4.1.1. Liquid Phase Cloud Forward Model Assumptions

The CLDPROP continuity algorithm uses a complex index of refraction dataset obtained at a laboratory super-cooled temperature of 265 K [*Kou et al.*, 1993], rather than the heritage 300 K measurements used in MOD06 [see *Platnick et al.*, 2017]. Empirically, the *Kou et al.* dataset was found to provide better consistency between the CER retrievals from the MODIS 2.13 µm and VIIRS 2.25 µm channels for relatively homogenous overcast marine boundary layer clouds. The impacts of *Kou et al.* on 2.x µm single scattering co-albedo and global CER retrievals are shown in Figures 4.1.1.1 and 4.1.1.2. For optically thick liquid clouds, the co-albedo change is expected to increase VIIRS 2.25 µm CER retrievals by roughly 1 µm, and decrease MODIS 2.13 µm CER retrievals by roughly 1.5 µm (Fig. 4.1.1.1). Substantial co-albedo impacts are also found in the 1.6 µm spectral region (not shown), though the impacts on VIIRS 1.61 µm vs. MODIS 1.64 µm CER retrieval differences are very small because of sufficiently close spectral response matching for the two sensors.

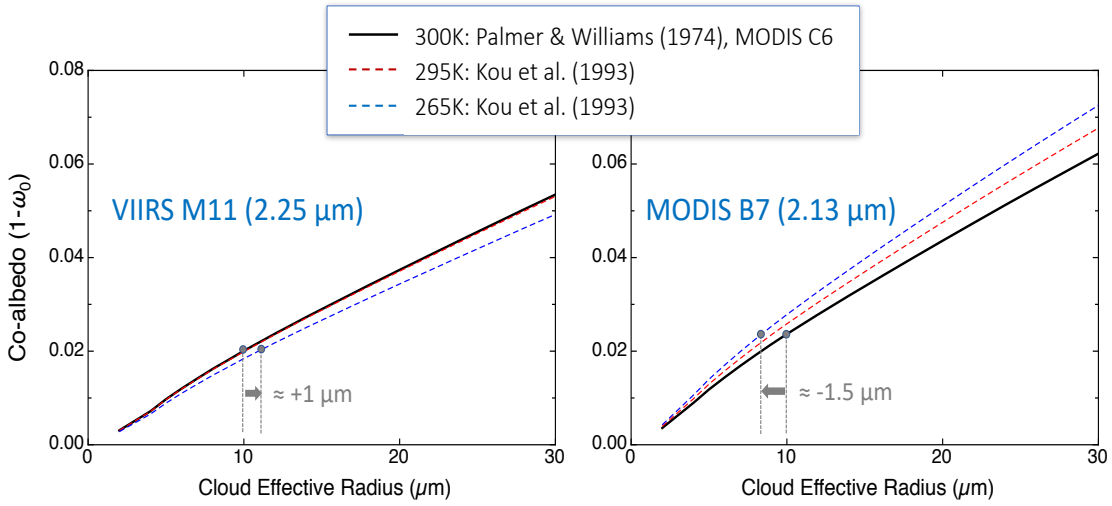

Figure 4.1.1.1. Sensitivity of 2.x µm single scattering co-albedo to the complex index of refraction measured by *Kou et al.* [1993] vs. that reported in *Palmer and Williams* [1974] used in the MOD06 algorithm. The approximate impact on CER retrievals is shown for optically thick (asymptotic) clouds.

For better consistency with the 265 K liquid water index of refraction dataset used in the CER retrievals from the 2.x and 1.6 µm channels, the continuity algorithm uses 265 K index of refraction interpolated from the 258 K and 269 K measurements of *Wagner et al.* [2005] for the 3.7 µm CER retrievals; overall, this results in a slight increase in 3.7 µm CER retrievals for both VIIRS and MODIS for an asymptotically optically thick cloud in that channel.

While the new index of refraction datasets provide better closure between the MODIS and VIIRS spectral CER retrievals, the relatively large impacts on the 2.x µm CER retrievals have not been separated unambiguously from potential inter-sensor relative radiometric differences in those channels (see Section 2.3). Note also that these new index of refraction datasets are being used for

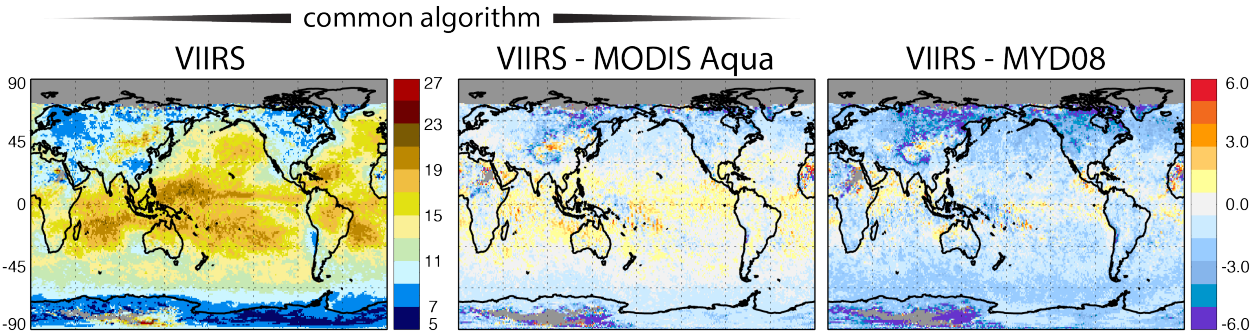

Figure 4.1.1.2. Even after the application of SWIR radiometric adjustments as described in Sect. 2.3, biases between liquid water mean CER_2.25 µm (VIIRS) and CER_2.13 µm (MODIS) remain substantial for Feb. 2014 (right panel). Pixel-level analysis of retrievals for homogeneous marine cloud scenes suggested a fundamental inconsistency in the radiative transfer forward model. Use of the index of refraction of *Kou et al.* [1993] improve the biases (center panel). Results are shown for the so-called "overcast" pixel population (see Sec. 4.1.3).

the CLDPROP continuity optical property algorithm only; incorporation into the MODIS MOD06 production stream is pending further study.

4.1.2. Cloud Optical Properties Thermodynamic Phase Determination

The basis of the CLDPROP cloud optical properties (**COP**) thermodynamic phase algorithm is the algorithm developed for the C6 MOD06 product, the details of which, in addition to monthly evaluations using co-located CALIOP cloud layer products, are provided in *Marchant et al.* [2016] and Section 2.4 and Appendix E of the MOD06 C6/C6.1 User's Guide [Link 3]. For C6/C6.1 MOD06, the COP phase algorithm employs a voting scheme consisting of numerous tests based on the IR thermodynamic phase results [*Baum et al.*, 2012], cloud top temperature retrievals, and dual phase spectral CER retrievals. The implementation of this phase algorithm in CLDPROP is modified, however, due primarily to the use of a new cloud top properties algorithm (see Section 3) and the mismatch between the MODIS B7 and VIIRS M11 SWIR channels in the 2.1 µm spectral region (see Table 4.1.1) that impacts the information content of the spectral CER tests.

The C6 MOD06 COP phase algorithm employs a cold cloud sanity check that overrides an undetermined phase or ambiguous liquid phase result provided that the IR phase indicates an ice cloud and that the cloud is cold (CTT < 240K) with the reported cloud top property solution provided by the CO_2-slicing technique (cloud top solution method being an indicator of high-altitude clouds). VIIRS, however, does not have IR channels in the 13 µm CO_2 absorption region that are required for the CO_2-slicing approach, and the C6 MOD06 cloud top algorithm has been replaced in CLDPROP by the ACHA cloud top retrieval (see Section 3.1.2) that uses only the 8.5, 10.8, and 12 µm IR window channels. Because the cloud top solution method information (CO_2-slicing vs IR-window) is exclusive to the MOD06 coupled CO_2-slicing/IR-window cloud top properties approach, the cold cloud sanity check has been modified for the CLDPROP COP phase algorithm, removing the dependence on the cloud top solution method.

An additional COP phase algorithm modification results from the spectral mismatch of the MODIS 2.13 µm (B7) and VIIRS 2.25 µm (M11) channels. The absorption by liquid cloud droplets and ice crystals differs throughout much of the SWIR spectrum, as ice crystals are generally more absorbing than liquid cloud droplets resulting in SWIR TOA reflectance that is generally darker for ice clouds than for liquid clouds. This information content is utilized in the C6 MOD06 COP

phase algorithm via comparing ice and liquid phase CER retrievals from the 1.64, 2.13, and 3.75 µm spectral channels. In the VIIRS 2.25 µm spectral channel, however, ice is substantially less absorbing than in the MODIS 2.13 µm channel, thus ice and liquid phase 2.25 µm CER retrieval differences provide ambiguous phase information (see Fig. 4.1.2.1). Early testing of the CLDPROP algorithms suggested that removing the 2.25 µm CER test from VIIRS, while simultaneously duplicating the 1.61 µm CER test, yields phase results roughly equivalent to those from MODIS where all three spectral CER retrievals are used (a caveat being MODIS pixels having inoperable 1.64 µm detectors, in which case the 2.13 µm CER test is duplicated). A pragmatic decision was therefore made to implement this approach in the initial CLDPROP COP phase algorithm. Development of a long-term phase algorithm strategy, including evaluation of potential alternate approaches, is ongoing. COP phase fraction statistics are shown in Sect. 4.2.

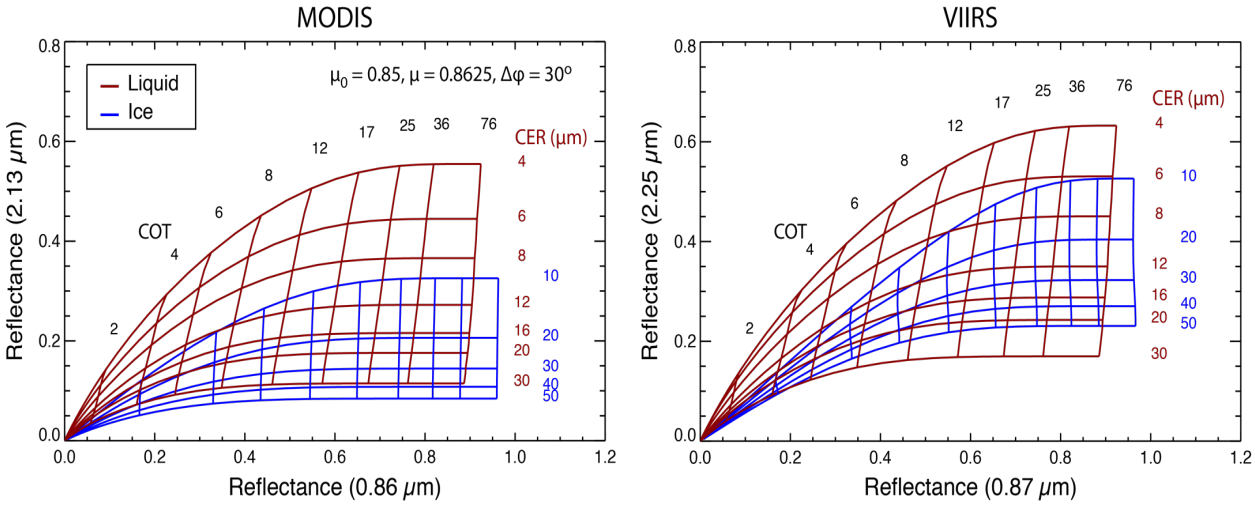

Figure 4.1.2.1. Example COT and CER solution space for liquid and ice phase clouds for the VNIR and 2.x µm channel combination.

4.1.3. MYD06 Datasets Absent from CLDPROP

In the C6/C6.1 MOD06 cloud product, numerous datasets are included that, in addition to the pixel-level uncertainties, can provide information on the quality of the pixel-level COT and CER retrievals and derived CWP. Among these are the results of the Clear Sky Restoral (**CSR**) algorithm [see Section 2.8 of the MOD06 User's Guide, Link 3] that attempts to identify pixels that are likely only partially cloudy, and a flag indicating the likely presence of multilayer clouds [*Wind et al.*, 2010; Section 2.10.1 of the MOD06 User's Guide, Link 3]; note that the CSR algorithm also identifies and "restores to clear sky" those pixels identified as "not clear" by the MOD35 cloud mask for reasons other than the presence of clouds, e.g., thick smoke/dust or bright sunglint. Both the partly cloudy (**PCL**) CSR and multilayer cloud tests provide useful information on retrieval quality as both are designed to identify pixels for which the homogeneous, plane-parallel cloud forward model assumption is expected to break down, thus introducing known but, in practice, unquantifiable retrieval errors. Due to the lack of M-band sub-pixel information (see Section 2.1) and missing water vapor and CO_2 absorbing channels in the SWIR and thermal IR on VIIRS, portions of the CSR PCL tests and the multilayer cloud algorithm in its entirety are omitted from both the MODIS and VIIRS CLDPROP products.

CSR changes for CLDPROP primarily involve the PCL tests, specifically the omission of the sub-pixel cloud mask variability test (CSR = 3) that is applied over water surfaces. Originally introduced in C5 MOD06, the sub-pixel variability test utilizes the 250 m VIS/NIR MOD35 cloud mask tests, and classifies a 1 km pixel as partly cloudy if 50% or fewer of its sixteen 250 m sub-pixels (i.e., ≤ 8) have positive cloud mask results. While such direct sub-pixel information is not available for the VIIRS M-bands, which was the impetus for omitting this test in CLDPROP for both MODIS and VIIRS, the utility of the 375 m I-bands is being explored as a means for reintroducing this test in some form on VIIRS in future CLDPROP versions. Additional CSR changes include a correction to the cloud edge detection test (CSR = 1), such that the test now accounts for pixel position within a scanline and does not yield spurious positive CSR = 1 results in bow-tie overlap regions and other aggregation boundaries. In MOD06, pixels in the first or last row of a scanline, particularly those in the bow-tie overlap regions towards swath edge, are potential unwarranted casualties to the cloud edge detection test due to clear sky pixels in the preceding or succeeding scan that are "adjacent" in the sensor swath pixel row/column ordering but are in fact located far apart geographically. In CLDPROP, the cloud edge CSR test now only considers adjacent pixels located within the same scanline.

Regarding multilayer cloud detection, the bulk of the tests implemented in MOD06 to identify such scenes rely on spectral channels located within the 0.94 μm water vapor absorption band or the 13 μm CO_2 absorption band (via CO_2-slicing results), all of which are missing on VIIRS. Because of this, and in the interest of expediency, the decision was made early in the CLDPROP development process to omit the multilayer cloud detection algorithm in its entirety from the initial product release. Nevertheless, previous investigations have shown that the 1.38 μm water vapor absorption channel included on both MODIS and VIIRS can provide some information on the presence of multilayer clouds. Efforts are underway to assess the information content of this channel for multilayer cloud detection in future versions of CLDPROP.

4.2. Continuity Assessment

An initial assessment of the continuity of the Version 1.1 CLDPROP-MODIS and CLDPROP-VIIRS cloud optical property products is presented here using spatial monthly maps and multiyear monthly time series of Level-3 (L3) statistics. Also shown are comparisons with the MODIS atmosphere team MYD08 product. All CLDPROP aggregations are from the CLDPROP_M3 monthly gridded products (see the CLDPROP_L3 User Guide, Link 10, for more details), and the VIIRS pixel-level retrievals used in the statistics make use of the radiometric adjustment factors shown in Table. 2.3.1.

4.2.1. Monthly Spatial Comparisons

The monthly spatial statistics comparisons focus on February 2014, the "golden month" used during CLDPROP algorithm development. Aggregations are performed on a 1° equal-angle grid, consistent with the MYD08 product. A pixel sampling scheme is employed for both MODIS and VIIRS, to limit computation time and to avoid inoperable detectors on Aqua MODIS; MODIS is sampled every fifth pixel, following the identical scheme employed by MYD08 (see Section 2.2 of the MOD08/MYD08 User Guide, Link 11), and VIIRS is sampled every fourth pixel excluding across-track rows having bow-tie deletions (see Sect. 2.2 above and Section 3.3 of the CLDPROP_L3 User Guide, Link 10). Moreover, VIIRS aggregations are limited to view angles

consistent with the MODIS swath (view zenith < 65.5°) to mitigate sampling biases due to the wider swath of VIIRS. Monthly retrieval means and fractions are calculated from pixel-weighted daily aggregations. Unless otherwise noted, the statistics are shown for daytime observations only.

Monthly COP phase fractions (i.e., the fractions of pixels that are identified by the COP phase algorithm as liquid, ice, or undetermined phase clouds) are shown in Fig. 4.2.1.1. Note that this is the phase fraction irrespective of the success of the optical property retrieval algorithm. In terms of pixel counts, the only difference between this population and that corresponding to CLDMSK cloudy fields-of-view (**FOV**s) is the removal of pixels flagged as CSR = 2 (Sect. 4.1.3). The center column shows CLDPROP-VIIRS minus CLDPROP-MODIS differences; the right column is CLDPROP-VIIRS minus MYD08. There is no broad improvement in the phase agreement for the CLDPROP algorithm for all three phase designations (liquid, ice, undetermined) compared to that between CLDPROP-VIIRS and MYD08, a result of the fact that the CLDPROP COP phase algorithm was directly ported from MYD06 with only minor modification (see Sect. 4.1.2). There remains a slight increase in liquid phase fraction for CLDPROP-MODIS compared with CLDPROP-VIIRS, along with a correspondingly smaller ice phase fraction for CLDPROP-MODIS; MYD08 appears to have smaller ice fractions over mid-latitude oceans, and larger ice and undetermined fractions over high-latitude land surfaces due to cloud fraction differences (see Fig. 4.2.1.4, top row).

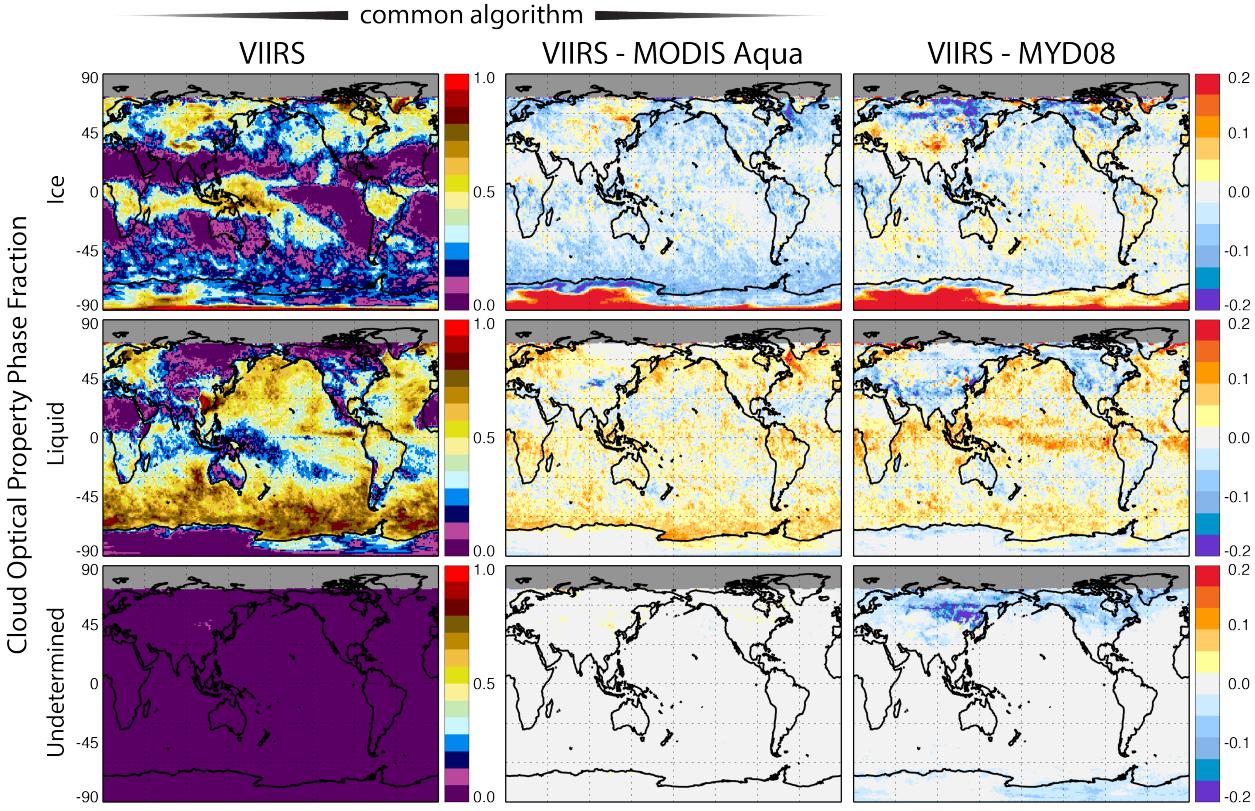

Figure 4.2.1.1. Gridded (1°) cloud optical property (COP) phase fractions for Feb. 2014 as described in the text.

Successful retrieval phase fractions for overcast clouds, i.e., the population of pixels from Fig. 4.2.1.1 that are identified as overcast by the CSR algorithm (CSR = 0, see Section 4.1.3) and result in a successful optical property retrieval, are shown in Figures 4.2.1.2 and 4.2.1.3 for ice and liquid

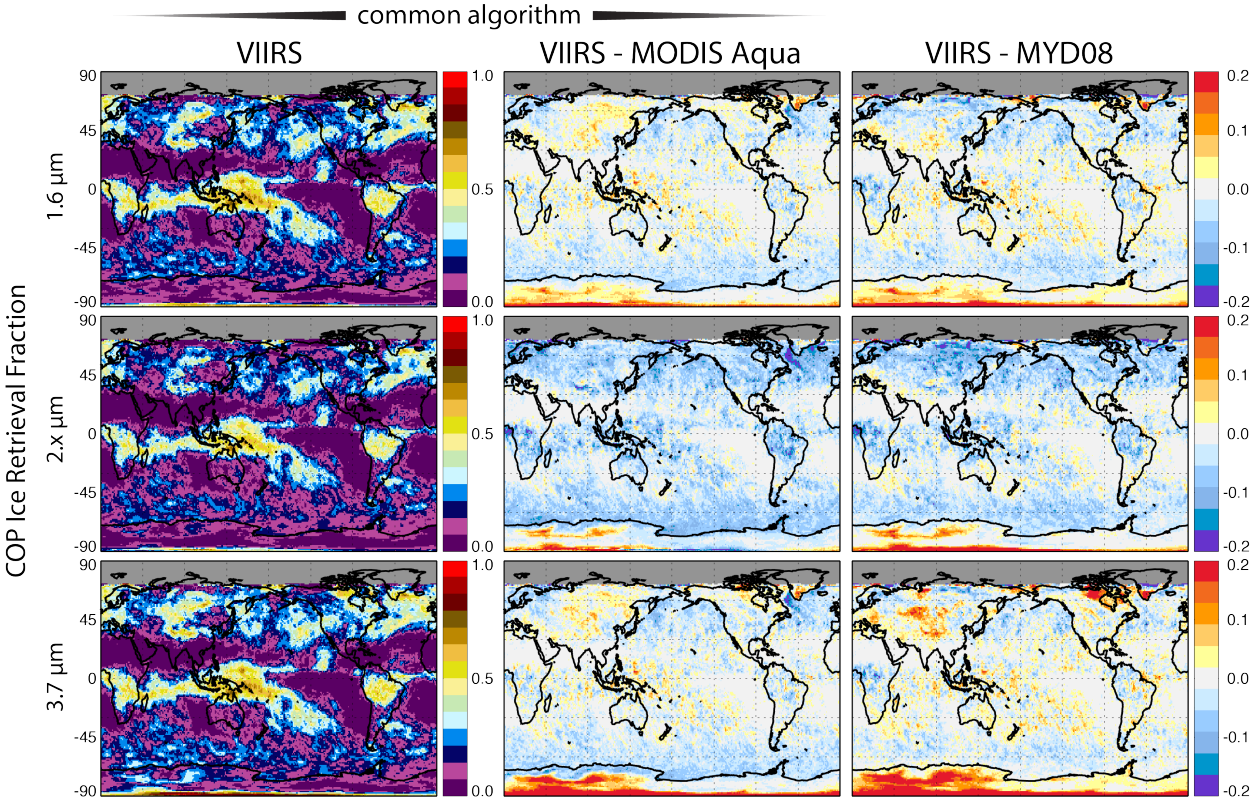

Figure 4.2.1.2. Gridded (1°) cloud optical property (COP) successful ice water phase retrieval fractions for the overcast (CSR = 0) pixel population for Feb. 2014.

phases, respectively. Successful retrievals can filter out incorrect phase determinations or multilayer phase clouds that present radiative signatures inconsistent with the algorithm's single-layer forward model. Since the retrieval success (or failure) rate also depends on the CER spectral channel used in the retrieval [e.g., *Cho et al.*, 2015], results are shown for the three core retrieval channel combinations for each phase. The inter-sensor and inter-algorithm difference images for the ice phase retrieval fractions (Fig. 4.2.1.2) are consistent with the ice phase fraction differences in Fig. 4.2.1.1 (note that the color bar scales are identical for all phase images). For the liquid phase retrieval fractions (Fig. 4.2.1.3), while the CLDPROP differences (center column) are consistent with the liquid phase fraction differences in Fig. 4.2.1.1, the CLDPROP-VIIRS minus MYD08 retrieval fraction differences (right column) are much larger over global oceans, with CLDPROP-VIIRS having significantly higher retrieval fractions. This is largely due to the exclusion of the sub-pixel cloud mask variability CSR test (CSR = 3) in CLDPROP that in MYD06 removes from the overcast pixel population those pixels over ocean that the 250 m cloud mask tests indicate are only partially cloudy (see Sect. 4.1.3). Because liquid phase clouds are generally more spatially heterogeneous than ice phase clouds, the exclusion of this CSR test disproportionately affects the liquid phase population, thus yielding a larger liquid phase overcast pixel population, and, in turn, larger successful retrieval fractions, over oceans in CLDPROP compared with MYD08.

Cloud optical thickness means separated by phase for the overcast pixel population are shown in Figure 4.2.1.4. Note the biases in the CLDPROP continuity algorithm for the liquid phase (middle column, bottom row) over the ocean, where CLDPROP-VIIRS COT is larger than CLDPROP-MODIS. To the extent that VIIRS radiometric adjustments were made using homogeneous liquid

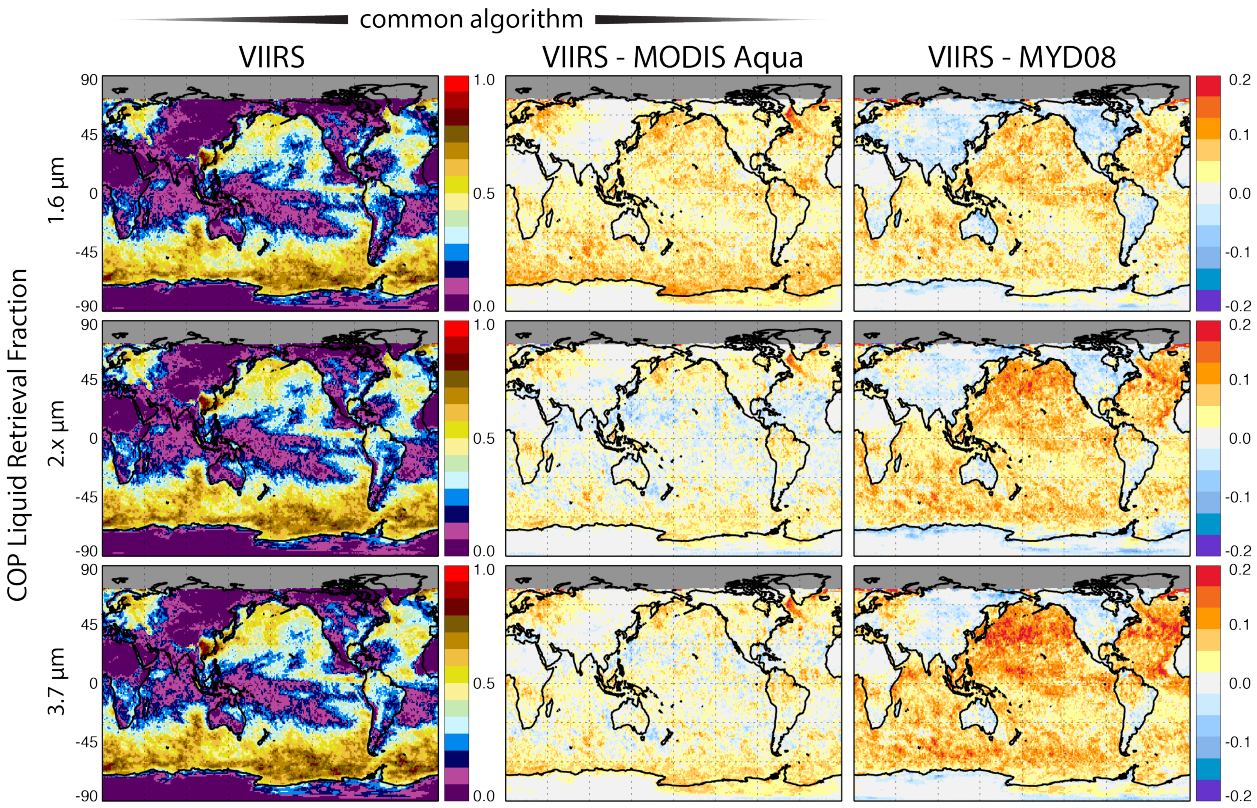

Figure 4.2.1.3. Gridded (1°) cloud optical property (COP) successful liquid water phase retrieval fractions for the overcast (CSR = 0) pixel population for Feb. 2014.

cloud maritime scenes (Section 2.3), consistent COT between the sensors for such scenes should already have been achieved by default. The positive continuity algorithm difference (VIIRS larger than MODIS) might indicate that the bias, at least in part, is due to inherent pixel FOV differences between the sensors that can affect overcast cloud sampling in broken cloudy scenes. The cause of the rather noisy results for ice clouds in Fig. 4.2.1.4 (i.e., positive and negative differences in the middle column, middle row), however, are not obvious.

To illustrate the impact of FOV differences between MODIS and VIIRS, Figures 4.2.1.5 and 4.2.1.6 show case study granules from 6 July, 2014, for an overcast scene and a broken cloudy scene, respectively, where the Aqua and SNPP orbits were in rough alignment and MODIS and VIIRS viewed the same geographic region within only a few minutes of each other. Fig. 4.2.1.5 shows the MODIS and VIIRS true color RGBs and geolocated CLDPROP COT retrievals (overcast pixels only, retrievals from the VNSWIR-2.x µm channel pair) for a stratocumulus cloud deck off the Kamchatka Peninsula observed by both MODIS and VIIRS at 0200 UTC. Histograms of liquid phase COT for the geographic region highlighted by the blue and red boxes in the MODIS and VIIRS COT plots, respectively, are also shown, as is the corresponding COT histogram from MYD06 (gray line); regional mean COT from each product is indicated within the parentheses in the respective plot labels. There is excellent agreement between the CLDPROP products and MYD06 for liquid phase COT for the relatively homogeneous clouds in this region, an indication that the VIIRS radiometric adjustments in Table 2.3.1 yield desirable results.

Fig. 4.2.1.6 shows similar plots for a broken cumulus scene over the central Pacific Ocean observed roughly ten minutes prior to the scene in Fig. 4.2.1.5 (MODIS and VIIRS observation

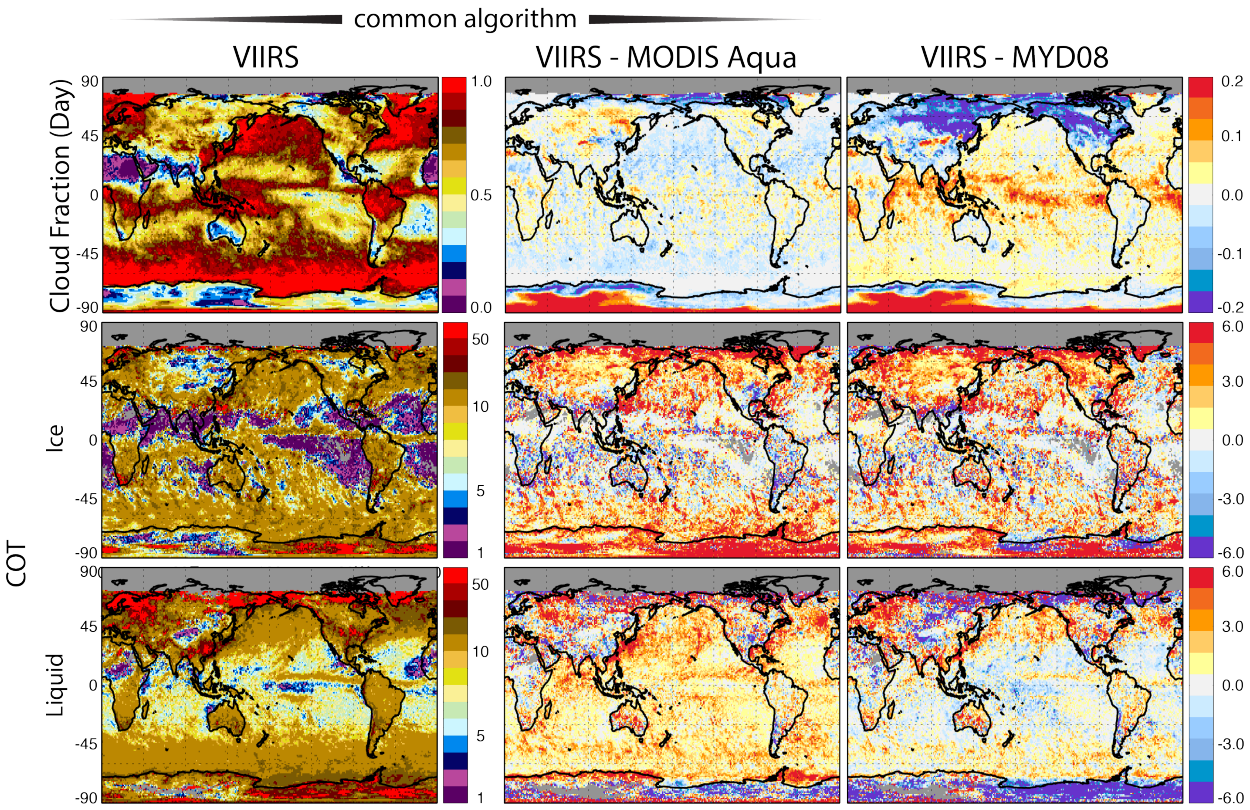

Figure 4.2.1.4. Mean 1° gridded cloud optical thickness for liquid and ice phase for the overcast (CSR = 0) pixel population for Feb. 2014. COT corresponds to the retrieval using the VNIR/2.x μm channel combination. For context, daytime cloud fraction is shown in the top row.

times 0150 and 0148 UTC, respectively). Here, the CLDPROP-MODIS (blue line) and CLDPROP-VIIRS (red line) liquid COT histograms (again, overcast pixels only) sharply disagree at large COT, with VIIRS exhibiting a long tail resulting in a considerably larger mean COT (6.0 versus 4.2 for CLDPROP-MODIS). MYD06 mean COT (gray line) is even larger (7.7) despite the fact that its histogram does not exhibit a long tail like CLDPROP-VIIRS.

The divergent COT histograms in Fig. 4.2.1.6 point toward some combination of sampling and FOV differences. Focusing first only on the divergence of CLDPROP-MODIS and MYD06, where FOV impacts are eliminated and only sampling differences remain, two underlying causes are at play, namely differences in the upstream cloud mask algorithms (CLDMSK generally yields higher cloud fraction over ocean than does MYD35, see Fig. 4.2.1.4) and the exclusion of the MYD06 sub-pixel variability CSR test (CSR = 3) in CLDPROP (again, see Sect. 4.1.3). These two factors collectively yield more overcast cloud pixels in CLDPROP-MODIS (and CLDPROP-VIIRS) compared to MYD06. Successively removing pixels from the CLDPROP-MODIS overcast cloud population that are not included in the same MYD06 population, namely those identified by MYD06 as partly cloudy (CSR = 3, gold line) and cloud edge (CSR = 1, brown line), and finally those identified by MYD35 as clear sky (green line), show that CLDPROP-MODIS COT agrees quite well with MYD06, as should be expected.

The divergence between CLDPROP-MODIS and CLDPROP-VIIRS, on the other hand, is likely primarily due to FOV differences that can have impacts on both sampling and the influence of

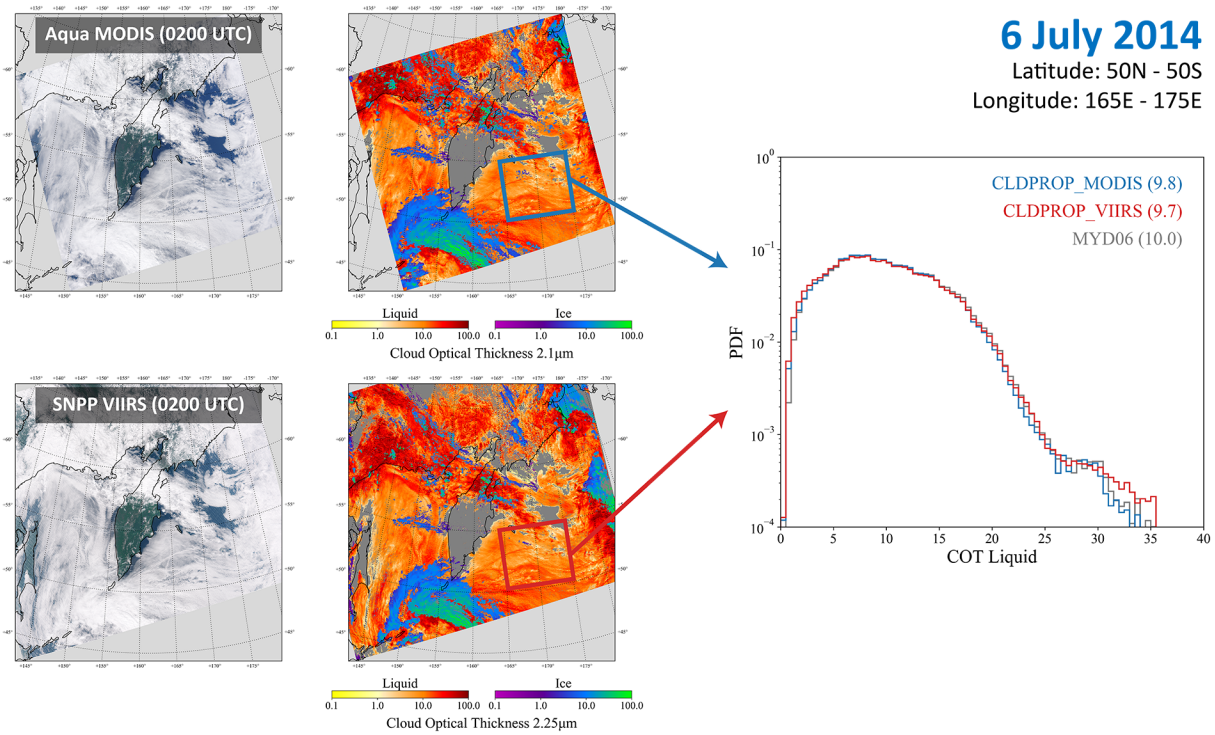

Figure 4.2.1.5. Overcast cloudy scene off the Kamchatka Peninsula observed concurrently by Aqua-MODIS (0200 UTC) and SNPP-VIIRS (0200 UTC) on 6 July 2014. Histograms of overcast (CSR = 0) liquid COT from CLDPROP-MODIS (blue line) and CLDPROP-VIIRS (red line), in addition to MYD06 (gray line), from the region highlighted in the granule imagery are shown at right. Mean COT for each histogram is shown in the parentheses.

cloud heterogeneity. Whereas the CLDPROP-VIIRS minus CLDPROP-MODIS liquid phase retrieval fraction differences for the VNSWIR-2.x μm channel pair are in the aggregate relatively small (Fig. 4.2.1.3, middle row, center panel), the sampling differences in this specific broken cloud scene likely are not negligible. Indeed, the liquid cloud retrieval fraction (i.e., fraction of successful optical property retrievals for overcast pixels) for the region in Fig. 4.2.1.6 is roughly 9% for CLDPROP-VIIRS compared to 12.5% for CLDPROP-MODIS. The implication of this sampling difference is that the higher fraction from the coarser resolution MODIS is more likely to include pixels that are not completely cloudy; note again that the MYD06 sub-pixel cloudiness CSR test is not applied in CLDPROP (MYD06 liquid retrieval fraction for this same region is roughly only 4%). Furthermore, such sub-pixel heterogeneity is expected to yield smaller retrieved COT due to radiative smoothing [e.g., *Kato et al.*, 2006], a consequence that will affect MODIS to a greater extent than VIIRS, since the across-swath pixel growth of VIIRS is limited by its onboard detector aggregation scheme (see Sect. 2.1, Fig. 2.1.2). Nevertheless, while FOV differences can plausibly explain the remaining COT differences between CLDPROP-MODIS and CLDPROP-VIIRS, further investigation is needed to disentangle the consequences of FOV differences on cloudy pixel sampling and sub-pixel heterogeneity in broken cloudy scenes.

Monthly mean cloud effective radius from the three core spectral channel pair combinations for the overcast pixel population (CSR = 0) are shown in Figures 4.2.1.7 and 4.2.1.8 for liquid and ice phase clouds, respectively. As discussed in Section 4.1.1, the CLDPROP-VIIRS minus MYD08 difference images for liquid clouds (Fig. 4.2.1.7, right column) use different complex index of

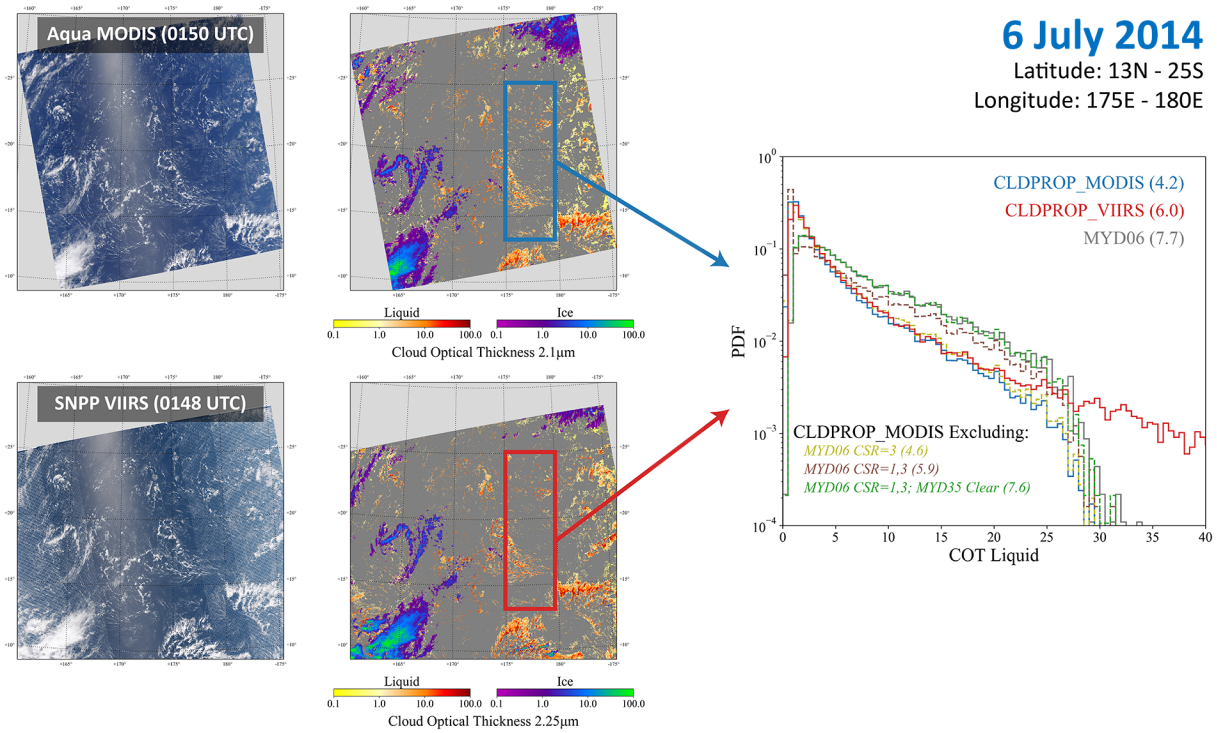

Figure 4.2.1.6. Similar to Fig. 4.2.1.5, except for a broken cloudy scene over the tropical Pacific Ocean observed concurrently by Aqua-MODIS (0150 UTC) and SNPP-VIIRS (0148 UTC) on 6 July 2014. Also shown are the CLDPROP-MODIS COT histograms excluding pixels identified by the MYD06 Clear Sky Restoral as being partly cloudy via sub-pixel heterogeneity tests (CSR = 3, gold line) and the cloud edge test (CSR = 1, brown line), and those identified by MYD35 as clear sky (green line).

refraction assumptions, so CER retrieval mean differences of the magnitude shown here (up to 3 μm or more) are expected, as are the substantially improved MODIS 2.1 μm and VIIRS 2.25 μm CLDPROP CER differences using the same *Kao et al.* 265 K refractive index assumption (center panel). Liquid CER differences from the 3.7 μm channels, on the other hand, flip signs (positive differences for CLDPROP-VIIRS minus MYD08, negative differences for CLDPROP-VIIRS minus CLDPROP-MODIS) and appear to have larger magnitudes when using the 265 K refractive index assumption of *Wagner et al.* [2005] (center column). The reasons for this behavior are at present unclear. Moreover, the CLDPROP ice phase CER (Fig. 4.2.1.8) show large differences (center column), particularly for the 2.x μm channel for which VIIRS retrieves significantly higher CER than does MODIS. It is not clear if this difference, like that of the liquid phase 2.x μm CER retrievals, is related to bulk ice complex index of refraction assumptions that were taken from C6 MOD06. Further investigation into both the 3.7 μm liquid CER differences and the 2.x μm ice CER differences is ongoing.

4.2.2. Monthly Time Series Comparisons

The single-month gridded analysis of Sect. 4.2.1 is extended to a monthly time series for a common Suomi NPP and Aqua record, namely April 2012 through August 2019. These time series are generated only for the latitudes between 60°N and 60°S, and thus exclude the polar regions. As

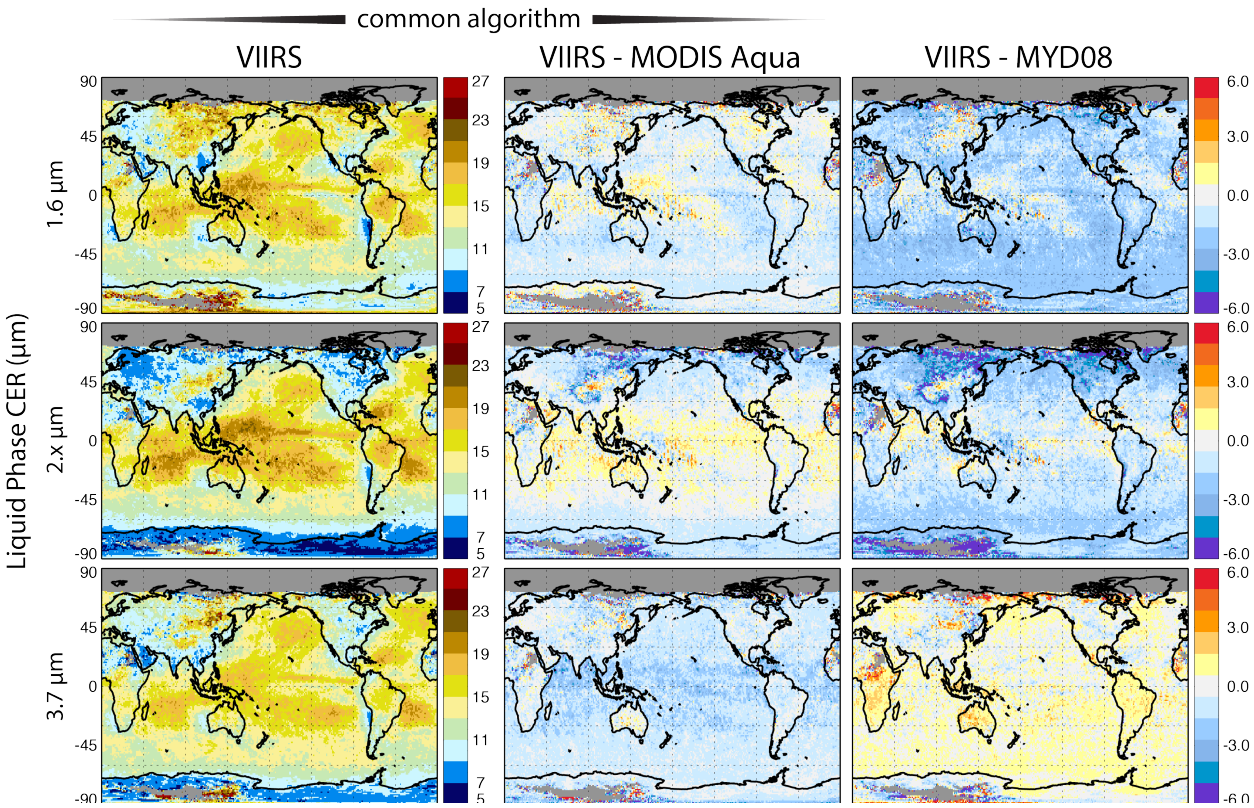

Figure 4.2.1.7. Mean 1° gridded effective radius (CER) for liquid phase clouds for Feb. 2014.

before, the regional means are calculated from pixel-weighted monthly aggregations from the Version 1.1 CLDPROP_M3 products, and all VIIRS aggregations are limited to view angles consistent with the MODIS swath (view zenith < 65.5°).

In the following figures (4.2.2.1-4.2.2.5), CLDPROP-VIIRS and CLDPROP-MODIS (and respective CLDMSK) products correspond to solid red and blue lines, respectively, while the standard MODIS products (MYD06 and MYD35, referred to collectively by the Level-3 MYD08 identifier) correspond to dotted blue lines. Therefore, the continuity paradigm of running both VIIRS and MODIS through a common algorithm to provide a useful cloud climate data record across the two sensors is supported when the solid blue line is relatively closer to the solid red line than the dotted blue line.

The daytime-only and total cloud fraction time series (from CLDMSK), and those of daytime CTP and CTH, are shown in Fig. 4.2.2.1. COP phase fraction (liquid and ice) time series are shown in Fig. 4.2.2.2, and COP successful retrieval fractions (overcast CSR = 0 pixels only) are shown in Fig. 4.2.2.3. Figs. 4.2.2.4 and 4.2.2.5 show the mean COT and CER time series, respectively.

The CLDMSK and CLDPROP common continuity product algorithms typically provide the smallest discrepancy between the VIIRS and MODIS mean properties, illustrated nicely by the daytime cloud fraction and cloud top properties time series in Fig. 4.2.2.1. One notable exception is liquid COT time series (Fig. 4.2.2.4) where the CLDPROP-MODIS mean is substantially smaller than either CLDPROP-VIIRS or MYD08. As noted in the discussion of COT spatial differences (Figs. 4.2.1.4-4.2.1.6), sensitivities with respect to inherent sensor pixel resolution

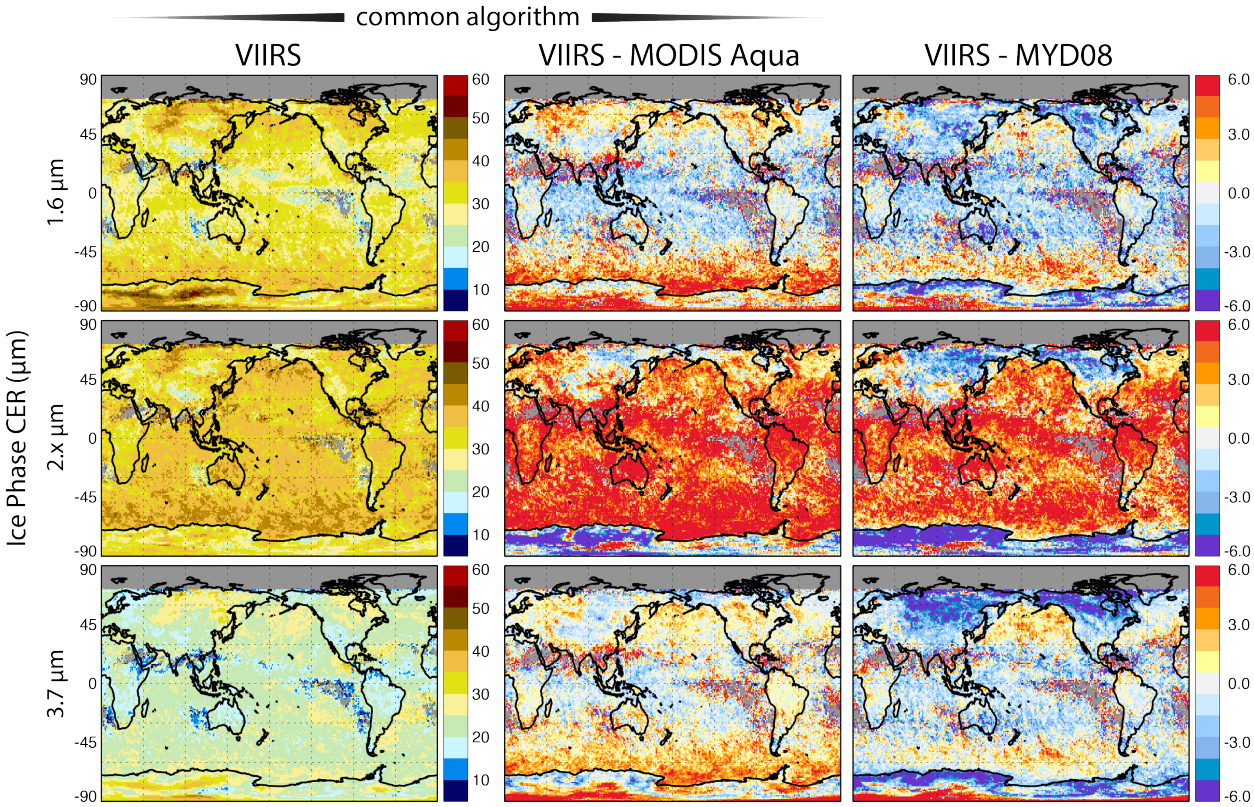

Figure 4.2.1.7. Mean 1° gridded effective radius (CER) for ice phase cloud for Feb. 2014.

need to be explored for broken and otherwise heterogeneous cloud scenes. A second exception is liquid 3.7 µm CER (Fig. 4.2.2.5) which is likely due, at least in part, to the CLDPROP-MODIS and MYD06 algorithms using different liquid water index of refraction datasets (Sect. 4.1.2). In other words, since the solid lines in that plot use a consistent index of refraction dataset, MYD08

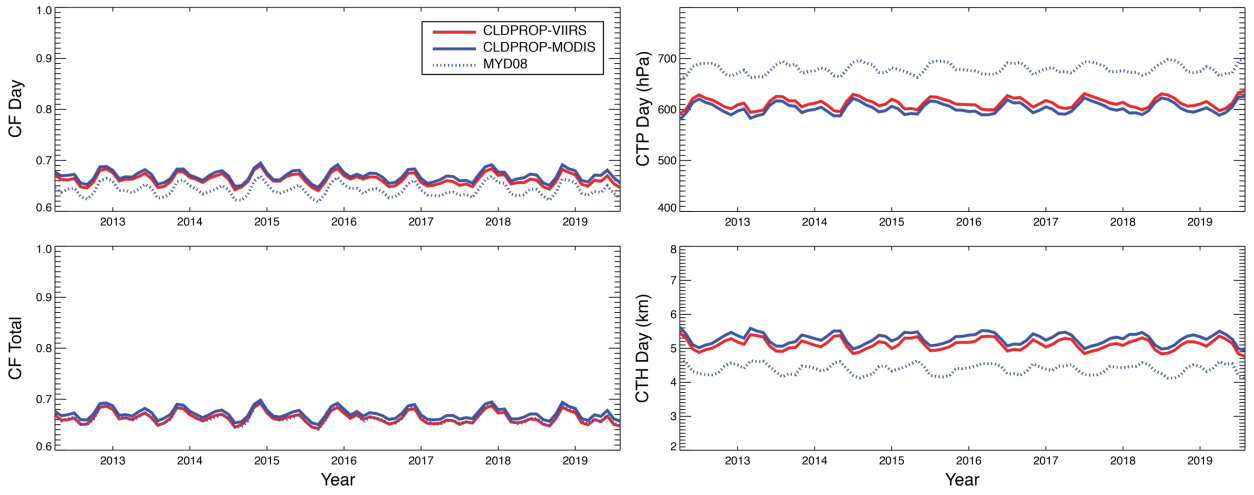

Figure 4.2.2.1. Monthly CLDMSK cloud fraction (CF), CLDPROP mean cloud top pressure and height (VIIRS and Aqua MODIS), and analogous MYD06/35 for the north Pacific (see text for details) for April 2012 through August 2019. The CLDPROP-VIIRS and CLDPROP-MODIS datasets correspond to solid red and blue lines, respectively, while the standard MODIS products (MYD35/06) correspond to dotted blue lines. Top left panel is for daytime observations only; the remaining panels are for combined daytime and nighttime observations.

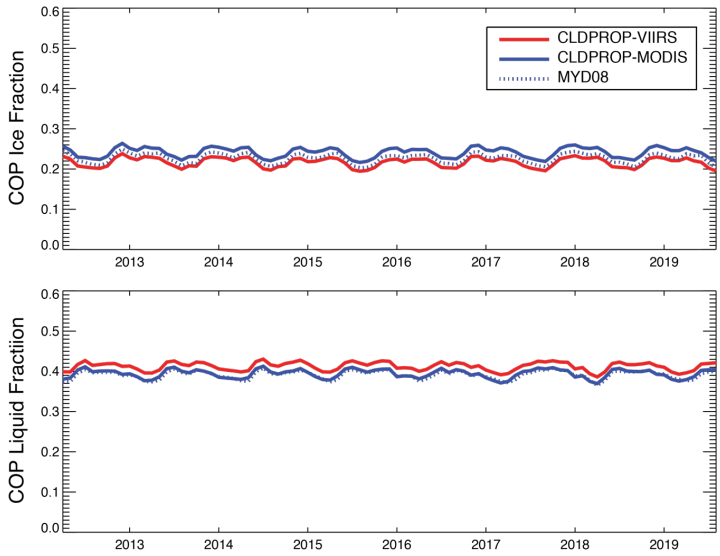

Figure 4.2.2.2. Same as 4.2.2.1 but for monthly cloud optical property phase fraction (PF) from CLDPROP (VIIRS and Aqua MODIS) and MYD06. Top and bottom rows are for ice and liquid phase clouds, respectively.

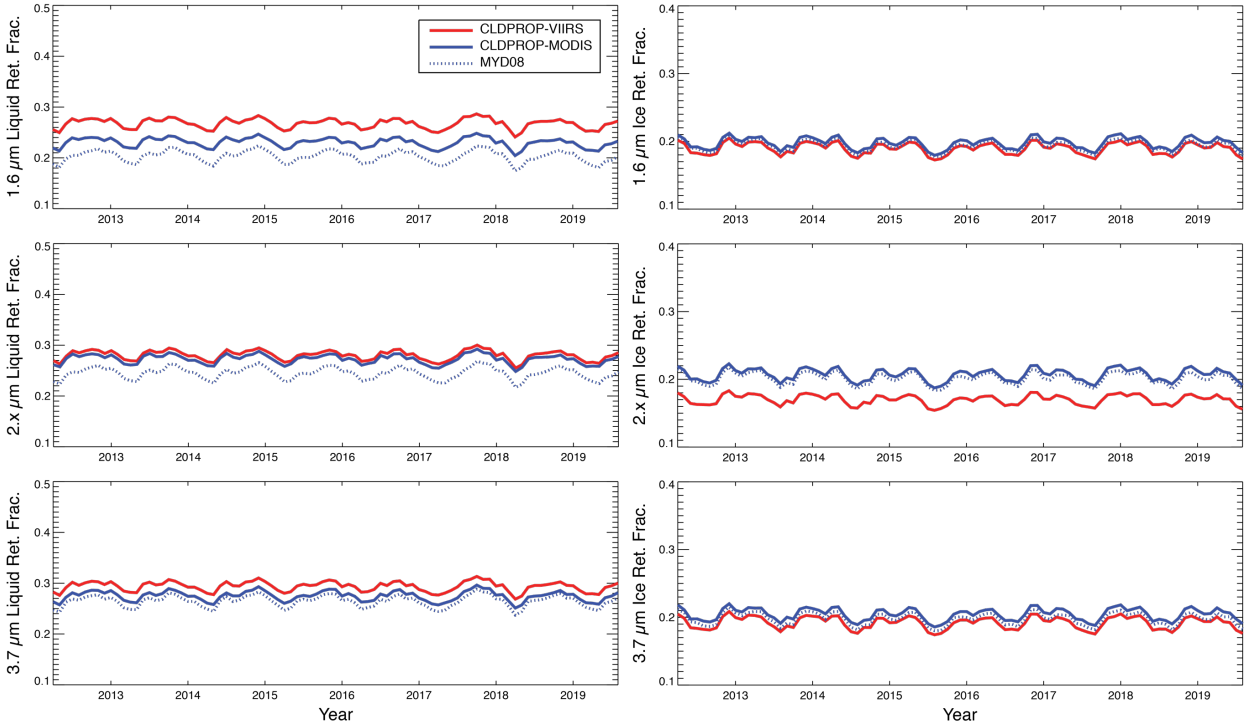

Figure 4.2.2.3. Same as 4.2.2.2 but for monthly cloud optical property successful retrieval fraction from CLDPROP (VIIRS and Aqua MODIS) and MYD06. Left column is for the VNIR-2.x µm retrieval, right column is for the VNIR-3.7 µm retrieval. Top and bottom rows are for ice and liquid phase clouds, respectively.

is showing agreement with VIIRS when it shouldn't – the right answer for the wrong reason. A third exception is the 2.x µm ice CER, where the CLDPROP-VIIRS mean is markedly larger than both CLDPROP-MODIS and MYD06 who are roughly in agreement; note also that the 2.x µm ice phase successful retrieval fraction (Fig. 4.2.2.3) shows similar agreement between CLDPROP-MODIS and MYD06 whereas CLDPROP-VIIRS is markedly smaller. Following the discussion

of the spatial means in Fig. 4.2.1.7, it is unclear whether these differences are related to the bulk ice complex index of refraction assumptions.

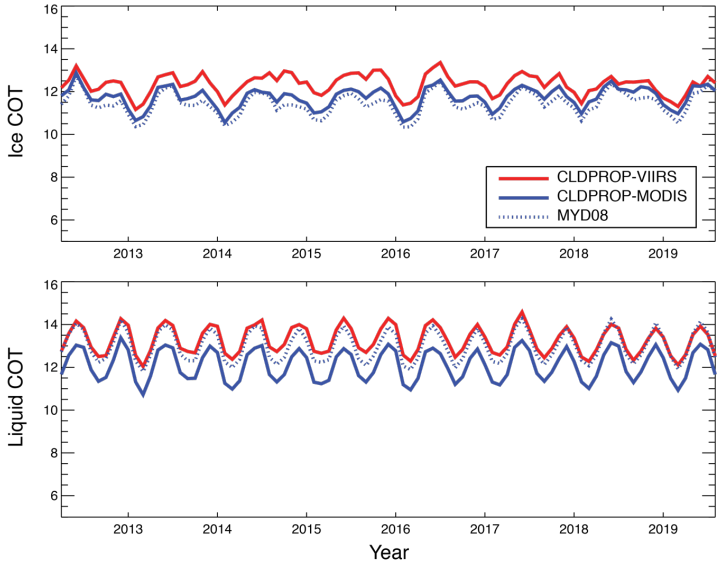

Figure 4.2.2.4. Same as 4.2.2.3 but for mean cloud optical thickness (COT) from CLDPROP (VIIRS and Aqua MODIS) and MYD06, for the VNIR-2.x µm retrieval.

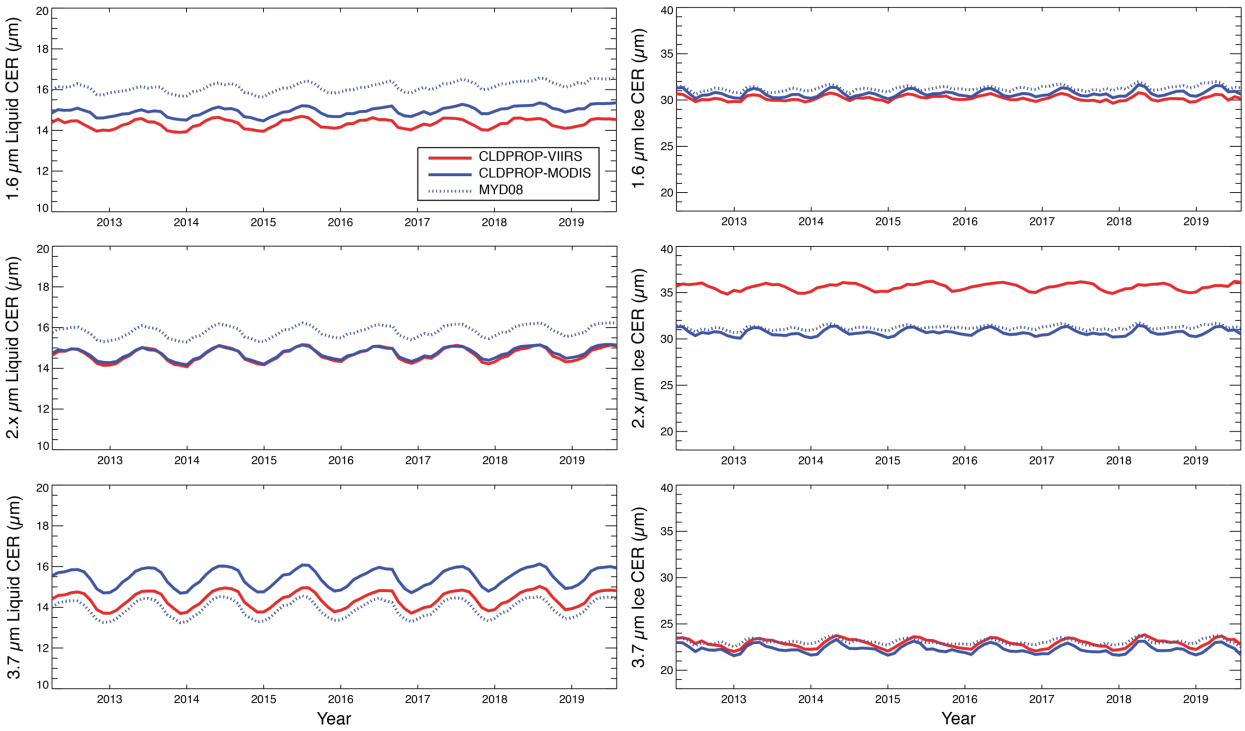

Figure 4.2.2.5. Same as 4.2.2.4 but for mean cloud optical property effective particle radius (CER) from CLDPROP (VIIRS and Aqua MODIS) and MYD06. Left column is for the VNIR-2.x µm retrieval, right column is for the VNIR-3.7 µm retrieval. Top and bottom rows are for ice and liquid phase clouds, respectively.

4.3. Ongoing Efforts

While a common cloud optical/microphysical property retrieval algorithm is now in production, a number of issues affecting product continuity between Aqua-MODIS and SNPP-VIIRS remain unresolved and require further investigation. Most involve understanding, addressing, and/or monitoring the impacts of sensor differences such as spatial resolution and relative radiometric consistency (see Sections 2.3, 2.4), while others involve algorithm assumptions such as liquid and ice cloud forward radiative models. Furthermore, a number of algorithm additions are currently in development and testing, including a 1.38 μm thin cirrus optical property retrieval based on the work of *Meyer and Platnick* [2010].

Sensor spatial resolution differences, particularly the divergent growth of MODIS and VIIRS pixel sizes towards scan edge, have significant implications on the impacts of sub-pixel heterogeneity and pixel population sampling (i.e., overcast vs cloud edge) and, ultimately, on the retrieval statistics derived from each sensor. As a reminder, this was an explanation for the monthly mean liquid phase COT divergence between the two sensors in broken cloud marine regimes despite the inter-sensor relative radiometry being set by homogeneous maritime cloud scenes (Sect. 4.2.1). Ice clouds may show pixel resolution impacts as well.

The differences in the ice phase CER retrieval statistics (e.g., monthly means in Fig. 4.2.1.7, regional time series in Fig. 4.2.2.5) from the MODIS 2.13 μm channel and the VIIRS 2.25 μm channel may indicate inappropriate forward radiative model assumptions, a conclusion similar to what prompted the change in refractive index for liquid water clouds (Sect. 4.1.1). Furthermore, it remains an open question whether the liquid water cloud forward radiative model change is truly appropriate on a global scale over the full range of liquid water cloud temperatures, or for the 3.7 μm channel.

Planned CLDPROP product additions include the 1.38 μm thin cirrus COT retrievals of *Meyer and Platnick* [2010], which have already been integrated into the CHIMAERA development environment that includes both the MOD06 and CLDPROP optical/microphysical retrieval algorithms (and those for other spaceborne and airborne sensors) and their shared code cores. While the 1.38 μm algorithm provides complementary COT information on optically thin cirrus for which the standard MOD06 and CLDPROP optical/microphysical property retrievals often fail, early testing has shown that it can also provide information on the presence of multilayer clouds. Work is ongoing towards developing appropriate 1.38 μm COT retrieval quality flags, a requirement for inclusion in future CLDPROP versions, as well as towards assessing the conditions under which it can appropriately be used for multilayer cloud detection.

5. REFERENCES

Ackerman, S. A., K. I. Strabala, W. P. Menzel, R. A. Frey, C. C. Moeller and L. E. Gumley (1998), Discriminating clear sky from clouds with MODIS, *J. Geophys. Res.: Atmos*, 103(D24), 32141–32157, doi: 10.1029/1998JD200032.

Baum, B. A., W. P. Menzel, R. A. Frey, D. C. Tobin, R. E. Holz, S. A. Ackerman, A. K. Heidinger, and P. Yang (2012), MODIS cloud-top property refinements for collection 6, *J. Appl. Meteorol. Climatol.*, 51(6), 1145–1163, doi:10.1175/JAMC-D-11-0203.1.

Cao, C., X. Xiong, R. Wolfe, F. DeLuccia, Q. Liu, S. Blonski, G. Lin, M. Nishihama, D. Pogorzala, H. Oudrari, and D. Hillger (2013), *Visible Infrared Imaging Radiometer Suite (VIIRS) Sensor Data Record (SDR) User's Guide*, NOAA Technical Report NESDIS 142A, 49 pp., U.S. Department of Commerce, National Oceanic and Atmospheric Administration, National Environmental Satellite, Data, and Information Service.

Cho, H.-M., Z. Zhang, K. Meyer, M. Lebsock, S. Platnick, A. S. Ackerman, L. Di Girolamo, L. C.-Labonnote, C. Cornet, J. Riedi, and R. E. Holz (2015), Frequency and causes of failed MODIS cloud property retrievals for liquid phase clouds over global oceans. *J. Geophys. Res.*, 120, 4132-4154, doi:10.1002/2015JD023161.

Hamann, U., A. Walther, B. Baum, R. Bennartz, L. Bugliaro, M. Derrien, P. N. Francis, A. Heidinger, S. Joro, A. Kniffka, H. Le Gléau, M. Lockhoff, H.-J. Lutz, J. F. Meirink, P. Minnis, R. Palikonda, R. Roebeling, A. Thoss, S. Platnick, P. Watts, and G. Wind (2014), Remote sensing of the cloud top pressure/height from SEVIRI: Analysis of ten current retrieval algorithms, *Atmos. Meas. Tech.*, 7, 2839–2867, doi:10.5194/amt-7-2839-2014.

Heidinger, A. (2011), GOES-R ABI Cloud Mask Algorithm Theoretical Basis Document, access at https://www.goes-r.gov/products/ATBDs/baseline/Cloud_CldMask_v2.0_no_color.pdf.

Heidinger, A. K., N. Bearson, M. J. Foster, Y. Li, S. Wanzong, S. Ackerman, R. E. Holz, S. Platnick, and K. Meyer (2018), Using sounder data to improve cirrus cloud height estimation from satellite images, *Submitted to J. Atmos. Oceanic Tech*.

Justice C.O., E. Vermote, J. Privette J., and A. Sei (2011), The Evolution of U.S. Moderate Resolution Optical Land Remote Sensing from AVHRR to VIIRS. *Land Remote Sensing and Global Environmental Change,* B. Ramachandran, C. Justice, and M. Abrams, Eds., Remote Sensing and Digital Image Processing, vol. 11. Springer, New York, NY., 781-806.

Kou, L. H., D. Labrie, and P. Chylek (1993), Refractive-indexes of water and ice in the 0.65- to 2.5-µm spectral range, *Applied Optics*, 32(19), 3531–3540.

Marchant, B., S. Platnick, K. Meyer, G. T. Arnold, J. Riedi (2016), MODIS Collection 6 shortwave-derived cloud phase classification algorithm and comparisons with CALIOP, *Atmos. Meas. Tech.*, 9(4), 1587–1599, doi:10.5194/amt-9-1587-2016.

Meyer, K., and S. Platnick (2010), Utilizing the MODIS 1.38 μm channel for cirrus cloud optical thickness retrievals: Algorithm and retrieval uncertainties, *J. Geophys. Res.: Atmos.*, 115(D24), doi:10.1029/2010JD014872.

Nakajima, T., and M. D. King (1990), Determination of the optical thickness and effective particle radius of clouds from reflected solar radiation measurements. Part 1. Theory, *J. Atmos. Sci.*, 47(15), 1878–1893, doi:10.1175/1520-0469(1990)047<1878:DOTOTA>2.0.CO;2.

Pavolonis, M. (2010), GOES-R ABI Cloud Type and Cloud Phase Algorithm Theoretical Basis Document, access at https://www.star.nesdis.noaa.gov/goesr/docs/ATBD/Cloud_Phase.pdf.

Platnick, S., K. G. Meyer, M. D. King, G. Wind, N. Amarasinghe, B. Marchant, G. T. Arnold, Z. Zhang, P. A. Hubanks, R. E. Holz, P. Yang, W. L. Ridgway, and J. Riedi (2016), The MODIS cloud optical and microphysical products: Collection 6 updates and examples from Terra and Aqua, *IEEE Trans. Geosci. Remote Sens.*, 55(1), 502–525, doi:10.1109/TGRS.2016.2610522.

Roebeling, R., B. Baum, R. Bennartz, U. Hamann, A. Heidinger, J. F. Meirink, M. Stengel, A. Thoss, A. Walther, and P. Watts (2015), Summary of the fourth cloud retrieval evaluation workshop, *Bull. Amer. Met. Soc.*, 96(4), ES71–ES74, doi:10.1175/BAMS-D-14-00184.1.

Sayer, A. M., N. C. Hsu, C. Bettenhausen, R. E. Holz, J. Lee, G. Quinn, and P. Veglio (2017), Cross-calibration of S-NPP VIIRS moderate-resolution reflective solar bands against MODIS Aqua over dark water scenes, *Atmos. Meas. Tech.*, 10(4), 1425–1444, doi:10.5194/amt-10-1425-2017.

Stubenrauch, C. J., W. B. Rossow, S. Kinne, S. Ackerman, G. Cesana, H. Chepfer, B. Getzewich, L. Di Girolamo, A. Guignard, A. Heidinger, B. Maddux, P. Menzel, P. Minnis, C. Pearl, S. Platnick, C. Poulsen, J. Riedi, S. Sun-Mack, A. Walther, D. Winker, S. Zeng, and G. Zhao, (2013), Assessment of global cloud datasets from satellites: Project and database initiated by the GEWEX Radiation Panel, *Bull. Am. Meteor. Soc.*, 94(7), 1031-1049, doi:10.1175/BAMS-D-12-00117.1.

Wagner, R., S. Benz, O. Möhler, H. Saathoff, M. Schnaiter, and U. Schurath (2005), Mid-infrared extinction spectra and optical constants of supercooled water droplets, *J. Phys. Chem. A*, *109*(32), 7099–7112, doi:10.1021/jp051942z.

Wielicki, B. A. et al. (2013), Achieving climate change Absolute accuracy in orbit, *Bull. Amer. Met. Soc.*, 94(10), 1519–1539, doi:10.1175/BAMS-D-12-00149.1.

Wind, G., S. Platnick, M. D. King, P. A. Hubanks, M. J. Pavolonis, A. K. Heidinger, P. Yang, and B. A. Baum (2010), Multilayer cloud detection with the MODIS near-infrared water vapor absorption band, *J. Appl. Meteorol. Climatol.*, 49(11), 2315–2333, doi:10.1175/2010JAMC2364.1.

Yang, P., L. Bi, B. A. Baum, K. N. Liou, G. W. Kattawar, M. I. Mishchenko, and B. Cole (2013), Spectrally consistent scattering, absorption, and polarization properties of

atmospheric ice crystals at wavelengths from 02 to 100 μm, *J. Atmos. Sci.*, 70, 330–347, doi:10.1175/JAS-D-12-039.1.

Zhang, Z., and S. Platnick (2011), An assessment of differences between cloud effective particle radius for marine water clouds from three MODIS spectral bands. *J. Geophys. Res.*, 116, D20215, doi:10.1029/2011JD016216.

Zhang, Z., A. S. Ackerman, G. Feingold, S. Platnick, R. Pincus, and H. Xue (2012), Effects of cloud horizontal inhomogeneity and drizzle on remote sensing of cloud droplet effective radius: Case studies based on large-eddy simulations. *J. Geophys. Res.,* 117, D19208, doi:10.1029/2012JD017655.

Appendix A. Variables in the CLDPROP L2 Product File

For completeness, **Tables A.1** and **A.2** below list all dimensions and scientific variables, respectively, in the CLDPROP file. Variables are organized by group (names in gray shaded cells) following product file convention.

Variable Dimensions	Value
number_of_pixels	1354 (MODIS); 3200 (VIIRS)
number_of_lines	granule-dependent
number_of_failure_metrics	3
number_of_reflectance_bands	6
number_of_cloud_mask_bytes	2
number_of_quality_assurance_bytes	4
number_of_wavelengths	7
number_of_ice_radii	12
number_of_liquid_radii	18

Variable Name	Long Name
cloud_model_data	
Asymmetry_Parameter_Ice	Ice particle asymmetry parameter
Asymmetry_Parameter_Liq	Liquid water droplet asymmetry parameter
Extinction_Efficiency_Ice	Ice particle extinction efficiency
Extinction_Efficiency_Liq	Liquid water droplet extinction efficiency
Single_Scatter_Albedo_Ice	Ice particle single scattering albedo
Single_Scatter_Albedo_Liq	Liquid water droplet single scattering albedo
geolocation_data	
latitude	Latitude from GMTCO or VGEOM
longitude	Longitude from GMTCO or VGEOM
sensor_azimuth	Sensor Azimuth Angle, Cell to Sensor
sensor_zenith	Sensor Zenith Angle, Cell to Sensor
solar_azimuth	Solar Azimuth Angle, Cell to Sun
solar_zenith	Solar Zenith Angle, Cell to Sun
geophysical_data	
Atm_Corr_Refl	Atmospherically corrected reflectance used during cloud optical and microphysical properties retrieval
Cloud_Effective_Emissivity	Cloud Effective Emissivity from NOAA CLAVR-x AWG algorithm at 11μm

Cloud_Effective_Radius	Cloud Particle Effective Radius two-channel retrieval using 2.2 um and either 0.65 um, 0.86 um or 1.24um (specified in Quality_Assurance) from best points: not failed in any way, not marked for clear sky restoral
Cloud_Effective_Radius_PCL	Cloud Particle Effective Radius two-channel retrieval using 2.2 um and either 0.65 um, 0.86 um or 1.24um (specified in Quality_Assurance) from points identified as partly cloudy from cloud edges
Cloud_Effective_Radius_16	Cloud Particle Effective Radius two-channel retrieval using 1.6 um and either 0.65 um, 0.86 um or 1.24um (specified in Quality_Assurance) from best points: not failed in any way, not marked for clear sky restoral
Cloud_Effective_Radius_16_PCL	Cloud Particle Effective Radius two-channel retrieval using 1.6um and either 0.65 um, 0.86 um or 1.24um (specified in Quality_Assurance) from points identified as partly cloudy from cloud edges
Cloud_Effective_Radius_1621	Cloud Particle Effective Radius two-channel retrieval using 2.2 um and 1.6um from best points: not failed in any way, not marked for clear sky restoral
Cloud_Effective_Radius_1621_PCL	Cloud Particle Effective Radius two-channel retrieval using 2.2 um and 1.6um from points identified as partly cloudy from cloud edges
Cloud_Effective_Radius_16_PCL	Cloud Particle Effective Radius two-channel retrieval using 3.7um and either 0.65 um, 0.86 um or 1.24um (specified in Quality_Assurance) from best points: not failed in any way, not marked for clear sky restoral
Cloud_Effective_Radius_37_PCL	Cloud Particle Effective Radius two-channel retrieval using 3.7um and either 0.65 um, 0.86 um or 1.24um (specified in Quality_Assurance) from points identified as partly cloudy from cloud edges
Cloud_Effective_Radius_Uncertainty	Cloud Effective Particle Radius from 2.2 um Relative Uncertainty (Percent) from both best points and points identified as cloud edge
Cloud_Effective_Radius_Uncertainty_16	Cloud Effective Particle Radius from 1.6 um Relative Uncertainty (Percent) from both best points and points identified as cloud edge
Cloud_Effective_Radius_Uncertainty_1621	Cloud Effective Particle Radius Relative Uncertainty (Percent) using 2.2 um and 1.6um from both best points and points identified as cloud edge
Cloud_Effective_Radius_Uncertainty_37	Cloud Effective Particle Radius from 3.7 um Relative Uncertainty (Percent) from both best points and points identified as cloud edge
Cloud_Mask	3-d byte arrary from which cloud mask information can be extracted
Cloud_Optical_Thickness	Cloud Optical Thickness two-channel retrieval using 2.2 um and either 0.65 um, 0.86 um or 1.24um (specified in Quality_Assurance) from best points: not failed in any way, not marked for clear sky restoral
Cloud_Optical_Thickness_PCL	Cloud Optical Thickness two-channel retrieval using 2.2 um and either 0.65 um, 0.86 um or 1.24um (specified in Quality_Assurance) from points identified as partly cloudy from cloud edges
Cloud_Optical_Thickness_16	Cloud Optical Thickness two-channel retrieval using 1.6um and either 0.65 um, 0.86 um or 1.24um (specified in

	Quality_Assurance) from best points: not failed in any way, not marked for clear sky restoral
Cloud_Optical_Thickness_16_PCL	Cloud Optical Thickness two-channel retrieval using 1.6um and either 0.65 um, 0.86 um or 1.24um (specified in Quality_Assurance) from points identified as partly cloudy from cloud edges
Cloud_Optical_Thickness_1621	Cloud Optical Thickness two-channel retrieval using 2.2 um and 1.6um from best points: not failed in any way, not marked for clear sky restoral
Cloud_Optical_Thickness_1621_PCL	Cloud Optical Thickness two-channel retrieval using 2.2 um and 1.6um from points identified as partly cloudy from cloud edges
Cloud_Optical_Thickness_37	Cloud Optical Thickness two-channel retrieval using 3.7um and either 0.65 um, 0.86 um or 1.24um (specified in Quality_Assurance) from best points: not failed in any way, not marked for clear sky restoral
Cloud_Optical_Thickness_37_PCL	Cloud Optical Thickness two-channel retrieval using 3.7um and either 0.65 um, 0.86 um or 1.24um (specified in Quality_Assurance) from points identified as partly cloudy from cloud edges
Cloud_Optical_Thickness_Uncertainty	Cloud Optical Thickness from 2.2 um Relative Uncertainty (Percent) from both best points and points identified as cloud edge
Cloud_Optical_Thickness_Uncertainty_16	Cloud Optical Thickness from 1.6 um Relative Uncertainty (Percent) from both best points and points identified as cloud edge
Cloud_Optical_Thickness_Uncertainty_1621	Cloud Optical Thickness Relative Uncertainty (Percent) using 2.2 um and 1.6um from both best points and points identified as cloud edge
Cloud_Optical_Thickness_Uncertainty_37	Cloud Optical Thickness from 3.7 um Relative Uncertainty (Percent) from both best points and points identified as cloud edge
Cloud_Phase_Cloud_Top_Properties	Cloud Phase Determination from NOAA CLAVR-x AWG algorithm
Cloud_Phase_Optical_Properties	Cloud Phase Determination Used in Optical Thickness/Effective Radius Retrieval
Cloud_Top_Height	Cloud Top Height from NOAA CLAVR-x AWG algorithm
Cloud_Top_Height_Uncertainty	Cloud Top Height uncertainty from NOAA CLAVR-x AWG algorithm
Cloud_Top_Pressure	Cloud Top Pressure from NOAA CLAVR-x AWG algorithm
Cloud_Top_Pressure_Uncertainty	Cloud Top Pressure uncertainty from NOAA CLAVR-x AWG algorithm
Cloud_Top_Temperature	Cloud Top Temperature from NOAA CLAVR-x AWG algorithm
Cloud_Top_Temperature_Uncertainty	Cloud Top Temperature uncertainty from NOAA CLAVR-x AWG algorithm
Cloud_Water_Path	Column Water Path two-channel retrieval using 2.2 um and either 0.65 um, 0.86 um or 1.24um (specified in Quality_Assurance) from best points: not failed in any way, not marked for clear sky restoral
Cloud_Water_Path_PCL	Column Water Path two-channel retrieval using 2.2 um and either 0.65 um, 0.86 um or 1.24um (specified in Quality_Assurance) from points identified as partly cloudy from cloud edges
Cloud_Water_Path_16	Column Water Path two-channel retrieval using 1.6um and either 0.65 um, 0.86 um or 1.24um (specified in Quality_Assurance)

	from best points: not failed in any way, not marked for clear sky restoral
Cloud_Water_Path_16_PCL	Column Water Path two-channel retrieval using 1.6um and either 0.65 um, 0.86 um or 1.24um (specified in Quality_Assurance) from points identified as partly cloudy from cloud edges
Cloud_Water_Path_1621	Column Water Path two-channel retrieval using 2.2 um and 1.6um from best points: not failed in any way, not marked for clear sky restoral
Cloud_Water_Path_1621_PCL	Column Water Path two-channel retrieval using 2.2 um and 1.6um from points identified as partly cloudy from cloud edges
Cloud_Water_Path_37	Column Water Path two-channel retrieval using 3.7um and either 0.65 um, 0.86 um or 1.24um (specified in Quality_Assurance) from best points: not failed in any way, not marked for clear sky restoral
Cloud_Water_Path_37_PCL	Column Water Path two-channel retrieval using 3.7um and either 0.65 um, 0.86 um or 1.24um (specified in Quality_Assurance) from points identified as partly cloudy from cloud edges
Cloud_Water_Path_Uncertainty	Cloud Water Path from 2.2 um Relative Uncertainty (Percent) from both best points and points identified as cloud edge
Cloud_Water_Path_Uncertainty_16	Cloud Water Path from 1.6 um Relative Uncertainty (Percent) from both best points and points identified as cloud edge
Cloud_Water_Path_Uncertainty_1621	Cloud Water Path Relative Uncertainty (Percent) using 2.2 um and 1.6um from both best points and points identified as cloud edge
Cloud_Water_Path_Uncertainty_37	Cloud Water Path from 3.7 um Relative Uncertainty (Percent) from both best points and points identified as cloud edge
IRW_Low_Cloud_Temperature_From_COP	Low Cloud Temperature from IR Window retrieval using cloud emissivity based on cloud optical thickness
Quality_Assurance	3-D byte array from which much info about quality (QA) of retrieval data can be extracted
Retrieval_Failure_Metric	Retrievals and other information for points that failed to retrieve via standard solution logic for retrieval using 2.2 um and either 0.65um, 0.86um or 1.2um (specified in Quality_Assurance)
Retrieval_Failure_Metric_16	Retrievals and other information for points that failed to retrieve via standard solution logic for retrieval using 1.6um and either 0.65um, 0.86um or 1.2um (specified in Quality_Assurance)
Retrieval_Failure_Metric_1621	Retrievals and other information for points that failed to retrieve via standard solution logic for retrieval using 2.2 um and 1.6um
Retrieval_Failure_Metric_37	Retrievals and other information for points that failed to retrieve via standard solution logic for retrieval using 3.7um and either 0.65um, 0.86um or 1.2um (specified in Quality_Assurance)

APPENDIX B. SUMMARY VARIABLE AND QUALITY ASSURANCE (QA) ASSIGNMENTS

The mapping of pixel retrieval outcome status to variable assignments, the mapping of QA outcome status to QA assignments, and retrieval failure outcome assignments all follow MOD06 conventions, and are given in Appendix B (Tables B.1, B.2, and B.3, respectively) of the MOD06 User's Guide [Link 3].

Cloud optical property QA flags are stored in two separate variables. The first variable, *Cloud_Mask*, contains cloud mask QA flags, which are copied from the CLDMSK_L2 product. The second variable, *Quality_Assurance*, contains product quality, retrieval processing, and scene characteristic flags. The bit assignments of these two QA variables are given in **Tables B.1** and **B.2** below.

Table B.1. Cloud_Mask variable in the CLDPROP_L2 file.

Variable: "Cloud_Mask" ***Description: Cloud Mask QA Flags*** ***Length: 2 bytes (16 bits)***			
Flag Name	Number of Bits	Bit Values	Bit Value Definitions
Cloud Mask Flag	1	0 1	Not determined Determined
Unobstructed FOV Quality Flag	2	0 1 2 3	Cloudy *(or Fill, if Cloud Mask Flag = 0)* Uncertain Probably Clear Confident Clear
Day or Night Path	1	0 1	Night *(or Fill, if Cloud Mask Flag = 0)* Day
Sunglint Path	1	0 1	Yes *(or Fill, if Cloud Mask Flag = 0)* No
Snow/Ice Background Path	1	0 1	Yes *(or Fill, if Cloud Mask Flag = 0)* No
Land or Water Path	2	0 1 2 3	Water *(or Fill, if Cloud Mask Flag = 0)* Coastal Desert Land
High Cloud Test 1.38um result	1	0 1	No / Not applied Might have cloud
High Cloud Test 1.38um applied?	1	0 1	Not applied Applied
Visible Reflectance Threshold test result	1	0 1	No / Not applied Might have cloud
Visible Reflectance Threshold test applied?	1	0 1	Not applied Applied
R0.86 / R0.65um test result	1	0 1	No / Not applied Might have cloud
R0.86 / R0.65um test applied?	1	0 1	Not applied Applied
Spares	2		TBD

Table B.2. Quality_Assurance variable in the CLDPROP_L2 file.

Variable: "Quality_Assurance" ***Description: Cloud Optical Property product quality and retrieval processing QA flags*** ***Length: 4 bytes (32 bits)***			
Flag Name	Number of Bits	Bit Values	Bit Value Definitions
VNSWIR-2.1 Retrieval Spectral Data QA	1	0 1	Some or all spectral data not available All spectral data available
VNSWIR-2.1 Retrieval Confidence QA	2	0 1 2 3	No confidence Marginal Good Very Good
VNSWIR-2.1 Retrieval Outcome	1	0 1	Failed/No attempt Successful
1.6-2.1 Retrieval Spectral Data QA	1	0 1	Some or all spectral data not available All spectral data available
1.6-2.1 Retrieval Confidence QA	2	0 1 2 3	No confidence Marginal Good Very Good
1.6-2.1 Retrieval Outcome	1	0 1	Failed/No attempt Successful
Primary retrieval processing path	3	0 1 2 3 4	No Cloud Mask No Cloud Water Cloud Ice Cloud Unknown Cloud
Rayleigh Correction	1	0 1	No Correction Correction
Band Used for Optical Thickness Retrieval	2	0 1 2 3	No attempt .645 micron .858 micron 1.24 micron
VNSWIR-2.1 Optical thickness out of bounds	1	0 1	No Yes
VIIRS Bow-tie pixel indicator	1	0 1	Normal Pixel Bow-Tie pixel
Clear Sky Restoral Type QA	2	0 1 2 3	Not Restored Restored Via Edge detection Restored Via Spatial Variance Restored using high resolution data
VNSWIR-1.6 Retrieval Outcome	1	0 1	Failed/No attempt Successful
VNSWIR-1.6 PCL Retrieval Outcome	1	0 1	Failed/No attempt Successful
VNSWIR-3.7 Retrieval Outcome	1	0 1	Failed/No attempt Successful
VNSWIR-3.7 PCL Retrieval Outcome	1	0 1	Failed/No attempt Successful
1.6-2.1 PCL Retrieval Outcome	1	0 1	Failed/No attempt Successful

VNSWIR-2.1 PCL Retrieval Outcome	1	0 1	Failed/No attempt Successful
Earth surface type used in optical thickness retrieval	2	0 1 2 3	ice-free ocean ice-covered ocean snow-free land snow-covered land
VNSWIR-1.6 Retrieval Spectral Data QA	1	0 1	Some or all spectral data not available All spectral data available
VNSWIR-3.7 Retrieval Spectral Data QA	1	0 1	Some or all spectral data not available All spectral data available
Spares	4	-	TBD

APPENDIX C. KEY ACRONYMS AND WEB LINKS

Acronyms

AIRS: Atmospheric Infrared Sounder, flown on the Aqua platform

ATBD: Algorithm Theoretical Basis Document

C5: Collection 5 MODIS Atmosphere Team processing stream (version), begun in mid-2006

C6: Collection 6 MODIS Atmosphere Team processing stream, began in Dec. 2013 and Nov. 2014 for Aqua and Terra L2 products, respectively

C6.1: Collection 6.1 MODIS Atmosphere Team processing stream, began in Sept. 2017 and Jan. 2018 for Terra and Aqua, respectively

CALIOP: Cloud-Aerosol Lidar with Orthogonal Polarization, a lidar instrument flow on the NASA CALIPSO mission

CFMIP: Cloud Feedback Modeling Intercomparison Project (http://cfmip.metoffice.com)

CER: Cloud Effective particle Radius

CHIMAERA: Cross-platform HIgh resolution Multi-instrument AtmosphEric Retrieval Algorithms. Cloud retrieval team's development environment that simultaneously supports multiple spaceborne and airborne platforms using the same science core.

CLDMSK: MODIS-VIIRS continuity cloud mask Level-2 product file ID

CLDPROP: MODIS-VIIRS continuity cloud-top and optical properties Level-2 product file ID

COP: Cloud Optical properties Phase (thermodynamic phase used in the optical property retrieval algorithm)

COT: Cloud Optical Thickness

CrIS: Cross-track Infrared Sounder, flown on the SNPP platform

CSR: Clear Sky Restoral algorithm

CTH: Cloud-Top Height

CTP: Cloud Top Pressure

CTT: Cloud-Top Temperature

CWP: Cloud Water Path (e.g., g m-2); LWP: Liquid Water Path; IWP: Ice Water Path

EOS: Earth Observing System, NASA's coordinated series of polar-orbiting and low inclination satellites for long-term global observations of the land surface, biosphere, solid Earth, atmosphere, and oceans

GOES-R AWG: NOAA Algorithm Working Group cloud code for the GOES-R ABI imager, similar to PATMOS-x

HDF: Hierarchical Data Format. MODIS data products are in HDF4.

IDPS: Interface Data Processing System, NOAA's vendor data production system

JPSS: Joint Polar Satellite System, NOAA's next-generation polar orbiting operational satellite series

LAADS: Land and Atmospheres Archive and Distribution System used to distribute MODIS Atmosphere Team products

L2: Level-2 products (pixel-level, 1km resolution at nadir for all optical property products)

L3: Level-3 products (1° aggregated/gridded for all MODIS Atmosphere Team products)

MOD06 /MYD06: MODIS Terra/Aqua cloud-top and optical properties Level-2 product file ID

MOD35/MYD35: MODIS Terra/Aqua cloud mask Level-2 product file ID

MODIS: Moderate Resolution Imaging Spectroradiometer

MWIR: Midwave Infrared (e..g., MODIS 3.7 μm channels)

NetCDF: Network Common Data Form. MODIS-VIIRS continuity products are in NetCDF-4.

PCL: pixels identified as "partly cloudy" by the CSR algorithm (CSR values of 1 and 2)

QA: Quality Assurance. Often refers to bit assignments used to qualitatively assign pixel-level retrieval accuracy or the accuracy of aggregated statistics. More generically, can refer to any approach for filtering/weighting retrieved pixels.

SDR: Sensor Data Record, NOAA designation for operational data products

SNPP: Suomi National Polar-orbiting Partnership

SWIR: Shortwave Infrared (e..g., MODIS 1.2, 1.6, and 2.1 μm MODIS channels)

TOA: Top of Atmosphere

VIIRS: Visible Infrared Imaging Radiometer Suite

VNIR: Visible and Near-Infrared (e..g., MODIS 0.66 and 0.86 μm channels, respectively)

VNSWIR: Refers to a retrieval using a Visible or Near-Infrared or SWIR channel as one of the channel pairs (e.g, VIS over land surfaces, NIR over ocean surfaces, 1.2 μm over snow/ice surfaces).

Web Links

Link 1: https://ladsweb.modaps.eosdis.nasa.gov/missions-and-measurements/viirs/MODIS_VIIRS_Cloud-Mask_UG_Feb_2019.pdf

Link 2: https://docs.google.com/document/d/1m2SatR91WIJcaAZweongcFCb6Wsx_xnRUcZxp94gXHk/edit

Link 3: https://modis-atmosphere.gsfc.nasa.gov/sites/default/files/ModAtmo/MODISCloudOpticalPropertyUserGuideFinal_v1.1_1.pdf

Link 4: https://sips.ssec.wisc.edu

Link 5: https://ladsweb.modaps.eosdis.nasa.gov/

Link 6: https://oceancolor.gsfc.nasa.gov/docs/technical/VIIRS_Level-1_DataProductUsersGuide.pdf

Link 7: https://worldview.earthdata.nasa.gov

Link 8: https://www.star.nesdis.noaa.gov/goesr/docs/ATBD/Cloud_Phase.pdf

Link 9: https://www.star.nesdis.noaa.gov/goesr/docs/ATBD/Cloud_Mask.pdf

Link 10: https://atmosphere-imager.gsfc.nasa.gov/sites/default/files/ModAtmo/L3_CLDPROP_User_Guide_v1.7.pdf

Link 11: https://atmosphere-imager.gsfc.nasa.gov/sites/default/files/ModAtmo/L3_ATBD_C6_C61_2019_02_20.pdf

APPENDIX D: CLOUD MODEL LUT SCATTERING PROPERTIES

The following tables give the scattering properties (g, ω_0, Q_e) for the liquid water and ice cloud radiative models used in the CLDPROP cloud optical/microphysical properties retrievals. Values are shown as a function of the Look-up Table (LUT) effective radii grid points and the MODIS and VIIRS spectral channels directly used in the retrieval algorithm. Band numbers correspond to the following nominal central wavelengths (CWL):

MODIS Band No.	1	2	5	6	7	20	31
CWL (µm)	0.66	0.86	1.24	1.64	2.13	3.75	11.03
VIIRS Band	**M5**	**M7**	**M8**	**M10**	**M11**	**M12**	**M15**
CWL (µm)	0.67	0.87	1.24	1.61	2.25	3.7	10.8

All table values below are reported in the CLDPROP L2 files in variables stored within the *cloud_model_data* group; specific variable names are given in each caption. Note that, because of the use of new super-cooled liquid water refractive indices (265K, see Section 4.1.1), the MODIS liquid water cloud properties for CLDPROP are different from those used in MOD06 (see Appendix D of the MOD06 User's Guide, Link 3).

Table D.1. MODIS liquid water asymmetry parameter (Variable: *Asymmetry_Parameter_Liq*). Note: CLDPROP only provides successful liquid water cloud retrievals for CER ≥ 4 µm.

MODIS Band/ CER (µm)	1	2	5	6	7	20	31
2	*0.805*	*0.785*	*0.767*	*0.808*	*0.850*	*0.794*	*0.423*
4	0.838	0.827	0.804	0.783	0.790	0.779	0.753
5	0.845	0.836	0.820	0.802	0.790	0.753	0.817
6	0.850	0.843	0.830	0.817	0.802	0.743	0.856
7	0.854	0.847	0.836	0.827	0.816	0.750	0.882
8	0.857	0.851	0.841	0.835	0.827	0.765	0.901
9	0.860	0.854	0.845	0.840	0.836	0.780	0.914
10	0.862	0.857	0.849	0.844	0.843	0.794	0.924
12	0.865	0.861	0.854	0.850	0.852	0.814	0.938
14	0.867	0.864	0.858	0.855	0.859	0.828	0.947
16	0.869	0.866	0.861	0.859	0.864	0.838	0.953
18	0.870	0.868	0.863	0.862	0.868	0.846	0.958
20	0.871	0.869	0.865	0.865	0.872	0.853	0.961
22	0.872	0.870	0.867	0.867	0.875	0.859	0.964
24	0.873	0.871	0.868	0.869	0.878	0.865	0.966
26	0.873	0.872	0.870	0.871	0.880	0.869	0.968
28	0.873	0.873	0.871	0.872	0.882	0.874	0.969
30	0.873	0.873	0.871	0.874	0.885	0.878	0.970

Table D.2. VIIRS liquid water asymmetry parameter (Variable: *Asymmetry_Parameter_Liq*). Note: CLDPROP only provides successful liquid water cloud retrievals for CER ≥ 4 µm.

VIIRS Band/ CER (µm)	M5	M7	M8	M10	M11	M12	M15
2	*0.801*	*0.785*	*0.767*	*0.805*	*0.859*	*0.791*	*0.441*
4	0.836	0.827	0.804	0.785	0.804	0.765	0.762
5	0.844	0.836	0.820	0.804	0.793	0.742	0.822
6	0.849	0.843	0.830	0.818	0.800	0.739	0.860
7	0.853	0.847	0.837	0.828	0.812	0.751	0.885
8	0.856	0.851	0.841	0.835	0.823	0.768	0.902
9	0.859	0.854	0.846	0.841	0.832	0.784	0.915
10	0.861	0.857	0.849	0.845	0.840	0.798	0.924
12	0.864	0.861	0.854	0.851	0.850	0.817	0.937
14	0.867	0.864	0.858	0.856	0.857	0.831	0.945
16	0.869	0.866	0.861	0.860	0.862	0.841	0.951
18	0.870	0.868	0.863	0.863	0.866	0.849	0.955
20	0.872	0.869	0.865	0.866	0.870	0.856	0.958
22	0.873	0.870	0.867	0.868	0.873	0.862	0.960
24	0.874	0.871	0.868	0.870	0.876	0.867	0.962
26	0.874	0.872	0.870	0.872	0.878	0.872	0.964
28	0.875	0.873	0.871	0.873	0.880	0.877	0.965
30	0.876	0.873	0.872	0.875	0.882	0.881	0.967

Table D.3. MODIS liquid water single scattering albedo (Variable: *Single_Scatter_Albedo_Liq*).

MODIS Band/ CER (µm)	1	2	5	6	7	20	31
2	*1.000*	*1.000*	*1.000*	*0.999*	*0.996*	*0.983*	*0.152*
4	1.000	1.000	1.000	0.997	0.989	0.971	0.295
5	1.000	1.000	0.999	0.996	0.986	0.959	0.345
6	1.000	1.000	0.999	0.995	0.983	0.947	0.384
7	1.000	1.000	0.999	0.995	0.980	0.937	0.415
8	1.000	1.000	0.999	0.994	0.977	0.928	0.439
9	1.000	1.000	0.999	0.993	0.975	0.919	0.458
10	1.000	1.000	0.999	0.992	0.972	0.912	0.473
12	1.000	1.000	0.999	0.991	0.967	0.898	0.494
14	1.000	1.000	0.998	0.990	0.963	0.885	0.506
16	1.000	1.000	0.998	0.988	0.958	0.873	0.513
18	1.000	1.000	0.998	0.987	0.953	0.862	0.516
20	1.000	1.000	0.998	0.986	0.949	0.851	0.516
22	1.000	1.000	0.998	0.984	0.945	0.840	0.515
24	1.000	1.000	0.997	0.983	0.940	0.830	0.513
26	1.000	1.000	0.997	0.982	0.936	0.820	0.511
28	1.000	1.000	0.997	0.981	0.932	0.810	0.508
30	1.000	1.000	0.997	0.979	0.927	0.801	0.506

Table D.4. VIIRS liquid water single scattering albedo (Variable: *Single_Scatter_Albedo_Liq*).

VIIRS Band/ CER (µm)	M5	M7	M8	M10	M11	M12	M15
2	*1.000*	*1.000*	*1.000*	*0.998*	*0.997*	*0.981*	*0.200*
4	1.000	1.000	1.000	0.996	0.993	0.965	0.361
5	1.000	1.000	0.999	0.995	0.991	0.951	0.413
6	1.000	1.000	0.999	0.994	0.989	0.938	0.452
7	1.000	1.000	0.999	0.994	0.987	0.927	0.482
8	1.000	1.000	0.999	0.993	0.985	0.917	0.504
9	1.000	1.000	0.999	0.992	0.983	0.909	0.520
10	1.000	1.000	0.999	0.991	0.982	0.901	0.533
12	1.000	1.000	0.999	0.989	0.978	0.886	0.548
14	1.000	1.000	0.998	0.988	0.975	0.872	0.555
16	1.000	1.000	0.998	0.986	0.972	0.859	0.556
18	1.000	1.000	0.998	0.985	0.969	0.846	0.553
20	1.000	1.000	0.998	0.983	0.966	0.834	0.548
22	1.000	1.000	0.998	0.982	0.963	0.823	0.542
24	1.000	1.000	0.997	0.980	0.960	0.812	0.535
26	1.000	1.000	0.997	0.979	0.957	0.802	0.529
28	1.000	1.000	0.997	0.977	0.954	0.792	0.523
30	1.000	1.000	0.997	0.976	0.951	0.782	0.518

Table D.5. MODIS liquid water extinction efficiency (Variable: *Extinction_Efficiency_Liq*).

MODIS Band/ CER (µm)	1	2	5	6	7	20	31
2	*2.291*	*2.403*	*2.531*	*2.977*	*3.251*	*2.697*	*0.375*
4	2.187	2.225	2.303	2.359	2.521	3.132	0.770
5	2.160	2.194	2.257	2.310	2.374	2.782	0.966
6	2.142	2.172	2.226	2.275	2.325	2.548	1.150
7	2.128	2.155	2.202	2.246	2.296	2.439	1.319
8	2.116	2.141	2.184	2.224	2.271	2.389	1.471
9	2.108	2.130	2.169	2.206	2.250	2.361	1.607
10	2.100	2.121	2.157	2.191	2.231	2.338	1.725
12	2.089	2.107	2.138	2.167	2.203	2.300	1.916
14	2.080	2.097	2.125	2.150	2.181	2.269	2.052
16	2.073	2.088	2.114	2.137	2.165	2.244	2.145
18	2.067	2.081	2.105	2.126	2.152	2.224	2.205
20	2.063	2.076	2.098	2.118	2.141	2.208	2.240
22	2.059	2.071	2.092	2.110	2.132	2.195	2.259
24	2.056	2.067	2.086	2.104	2.124	2.184	2.266
26	2.053	2.064	2.082	2.098	2.118	2.174	2.266
28	2.050	2.061	2.078	2.094	2.112	2.165	2.261
30	2.048	2.058	2.074	2.089	2.107	2.157	2.254

Table D.6. VIIRS liquid water extinction efficiency (Variable: *Extinction_Efficiency_Liq*).

VIIRS Band/ CER (µm)	M5	M7	M8	M10	M11	M12	M15
2	*2.298*	*2.406*	*2.528*	*2.938*	*3.174*	*2.844*	*0.346*
4	2.193	2.225	2.302	2.354	2.632	3.061	0.765
5	2.165	2.195	2.257	2.307	2.414	2.712	0.983
6	2.146	2.173	2.225	2.271	2.340	2.510	1.192
7	2.131	2.156	2.201	2.243	2.308	2.423	1.386
8	2.120	2.143	2.183	2.221	2.284	2.382	1.562
9	2.111	2.131	2.169	2.203	2.262	2.355	1.718
10	2.103	2.122	2.157	2.188	2.243	2.333	1.853
12	2.091	2.108	2.138	2.165	2.213	2.294	2.063
14	2.082	2.097	2.124	2.149	2.191	2.263	2.204
16	2.075	2.089	2.114	2.136	2.173	2.239	2.290
18	2.069	2.082	2.105	2.125	2.160	2.220	2.336
20	2.064	2.076	2.098	2.116	2.148	2.204	2.354
22	2.060	2.072	2.091	2.109	2.139	2.191	2.355
24	2.057	2.068	2.086	2.103	2.130	2.180	2.346
26	2.054	2.064	2.082	2.097	2.123	2.170	2.332
28	2.051	2.061	2.078	2.092	2.117	2.162	2.315
30	2.049	2.058	2.074	2.088	2.112	2.154	2.299

Table D.7. MODIS ice asymmetry parameter (Variable: *Asymmetry_Parameter_Ice*).

MODIS Band/ CER (µm)	1	2	5	6	7	20	31
5	0.748	0.749	0.752	0.769	0.802	0.787	0.873
10	0.751	0.753	0.756	0.769	0.790	0.798	0.931
15	0.752	0.754	0.759	0.775	0.799	0.833	0.952
20	0.753	0.755	0.760	0.780	0.807	0.860	0.960
25	0.753	0.756	0.761	0.784	0.815	0.881	0.965
30	0.753	0.756	0.762	0.789	0.821	0.898	0.968
35	0.753	0.756	0.762	0.793	0.828	0.912	0.970
40	0.753	0.756	0.763	0.797	0.833	0.922	0.972
45	0.753	0.756	0.764	0.800	0.839	0.931	0.973
50	0.753	0.757	0.764	0.804	0.844	0.937	0.974
55	0.753	0.757	0.764	0.807	0.849	0.943	0.975
60	0.753	0.757	0.765	0.811	0.854	0.947	0.975

Table D.8. VIIRS ice asymmetry parameter (Variable: *Asymmetry_Parameter_Ice*).

VIIRS Band/ CER (µm)	M5	M7	M8	M10	M11	M12	M15
5	0.748	0.749	0.752	0.767	0.816	0.783	0.873
10	0.751	0.753	0.756	0.770	0.788	0.800	0.928
15	0.752	0.754	0.758	0.777	0.792	0.836	0.952
20	0.753	0.755	0.760	0.782	0.796	0.864	0.962
25	0.753	0.756	0.761	0.787	0.800	0.885	0.968
30	0.754	0.756	0.762	0.792	0.802	0.902	0.972
35	0.754	0.756	0.762	0.797	0.805	0.915	0.975
40	0.754	0.756	0.763	0.801	0.808	0.925	0.977
45	0.754	0.757	0.763	0.805	0.810	0.933	0.978
50	0.754	0.757	0.764	0.809	0.812	0.939	0.979
55	0.754	0.757	0.764	0.813	0.814	0.944	0.980
60	0.754	0.757	0.764	0.817	0.817	0.949	0.981

Table D.9. MODIS ice single scattering albedo (Variable: *Single_Scatter_Albedo_Ice*).

MODIS Band/ CER (µm)	1	2	5	6	7	20	31
5	1.000	1.000	0.999	0.991	0.981	0.887	0.317
10	1.000	1.000	0.999	0.981	0.962	0.804	0.424
15	1.000	1.000	0.998	0.972	0.946	0.755	0.466
20	1.000	1.000	0.998	0.964	0.930	0.717	0.485
25	1.000	1.000	0.997	0.955	0.915	0.686	0.497
30	1.000	1.000	0.996	0.946	0.900	0.662	0.504
35	1.000	1.000	0.996	0.938	0.886	0.642	0.509
40	1.000	1.000	0.995	0.930	0.873	0.626	0.513
45	1.000	1.000	0.994	0.922	0.861	0.613	0.515
50	1.000	1.000	0.994	0.915	0.849	0.602	0.518
55	1.000	1.000	0.993	0.907	0.838	0.593	0.520
60	1.000	1.000	0.992	0.900	0.827	0.586	0.521

Table D.10. VIIRS ice single scattering albedo (Variable: *Single_Scatter_Albedo_Ice*).

VIIRS Band/ CER (µm)	M5	M7	M8	M10	M11	M12	M15
5	1.000	1.000	0.999	0.989	0.994	0.866	0.336
10	1.000	1.000	0.999	0.978	0.988	0.784	0.444
15	1.000	1.000	0.998	0.967	0.983	0.736	0.483
20	1.000	1.000	0.998	0.957	0.978	0.700	0.499
25	1.000	1.000	0.997	0.947	0.973	0.671	0.507
30	1.000	1.000	0.996	0.937	0.967	0.648	0.511
35	1.000	1.000	0.996	0.928	0.962	0.629	0.513
40	1.000	1.000	0.995	0.918	0.957	0.615	0.514
45	1.000	1.000	0.994	0.910	0.952	0.603	0.515
50	1.000	1.000	0.994	0.901	0.947	0.593	0.516
55	1.000	1.000	0.993	0.893	0.942	0.585	0.516
60	1.000	1.000	0.993	0.885	0.937	0.578	0.517

Table D.11. MODIS ice extinction efficiency (Variable: *Extinction_Efficiency_Ice*).

MODIS Band/ CER (µm)	1	2	5	6	7	20	31
5	2.109	2.138	2.162	2.170	2.198	2.399	1.219
10	2.065	2.086	2.107	2.128	2.100	2.199	1.601
15	2.048	2.066	2.080	2.098	2.081	2.168	1.750
20	2.039	2.054	2.065	2.080	2.067	2.141	1.819
25	2.032	2.044	2.055	2.067	2.057	2.120	1.860
30	2.027	2.038	2.048	2.058	2.049	2.105	1.885
35	2.024	2.033	2.043	2.051	2.044	2.094	1.902
40	2.021	2.029	2.038	2.046	2.039	2.085	1.913
45	2.019	2.026	2.035	2.042	2.036	2.078	1.922
50	2.017	2.024	2.032	2.039	2.033	2.072	1.929
55	2.015	2.022	2.029	2.036	2.030	2.067	1.934
60	2.014	2.020	2.027	2.034	2.028	2.062	1.939

Table D.12. VIIRS ice extinction efficiency (Variable: *Extinction_Efficiency_Ice*).

VIIRS Band/ CER (µm)	M5	M7	M8	M10	M11	M12	M15
5	2.114	2.140	2.162	2.154	2.248	2.377	1.049
10	2.068	2.087	2.107	2.116	2.093	2.210	1.513
15	2.049	2.067	2.079	2.089	2.080	2.175	1.718
20	2.040	2.055	2.065	2.073	2.066	2.146	1.815
25	2.034	2.045	2.055	2.061	2.056	2.125	1.867
30	2.029	2.039	2.048	2.052	2.049	2.109	1.896
35	2.026	2.034	2.043	2.046	2.044	2.097	1.912
40	2.023	2.030	2.038	2.041	2.039	2.088	1.922
45	2.020	2.027	2.035	2.038	2.036	2.080	1.929
50	2.018	2.024	2.032	2.035	2.033	2.074	1.935
55	2.016	2.022	2.029	2.032	2.030	2.069	1.939
60	2.015	2.021	2.027	2.030	2.028	2.064	1.943

APPENDIX E: CLOUD TOP PROPERTIES PHASE FLOW CHARTS AND TESTS

Here we summarize the logic flow chart and cloud type tests used in the CLDPROP cloud top properties thermodynamic phase algorithm (see Section 3.1.1). The cloud top properties phase product, derived from the NOAA algorithm run in the CLAVR-x processing system, determines the solution path for the ACHA cloud top height algorithm, and is separate from the cloud optical properties phase algorithm (see Section 4.1.2).

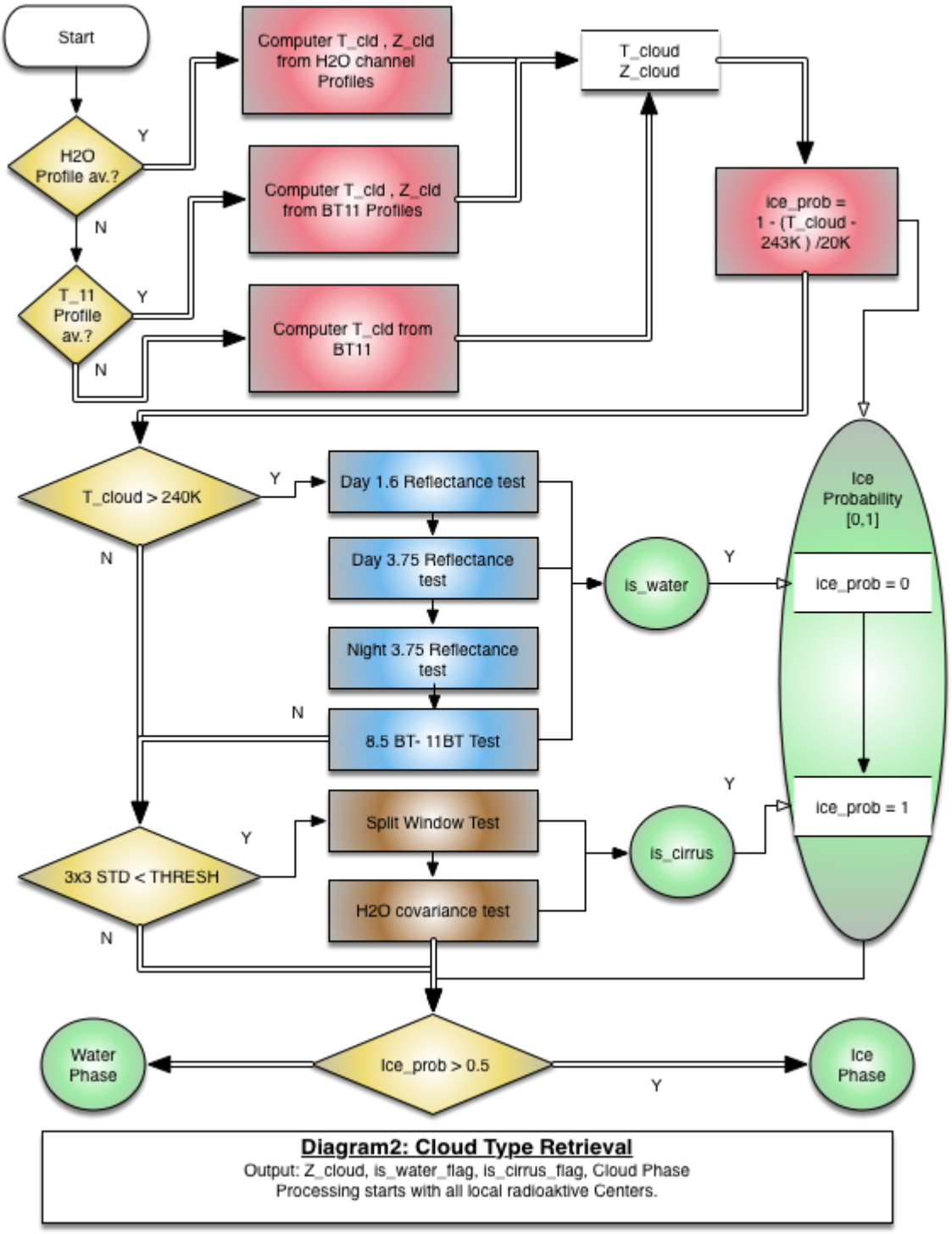

Figure E1. Determination of initial cloud phase by computing the ice probability.

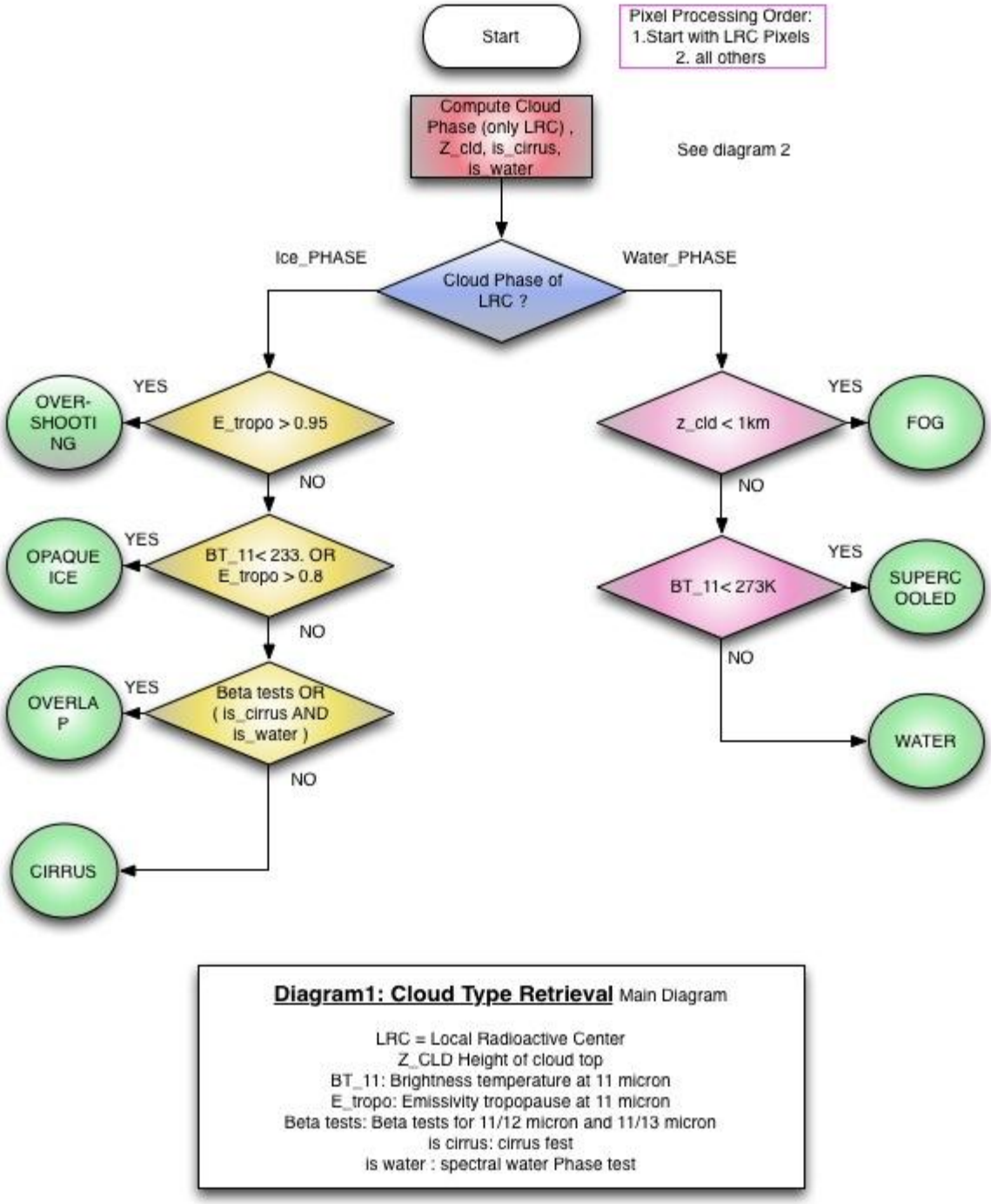

Figure E2. Determination of cloud type when cloud phase (ice or water, from Fig. E.1) is known.

Cloud Type Tests

Beta (β) Test

The β parameter is directly linked to cloud microphysics. It can be constructed using any two-channel pair of cloud emissivities (ε) as follows:

$$\beta = \frac{\log(1-\varepsilon_1)}{\log(1-\varepsilon_2)}$$

Purpose: Utilize the cloud phase information offered by β(11μm/12μm) to identify overlapped clouds.

Logic:

$$\boldsymbol{If}\left(\beta\left[\frac{11\mu m}{12\mu m}\right] > 0\ \boldsymbol{AND}\ \beta\left[\frac{11\mu m}{12\mu m}\right] < B_{overlap_{threshold}}\right)\ \boldsymbol{Then}\ TRUE$$

where $B_{overlap\_threshold} = 0.95$

Daytime 1.6 μm reflectance liquid water test

Purpose: Utilize 1.6 μm reflectance to determine if a cloud is liquid water.

Logic:

$$\boldsymbol{If}\left(\theta_0 < 80°\ \boldsymbol{AND}\ R_{1.6\mu m} < 20\ \boldsymbol{AND}\ R_{1.6\mu m} > 30\right)\ \boldsymbol{Then}\ TRUE$$

where θ_0 is the solar zenith angle and $R_{1.6\mu m}$ is the observed TOA reflectance at 1.6 μm.

Daytime 3.75μm reflectance liquid water test

Purpose: Utilize 3.75 μm emissivity and reflectance in daytime to determine if a cloud is liquid water.

Logic:

$$\boldsymbol{If}\left(\theta_0 < 80°\ \boldsymbol{AND}\ \varepsilon_{3.75\mu m} > 0.9\ \boldsymbol{AND}\ R_{3.75\mu m} > 20\right)\ \boldsymbol{Then}\ TRUE$$

where $\varepsilon_{3.75\mu m}$ is the emissivity and $R_{3.75\mu m}$ the TOA reflectance at 3.75 μm.

Nighttime 3.75μm reflectance liquid water test

Purpose: Utilize 3.75μm reflectance at night to determine if a cloud is liquid water.

Logic:

$$\boldsymbol{If}\left(\theta_0 > 80° \ \boldsymbol{AND}\ R_{3.75\mu m} > 5\right)\boldsymbol{Then}\ TRUE$$

Split window liquid water test

Purpose: Utilize the brightness temperature difference between 8.5 μm and 11 μm ($BTD_{8.5\mu m\text{-}11\mu m}$) to determine if a cloud is liquid water.

Logic:

$$\boldsymbol{If}\left(BTD_{8.5\mu m-11\mu m} < -1\right)\boldsymbol{Then}\ TRUE$$

3x3 STD Test

Purpose: Pre-test for cirrus cloud using the 3x3 pixel 11 μm brightness temperature ($BT_{11\mu m}$) standard deviation (STD_{3x3}); if true, proceed to the split window cirrus test.

Logic:

$$\boldsymbol{If}\left(STD_{3x3}\left[BT_{11\mu m}\right] < 4\right)\boldsymbol{Then}\ TRUE$$

2.1.1.7 Split window cirrus test

Purpose: Test for cirrus cloud.

Logic:

PART I

$$\boldsymbol{If}\left(BT_{11\mu m,clear} \leq 265\right)\boldsymbol{Then}$$

$$Correction_{H_2O} = 0.5$$

$$\boldsymbol{Else}$$

$$Correction_{H_2O} = \left(BT_{11\mu m,clear} - BT_{12\mu m,clear}\right)\frac{\left(BT_{11\mu m} - 260\right)}{\left(BT_{11\mu m,clear} - 260\right)}$$

PART II

$$FMFT = BT_{11\mu m} - BT_{12\mu m} - Correction_{H_2O}$$

$$\boldsymbol{If}(FMFT > 1)\ \boldsymbol{Then}\ TRUE$$

Here FMFT refers to the AVHRR heritage “four minus four test” that used the AVHRR channels 4 and 5.